Rhodes College Digital Archives - DLynx

Design, synthesis and analysis of novel dopaminergic and catecholic ligands as inhibitors of catechol-O-methyltransferase

Item Type	Thesis
Authors	Hatstat, Anna Katherine
Publisher	Memphis, Tenn. : Rhodes College
Rights	Rhodes College owns the rights to the archival digital objects in this collection. Objects are made available for educational use only and may not be used for any non-educational or commercial purpose. Approved educational uses include private research and scholarship, teaching, and student projects. For additional information please contact archives@rhodes.edu. Fees may apply.
Download date	2025-07-12 03:20:11
Link to Item	

Design, synthesis and analysis of novel dopaminergic and catecholic ligands as inhibitors
of catechol-*O*-methyltransferase

Anna Katherine Hatstat

Department of Chemistry
Rhodes College
Memphis, Tennessee

2016

Submitted in partial fulfillment of the requirements for the Bachelor of Science degree
with Honors in Chemistry

This Honors paper by Anna Katherine Hatstat has been read and approved for Honors in the Department of Chemistry

Dr. Mauricio Cafiero
Project Advisor

_____

Dr. Larryn W. Peterson
Second Reader

_____

Dr. Brian Larkins
Extra-Departmental Reader

_____

Dr. Mauricio Cafiero
Department Chair

_____

Acknowledgements

Contents

List of Figures and Tables

Abstract

L-DOPA, a dopamine precursor, is commonly used as a pharmacological treatment for patients with conditions such as Parkinson's disease. Therapeutic L-DOPA, as well as the dopamine derived from L-DOPA, can be deactivated via metabolism by catechol-*O*-methyltransferase (COMT). The targeted inhibition of the COMT enzyme prolongs the effectiveness of L-DOPA and dopamine, resulting in a net increase in pharmacological efficiency of the treatment strategy. Two classes of novel derivatives have been proposed and analyzed through *in silico* models that apply density functional theory and Møller–Plesset perturbation theory methods. The inhibitory capacities of the ligands were determined by the relative binding affinity of each ligand in the active site model. Three active site models were analyzed in order to compare computational methods and simulate physiological conditions. The lipophilicity of the proposed ligands was determined computationally as well. Following the completion of the computational analysis, several of the proposed catecholic ligands, namely 3,4-dihydroxybenzonitrile, 2-(3,4-dihydroxyphenyl)acetonitrile and 3-(3,4-dihydroxyphenyl)propanenitrile, were synthesized and analyzed experimentally to confirm structure and purity and to determine lipophilicity.

1.   Introduction

Catechol-*O*-methyltransferase (COMT) is an enzyme involved in the metabolism of catecholamines and catechols, producing inactive, methylated metabolites of its substrates and thereby affecting the ability of the catecholamines to act as signaling agents in the body. Catecholamines, which include dopamine, norepinephrine and epinephrine, can act as hormonal signals or neurotransmitters, inducing activity in the body and brain, respectively. Inhibition of COMT can prevent the metabolism of these molecules, thus prolonging the activity of the signaling agents. In order to identify viable inhibitors of COMT and to understand their biological activity, a computational and experimental study including the design, synthesis and analysis of novel inhibitors of COMT has been performed.

The metabolic activity of COMT occurs in the active site of the enzyme (Figure 1), which is located between two dimerized subunits. The active site has organometallic character due to the presence of a magnesium ion, which in one monomer is coordinated with Asp141, Asp169, and Asn170.[1,2,3] The magnesium complex is near residues Glu199 and Lys144, which complete a hydrophilic pocket of charged amino acids.[1,2,3] The opposite side of the active site consists of non-polar and aromatic residues (Trp38, Met40, Asn41, Val42, Pro174, Trp253, Val388, Leu413, Met416), creating a hydrophobic region.[2]

Figure 1: Crystal structure of COMT (PDB ID: 2CL5)[2]

The crystal structure of the active site was first elucidated by Rodrigues et al.[4] and was further studied by Palma et al.[2]

Catecholic ligands bound in the active site coordinate with the magnesium residue (as the sixth ligand in an octahedral complex) via one of the two characteristic phenolic hydroxyl groups. The other hydroxyl group is oriented toward Lys144, which extracts a proton, leaving a deprotonated ligand.[2] The deprotonated ligand interacts with an electron-deficient region of co-factor S-adenosyl-L-methionine (SAM), resulting in the transfer of a methyl group from SAM onto the ligand and producing a methylated metabolite (Figure 2).[2]

Competitive inhibition of COMT can prevent the metabolism of catecholic ligands into methylated metabolites. The strategic inhibition of COMT can be used in treatment strategies

Figure 2: Metabolism scheme of L-DOPA and dopamine. COMT can metabolize both L-DOPA and dopamine, affecting the amount of either molecule available to be converted into dopamine (L-DOPA) or to act as a hormonal signal or neurotransmitter (dopamine)[3,5,7,9]

for conditions resulting from catecholic dysfunctions such as Parkinson's disease (PD). PD results from the degeneration of the substantia nigra, a region of the midbrain that has dopaminergic innervations to other brain regions such as the basal ganglia. The loss of dopaminergic signaling from the substantia nigra results in the characteristic movement-related dysfunction associated with PD. Traditionally, PD is treated pharmacologically with the oral administration of 3,4-dihydroxy-L-phenylalanine (L-DOPA), a dopamine precursor.[5] Dopamine cannot cross the blood brain barrier (BBB), but L-DOPA is able to cross via the LAT1 transporter, which transports large, neutral amino acids across the BBB.[1,6] Once administered to the body or present in the brain, L-DOPA is converted to dopamine by DOPA decarboxylase.[7] Orally administered L-DOPA is not a targeted treatment, and very little of the administered dose reaches the brain to correct for the loss of dopaminergic signaling.[1] To prevent the metabolism of L-DOPA to dopamine in the body and thus increase the amount of L-DOPA available to reach the brain, L-DOPA is typically administered with a DOPA decarboxylase inhibitor such as carbidopa or benserazide.[8]

The effectiveness of L-DOPA treatments can be further prolonged by the administration of a COMT inhibitor in conjunction with L-DOPA and a decarboxylase inhibitor. COMT is involved, with monoamine oxidase and aldehyde dehydrogenase, in a two-step metabolism of dopamine into homovanillic acid, and it can also metabolize L-DOPA into 3-*O*-methyldopa (Figure 2).[3,5,9] COMT is ubiquitously expressed in both the brain and the body. In the body, it can act to metabolize L-DOPA to 3-*O*-methyldopa, preventing L-DOPA from reaching the brain and subsequently being converted to dopamine. Once in the brain, L-DOPA can be prematurely metabolized to 3-*O*-

methyldopa, and dopamine derived from L-DOPA can be metabolized by COMT to 3-methoxytyramine. Inhibition of COMT in the body can increase the amount of L-DOPA available to reach the brain, while inhibition in the brain can increase the amount of L-DOPA in the brain available to become dopamine, and prolong the effectiveness of dopamine derived from L-DOPA in the brain.

Because of the implication of COMT inhibition in the treatment of dopamine or catecholamine related disorders, several generations of COMT inhibitors have been previously proposed and studied. First generation inhibitors were primarily simple catechols such as protocatechuric acid, caffeic acid, and dopacetamine (Figure 3a).[10] Though the early inhibitors showed moderate inhibitory effects, many had short half-lives and were thus ineffective as COMT inhibitors because they would have to be administered frequently to produce a prolonged effect.[10] First generation inhibitor U-0521 (Figure 3a), in particular, showed favorable effects when administered in animal models[11] but failed to elicit activity in Parkinsonian patients.[12] Other early inhibitors such as pyrogallol and its derivatives did not retain the catecholic structure but rather contained a trihydroxybenzene structure (Figure 3b).[13,14] Pyrogallol displayed inhibitory activity similar to that of catechol but was slightly more potent, which may have resulted from additional intermolecular forces between the third hydroxyl group and the active site.[15] Like simple catechols, pyrogallol and its derivatives had a short-half life and limited efficacy as COMT inhibitors.[15]

Early second generation inhibitors included electron donating or electron withdrawing groups in positions adjacent to the catechol hydroxyl groups, and inhibitors with electron withdrawing groups in the adjacent position were the most effective.[15,16]

Most second generation inhibitors include a nitrocatechol moiety through which the ligands bind in COMT. The most effective meta-nitrated inhibitors are nitecapone and entacapone, though other meta-nitrated inhibitors have been proposed as well (Figure 3c). Nitecapone is a tight binding inhibitor that acts only in the periphery as it in unable to cross the BBB.[17,18] It has been effective in a dose-dependent manner when administered in animal models, with little acute toxicity.[19] Entacapone, like nitecapone, is a peripheral, meta-nitrated inhibitor, but, unlike nitecapone, it is fully reversible. Entacapone is longer-acting than nitecapone but has relatively low bioavailability, requiring administration of higher and more frequent doses.[20] Further investigation of nitrocatechol inhibitors led to the development of acetylated nitrocatechols such as Ro41-0960, tolcapone, nebicapone, and BIA 3-335 (Figure 3c). Ro41-0960, with its fluorinated substituent, had greater in vivo efficacy compared to simpler acetylated inhibitors. Ro41-0969 dose-dependently blocked the formation of 3-O-methyldopa and homovanillic acid produced by COMT metabolism of L-DOPA and dopamine, respectively.[16] Tolcapone is a tight binding but reversible inhibitor that acts in both the periphery and in the brain with long-lasting effects.[17,18] Nebicapone has similar potency to tolcapone but has a shorter duration and weaker activity in the brain.[19] BIA 3-335 has better peripheral selectivity than tolcapone but has very poor BBB penetration because of the increased polarity caused by the piperazinyl nitrogen atoms and various hydrogen bond acceptors.[20]

This progression of COMT inhibitor design has led to the identification of inhibitors with drastic variation in the substituents on the catecholic ring (Figure 3a-c).[20] The structures of early and current inhibitors deviate from the dopaminergic or catehcolic

structure of endogenous ligands, so this investigation proposed and analyzed novel small molecule dopaminergic and catecholic derivatives as potential inhibitors of COMT.

a) Simple catechols and derivatives

| Catechol | Protocatechuric acid | Caffeic acid |

Quercetin   U-0521

b) Pyrogallol and derivatives

Pyrogallol   Gallic acid

c) Nitrocatechols

Nitecapone   Entacapone   Ro41-0960

Tolcapone   Nebicapone (BIA3-202)   BIA3-335
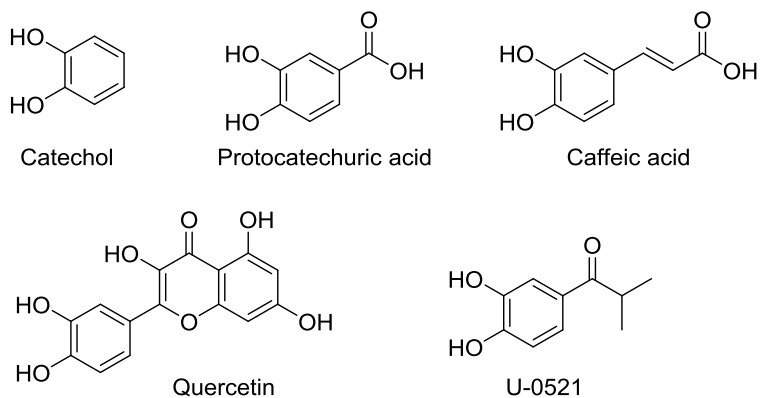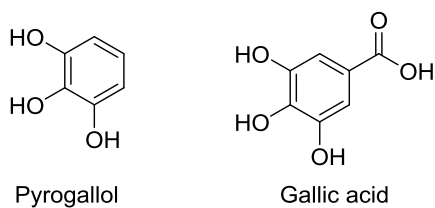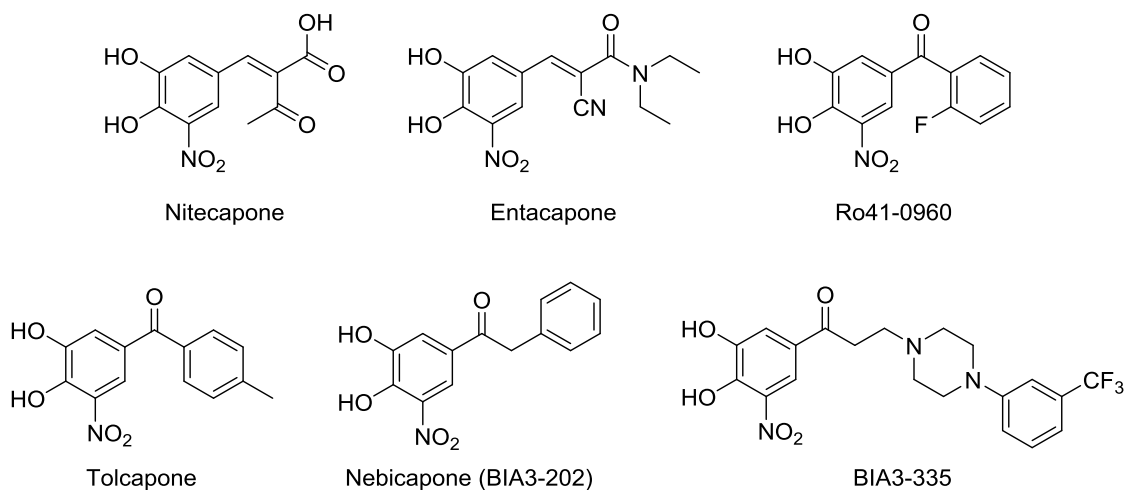
Figure 3: Previously studied COMT inhibitors, including a) simple catechols, b) pyrogallol and derivatives and c) nitrocatechols[10-20]

Two generations of potential COMT inhibitors were proposed in this

investigation, with the first generation characterized as dopaminergic derivatives (Figure

4) and the second generation characterized as catecholinergic derivatives (Figure 5). The

ligands were first studied computationally through a quantum mechanics-based study of

ligand binding affinity in the enzymatic active site. The conformations of the derivatives

bound in the COMT active site, were optimized using M062X, a Density Functional

Theory (DFT) method, in various computational models that applied both *in vacuo* and

solvated (via the Polarizable Continuum Model proposed by Tomasi et al.) conditions.[25]

M062X was chosen as the method by which to optimize the ligand-active site complexes

because of its ability to accurately model a wide range of interactions and its favorable

results in previous investigations of active site models.[26-28] Electronic interaction energies

for the optimized ligands were determined with both M06L,[29] a DFT method, and MP2.[30]

M06L has been shown to be accurate in calculations involving transition metals,[29] while

MP2 is known to be the most economical and accurate post-Hartree Fock method.[30,32] For

DFT methods, M06L was chosen over M062X for the determination of counterpoise

corrected interaction energies because the most dominant interaction in the active site
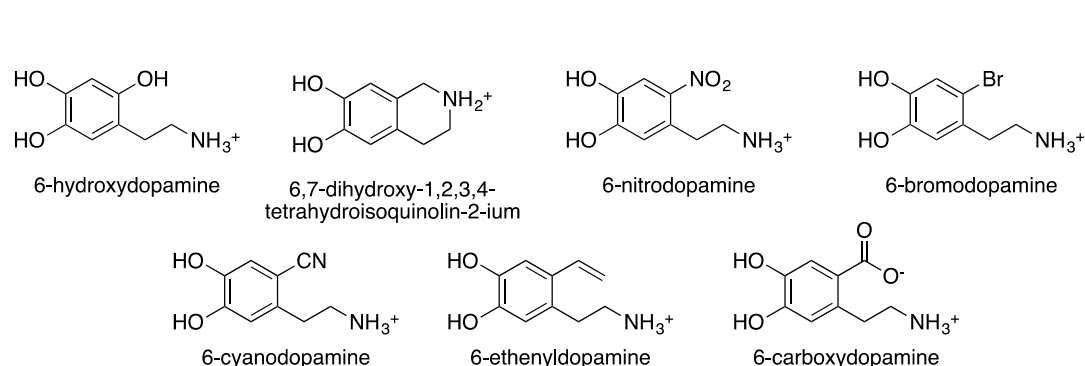
Figure 4: First generation ligands, which are dopaminergic derivatives and
contain an ethylamine tail

exists between the ligand and the magnesium residue. M06L was used for all subsequent interaction energy calculations for consistency and to allow for the determination of total electronic interaction energy by summation. The application of the Polarizable Continuum Model (PCM)[25] in some optimization models simulates the electrostatic and hydrostatic effects of aqueous solvation and provides a better measurement of intermolecular forces by improving charge distribution in the system. Bigler et al. found that the application of PCM with MP2 and M062X showed good agreement.[28] The application of solvation through PCM establishes a more physiologically relevant computational model, though considerations for solvation can be computationally expensive.

Metabolism of ligands by COMT produces a singly methylated metabolite, as seen in dopamine metabolite homovanillic acid (Figure 2). The position of methylation depends on the orientation of the ligand when it binds in the active site through coordination with the magnesium ion. All proposed inhibitors contain a catecholic structure, with two phenolic hydroxyl substituents. If the ligand binds through the 4-hydroxyl group to magnesium ion with the 3-hydroxy (relative to the dopaminergic ethylamine tail) closer to Lys144, the 3-*O*-methylated metabolite will be produced
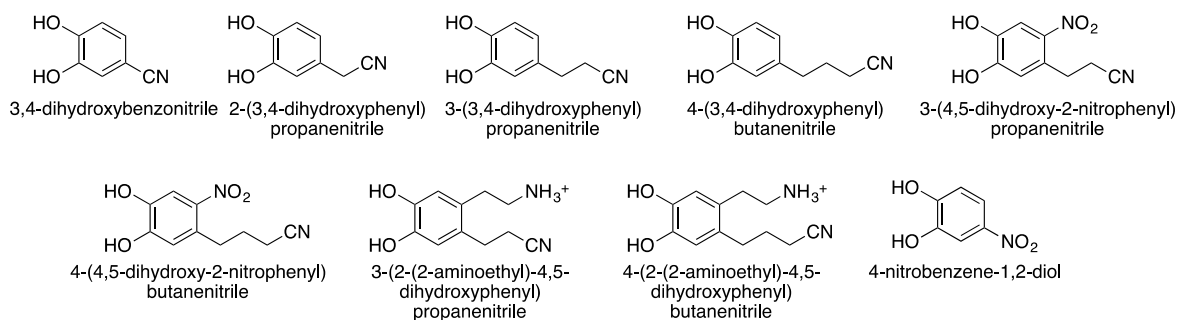
Figure 5: Second generation ligands, which contain catecholic structure with varied substituents

(Figure 6). Conversely, binding to magnesium through the 3-OH group, leaving the 4-hydroxyl group accessible for methylation, produces the 4-*O*-methylated metabolite (Figure 6). When considering inhibitor efficacy in this investigation, both the 3-deprotonation and 4-deprotonation positions were considered, representing the 3-methoxy and 4-methoxy metabolism positions, respectively. Thus, the proposed computational model compares deprotonation position in addition to method accuracy and relative inhibitory capacity measured as electronic interaction energy. Deprotonation position preference is an important consideration because metabolite effects and activity must be considered in the drug design process. Computational analysis will provide an indication of binding preference and, subsequently, metabolite structure, which will provide information about how the ligands interact with the active site and how metabolism will affect their structures.

Though computational analysis can provide a relative comparison of the interaction energy of different ligands in the same enzymatic active site, the computational binding affinity would be more reliable if validated by experimental, *in*
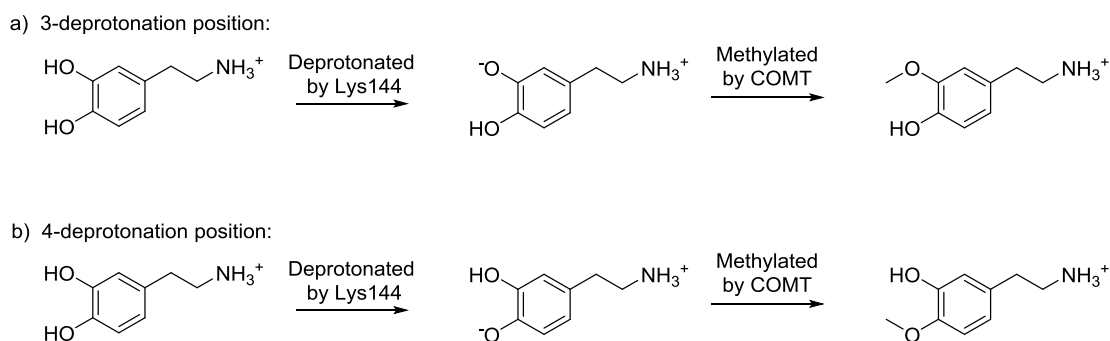
Figure 6: Schemes depicting the deprotonation and methylation of dopamine in the 3-deprotonation (a) and 4- deprotonation (b) position. 3-*O*-Methyl and 4-*O*-methyl metabolites can be produced from ligand metabolism by COMT

vitro results. To determine the binding affinity of ligands through *in vitro* analysis, the ligands of interest must first be synthesized. The first generation ligands proposed in the computational study have been successfully synthesized or their syntheses are currently in progress,[32] so this investigation details the synthesis of three of the second generation ligands, namely 3,4-dihydroxybenzonitrile, 2-(3,4-dihydroxyphenyl)acetonitrile, and 3-(3,4-dihydroxyphenyl)propanenitrile. After the structure and purity of the synthesized molecules have been confirmed, the binding affinity of the molecules as ligands of COMT can be determined through a microplate screening assay proposed by Kurkela et al. (2004).[33] The results from this assay will provide more accurate measurement of the biological activity of the ligands, thus validating the computational methods established in this study.

To further understand the biological activity of the ligands proposed in this investigation, computational and experimental determinations of ligand lipophilicity were performed. Lipophilicity provides a measure of ligand solubility as the partition coefficient, or logP, and is important to consider because it is a property that affects the absorption, distribution, metabolism and excretion of drugs. The value of logP can be determined according to the following derivation:

$$logP = log\frac{[Ligand_{octanol}]}{[Ligand_{water}]} \qquad \text{(Eq. 1)}$$

$$logP = log(e^{\frac{-\Delta G_{total}}{RT}}) \qquad \text{(Eq. 2)}$$

$$\Delta G_{total} = \Delta G_{octanol} - \Delta G_{water} \qquad \text{(Eq. 3)}$$

LogP can be determined computationally by calculating the free energy (ΔG) of each ligand in both water and octanol and using the ΔG_{total} to find logP according to Equation 2. Experimentally, logP can be determined based on the solubility of the ligand in a

solution containing both octanol and water. Common approaches include the shake-flask method,[34] which requires agitation of a solution containing n-octanol, water and a known concentration of the molecule of interest. Following agitation, the layers are separated and each is analyzed by high performance liquid chromatography to determine the concentration of ligand in solution.[33] From this analysis, the ratio of $\frac{[Ligand_{octanol}]}{[Ligand_{water}]}$ can be determined and used to find logP according to Equation 1.

LogD, which accounts for solubility of the ligand in different protonation states, is determined according to the following equation, where f indicates the fraction of ligand in each protonation state, P is the partition coefficient of the ligand, N represents the neutral from of the ligand and I represents the ionized form of the ligand:

$$logD = \log\{f^N P^N + f^I P^I\} \qquad \text{(Eq. 4)}$$

The partition coefficient of each ligand, in either the neutral or protonated form, can be determined according to the method described for logP (Eq. 1-3). The fraction of each ligand is determined according to the following derivation:

$$pH = pKa + \log(\frac{[Base]}{[Acid]}) \qquad \text{(Eq. 5)}$$

$$pH - pKa = \log(\frac{[Base]}{[Acid]}) \qquad \text{(Eq. 6)}$$

$$10^{pH-pKa} = \log(\frac{[Base]}{[Acid]}) \qquad \text{(Eq. 7)}$$

where the acidic form has fully protonated substituents (i.e. protonated ethylamine tail on dopamine) and the basic form of the ligand is the neutral conformation, so

$$\frac{Base}{Acid} = \frac{Neutral\ Form}{Ionized\ Form} \qquad \text{(Eq. 8)}$$

Once the ratio of base to acid is calculated:

$$f^N = \frac{N}{N+I} \tag{Eq. 9}$$

$$\frac{1}{f^N} = \frac{N+I}{N} = \frac{N}{N} + \frac{I}{N} = 1 + \frac{I}{N} = 1 + \frac{Acid}{Base} \tag{Eq. 10}$$

So,

$$f^N = \frac{1}{1 + \frac{Acid}{Base}} \tag{Eq. 11}$$

$$f^I = 1 - f^N \tag{Eq. 12}$$

By computationally determining the pKa of the ligand with considerations for physiological conditions (pH = 7.4), the ratio of basic form to acidic form can be determined, thus allowing for the determination of f^N and f^I. Once f^N and f^I have been calculated, logD can be determined according to Equation 4.

By analyzing the behavior of the proposed ligands with computational and experimental techniques in order to determine the biological behavior and solubility of the molecules, an interdisciplinary understanding of molecular behavior in enzymatic active sites can be established. The combination of experiment and computation allows for validation of techniques while providing a more thorough understanding of the proposed molecules as inhibitors of catechol-*O*-methyltransferase.

2.   Computational Methods

2.1.   *Crystal Structure*

A crystal structure of catechol-*O*-methyltransferase, with ligand BIA 8-176, a known COMT inhibitor, bound in the active site was retrieved from the Protein Data Bank (PDB ID: 2CL5).[2] The active site was extracted from the crystal structure. Amino acids of interest were included in the active site based on proximity to the ligand. All

amino acids retained in the active site model were between 3 and 4 angstroms from the bound ligand and include Trp38, Met40, Asn41, Val42, Lys144, Asp141, Asp169, Asn170, Pro174, Glu199, Trp253, Val388, Leu413, and Met416.

2.2. *Optimization Models*

Three computational models were established and analyzed through this investigation. In all models, the active site-ligand complex was optimized using M062X/6-31G with the conditions described below.

2.2.1. *VR Model*

Ligand-active site complexes were optimized with the described method assuming gas phase conditions and with rigid amino acid side chains. Thus, in the VR model, only the positions of the ligand and added protons were optimized while the conformation of the amino acid side chains was retained as resolved in the original active site structure.

2.2.2. *SR Model*

Ligand-active site complexes were optimized with the described method with rigid amino acid side chains (VR model), but implicit solvation was applied through the Polarizable Continuum Model (PCM) as described by Tomasi et al.[25] PCM applies the electrostatic and hydrostatic forces that would be present if the ligand and active site were in solution, allowing for a more accurate and reliable model of a physiological system.

2.2.3. SX Model

Ligand-active site complexes were optimized with the described method with implicit solvation through PCM and with non-rigid amino acid side chains. Thus, the ligand, the R-groups of the amino acid residues, and added protons were allowed to optimize, while the backbone of the amino acid remained rigid, retaining the overall size of the active site and amino acid distribution.

2.3.   Interaction Energies

Counterpoise corrected interaction energies were determined for the optimized ligand-active site complex through a summation of interaction energies between the ligand and each individual amino acid. Interaction energies were calculated with M06L and MP2, each with the 6-311+G* basis set, for the VR and SR model. SX interaction energies were calculated with M06L/6-311+G* only due to strong agreement between M06L and MP2 in previous studies[13] and in the VR and SR model analysis.

2.4.   Ligands

Each ligand proposed in this investigation was studied in the VR, SR, and SX models. Deprotonation of the ligand can occur in two conformations (Figure 6), depending on which phenolic hydroxyl group is in closer proximity to Lys144, which extracts a proton and allows for methylation of the ligand at the deprotonated position. The positions of deprotonation and subsequent methylation will be referred to as 3-dp and 4-dp, representing deprotonation in the 3- and 4- position relative to the

dopaminergic aminoethyl tail, respectively (Figure 6). Both conformations of each ligand in the active site were investigated in the VR, SR, and SX models.

Two generations of ligands were proposed in this investigation. The first generation of ligands (Figure 4) retains the dopaminergic structure and contains various substituents in the 6-position relative to the ethylamine tail. The second generation of ligands retains the dihydroxyphenyl structure of catecholic molecules but contains an alkyl nitrile of various lengths or an alkyl nitrile substituent and an ethylamine or nitro substituent (Figure 5).

2.5. *LogP and LogD Calculations*

Computational measures of partition coefficients (logP) were determined for both the first and second generation ligands. LogP was determined for ligands with all ionizable substituents fully protonated (deprotonated for amines), while logD considers the ligand at physiological pH. For determination of logP, ligands were optimized twice with M062X/6-311+G* using n-octanol and water via PCM for the optimizations, separately. The harmonic vibrational frequencies of the ligands were determined in the optimization, producing the total free energy of the molecule (ΔG_{total}).

A relative value for pKa was determined computationally using OLYP/3-21G*, applying implicit solvation through PCM. The pKa of both the acidic (protonated) form and basic (neutral) form of the ligand were determined
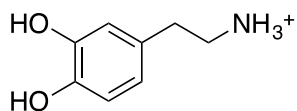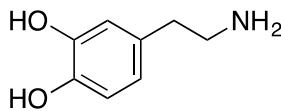
Figure 7: Protonation state of dopamine at a) physiological conditions (pH = 7.4) and b) in a neutral state

using the described method. Once pKa values and partition coefficient values were obtained, the relative values of logD were determined according to Equations 4-12 for all ligands which could be ionized at physiological pH (contained either an amino group or carboxyl group) (Figure 7).

3.   Synthetic Methods

3.1.   *General Methods*

Unless otherwise indicated, all anhydrous solvents were commercially obtained and stored in Sure-Seal bottles under argon. All other reagents and solvents were purchased as the highest grade available from Acros or Sigma-Aldrich and were used without further purification. All moisture-sensitive reactions were carried out using dry solvents and under slight pressure of ultra-pure argon. Commercially available disposable syringes were used for transferring reagents and solvents. All single syntheses were conducted in conventional flasks under an atmosphere of dry argon. Proton (^{1}H) and carbon (^{13}C) NMR spectra were recorded on a Varian 400 MHz spectrometer. Chemical shifts (δ) are reported in parts per million (ppm) referenced to ^{1}H (CHCl$_3$ at 7.26, DMSO at 2.50), ^{13}C (CDCl$_3$ at 77.16, DMSO at 39.52). Coupling constants (J) are reported in Hz throughout. Column chromatography was conducted using silica gel (Silicycle 55-65 Å). Purity of the compounds was confirmed via HPLC analysis with Shimadzu LC-6AD pumps, SPD-M20A PDA, CBM-20A communication and ThermoScientific column (hypersil gold, 250 x 4.6, particle size = 5 μm). HRMS analysis was conducted at UC Riverside High Resolution Mass Spectrometry facility on a Waters GCT high resolution mass spectrometer with EI/CI and LIFDI capabilities (NSF grant CHE-0742001).

3.2.   Abbreviations

Reagents used in the subsequent syntheses are abbreviated as follows: Boron tribromide, BBr$_3$; dichloromethane, DCM; sodium sulfate, Na$_2$SO$_4$; dimethyl sulfoxide, DMSO; tetrahydrofuran, THF; N-bromosuccinimide, NBS; triphenylphosphine, PPh$_3$; sodium thiosulfate, NaS$_2$O$_3$; sodium hydroxide, NaOH; magnesium sulfate, MgSO$_4$; triphenylphosphine oxide, PPh$_3$O; chloroform, CDCl$_3$; potassium cyanide, KCN; dimethylformamide, DMF.

*3.3.   3,4-Dihydroxybenzonitrile (**2**)*

BBr$_3$ (1 M in DCM, 12.25 mL, 12.25 mmol) was added dropwise, under argon gas, to 3,4-dimethoxybenzonitrile (**1**) (500 mg, 3.06 mmol) in DCM (3 mL) at 0 °C. The reaction was stirred at 0 °C for 2 h and was allowed to slowly warm to room temperature (rt). After an additional 1 h and 15 min of stirring, the solution was concentrated under reduced pressure and was then redissolved in ethyl acetate (15 mL). The ethyl acetate solution was washed with brine (3 x 15 mL) and the organic layer was dried over Na$_2$SO$_4$ and concentrated, yielding 3,4-dihydroxybenzonitrile (**2**) as a yellow solid (338 mg, 81.3% yield). ^{1}H NMR (400 MHz, DMSO-d_6) δ ppm 6.86 (d, *J*=8.22 Hz, 1 H) 7.05 (d, *J*=1.96 Hz, 1 H) 7.08 (dd, *J*=8.22, 1.96 Hz, 1 H) 9.66 (br. s., 1 H) 10.12 (s, 1 H); HRMS m/z [M-H]- calcd for C$_7$H$_4$NO$_2$: 134.0248. Found: 134.0253; HPLC retention time: 6.634 minutes.

3.4.   2-(3,4-Dihydroxyphenyl)acetonitrile (**4**)

BBr$_3$ (1 M in DCM, 10.15 mL, 10.15 mmol) was added dropwise, under argon gas, to 2-(3,4-dimethoxyphenyl)acetonitrile (**3**) (300 mg, 1.69 mmol) in DCM at 0 °C. The reaction was stirred for 2 h and 15 min, warmed to rt and stirred for an additional 45 min. The solution was concentrated under reduced pressure and was immediately redissolved in ethyl acetate (15 mL). The ethyl acetate solution was washed with brine (3 x 15 mL), and the organic layer was dried over Na$_2$SO$_4$ and concentrated, yielding 2-(3,4-dihydroxyphenyl)acetonitrile (**4**) as an off-white solid (145 mg, 57.3% yield). ^{1}H NMR (400 MHz, DMSO-d_6) δ ppm 3.80 (s, 2 H) 6.57 (dd, J=7.8, 2.0 Hz, 0 H) 6.70 (d, J=7.8 Hz, 0 H) 6.71 (d, J=2.0 Hz, 0 H) 8.94 (s, 1 H) 9.06 (s, 1 H); HRMS m/z [MNH4+] calcd for C$_8$H$_{11}$N$_2$O$_2$: 167.0815. Found: 167.0813; HPLC retention time: 6.987 minutes.

3.5.   4-(2-Bromoethyl)-1,2-dimethoxybenzene (**6**)

2-(3,4-Dimethoxyphenyl)ethanol (**5**) (750 mg, 4.12 mmol) and PPh$_3$ (1076 mg, 4.12 mmol) in THF (7 mL) was stirred for 1 h at 0 °C. NBS (732 mg, 4.12 mmol) was added in one portion and the solution was allowed to slowly warm to rt and was stirred overnight (18 h). The reaction was quenched with NaS$_2$O$_3$ (5 mL, 10% w/v). The solution was diluted with DCM (10 mL) and washed twice with 1 M NaOH solution (2 X 5 mL) and once with H$_2$O (5 mL). The organic layer was separated, dried over MgSO$_4$ and condensed under reduced pressure. PPh$_3$O byproduct was precipitated with addition of diethyl ether and removed, and diethyl ether was evaporated. The crude product was purified via flash chromatography (1:1 hexanes:ethyl acetate) and product (**6**) was isolated as a brown oil (530 mg, 53% yield). ^{1}H NMR (400 MHz, CDCl$_3$-d) δ ppm 3.12

(d, *J*=7.83 Hz, 2 H) 3.56 (d, *J*=7.83 Hz, 2 H) 3.88 (s, 3 H) 3.89 (s, 3 H) 6.72 - 6.86 (m, 3 H); Rf (1:1 hexanes:ethyl acetate): 0.79.

3.6.   3-(3,4-Dimethoxyphenyl)propanenitrile (*7*)

KCN (204 mg, 3.13 mmol) and 4-(2-bromoethyl)-1,2-dimethoxybenzene (**6**) (530 mg, 2.09 mmol) were dissolved in DMF (24 mL) under Ar. The solution was stirred overnight at rt. Deionized water (40 mL) was added to quench the rxn, and the solution was extracted with DCM (3 x 20 mL). The combined organic layer was washed with water (20 mL) and brine (20 mL), dried over Na_2SO_4 and condensed under reduced pressure. The product was purified via flash column chromatography (1:1 hexanes:ethyl acetate) to produce 3-(3,4-dimethoxyphenyl)propanenitrile (**7**) as a clear oil (186 mg, 72% yield). ^{1}H NMR (400 MHz, $CDCl_3$-*d*) δ ppm 2.60 (t, *J*=7.43 Hz, 2 H) 2.90 (t, *J*=7.43 Hz, 2 H) 3.87 (s, 3 H) 3.88 (s, 3 H) 6.74 - 6.86 (m, 3 H); Rf (1:1 hexanes:ethyl acetate): 0.58.

3.7.   3-(3,4-Dihydroxyphenyl)propanenitrile (*8*)

BBr_3 (1 M in DCM, 8.83 mL, 8.83 mmol) was added dropwise to 3-(3,4-dimethoxyphenyl)propanenitrile (**7**) (422 mg, 2.21 mmol) in DCM (2.5 mL) and the solution was stirred at 0 °C for 3 h. The solution was immediately concentrated under reduced pressure and redissolved in ethyl acetate. The organic layer was washed with brine, dried over Na_2SO_4 and concentrated under reduced pressure to yield 3-(3,4-dihydroxyphenyl)propanenitrile (**8**) as a white solid (218 mg, 61% yield). ^{1}H NMR (400 MHz, DMSO-*d*$_6$) δ ppm 2.68 (s, 4 H) 6.51 (dd, *J*=8.2, 2.0 Hz, 1 H) 6.64 (d, *J*=2.0 Hz, 1

H) 6.65 (d, *J*=8.2 Hz, 1 H) 8.78 (br. s., 2 H); HRMS m/z [MNH4]+ calcd for $C_9H_{13}N_2O_2$:

181.0972. Found: 181.0968; HPLC retention time: 7.600 minutes.

4.   Results and Discussion

4.1.   *Optimization and Structure*

The optimized structures of all ligands in the VR model, oriented with the 3-OH

group nearer to Lys144, modeling the 3-deprotonation position, and oriented with the 4-

OH group nearer to Lys144, modeling the 4-deprotonation position, are shown in

Appendix A. Structures of the optimized ligand-active site complexes for all ligands in

the 3-dp and 4-dp conformation in both the SR and SX model are included in subsequent

| 3-dp, VR Model | 3-dp, SR Model | 3-dp, SX Model |
| 4-dp, VR Model | 4-dp, SR Model | 4-dp, SX Model |
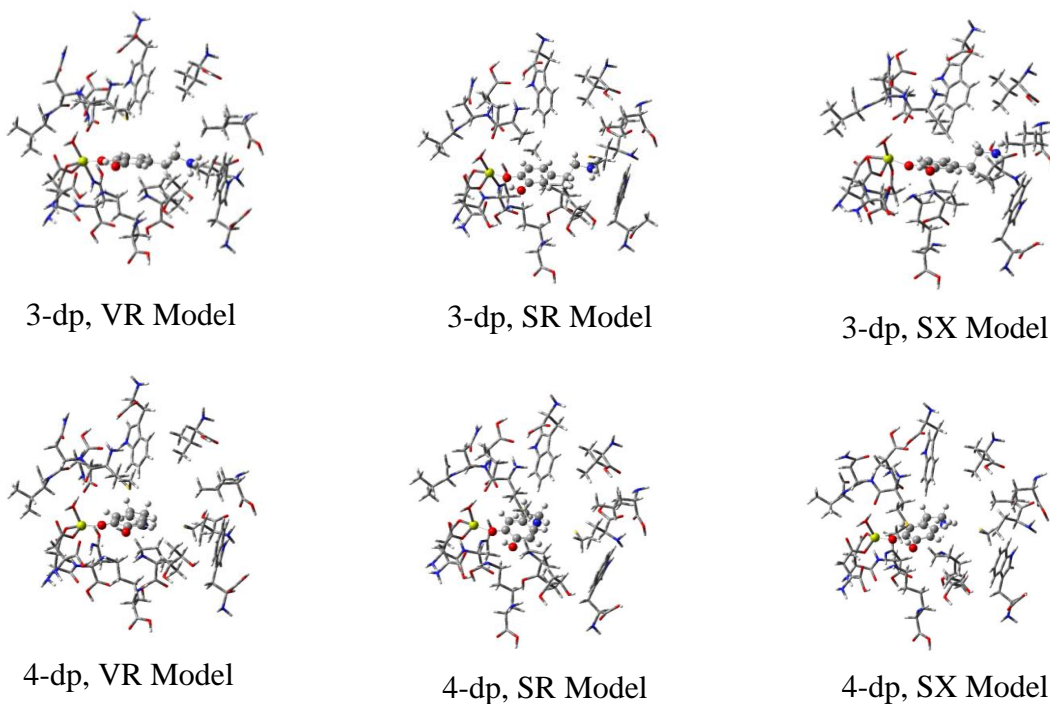
Figure 8: Optimized structures of dopamine in the COMT active site. All three optimization models, with dopamine in both the 3- and 4-deprotonation (dp) position shown. Structures optimized using M062X/6-31G in the Gaussion09 platform.

appendices (Appendix B and C). Representative figures of the ligand-active site complexes show dopamine, in both the 3-dp position and 4-dp position, in all optimization models (Figure 8).

4.2. *VR Model Interaction Energies*

Analysis of counterpoise corrected interaction energies of ligands in the VR model, which required optimization with *in vacuo* conditions and rigid amino acid side chains, revealed several amino acid residues that contribute strongly to overall ligand binding activity in the COMT active site. The key residues, which include Lys144, Asp149, the Asp169/Asn170 dipeptide, and Glu199, are the only charged amino acids in the active site and are all clustered around or coordinated with the Mg^{2+} residue, creating a highly charged, hydrophilic pocket at one side of the active site (Figure 9). The pocket of charged, hydrophilic amino acid residues contribute more strongly to the overall binding affinity than the other residues, with the Mg^{2+} ion contributing most significantly through coordination with the ligand. The remaining residues form a hydrophobic pocket in the active site and interact with the ligand through dispersion-type forces.
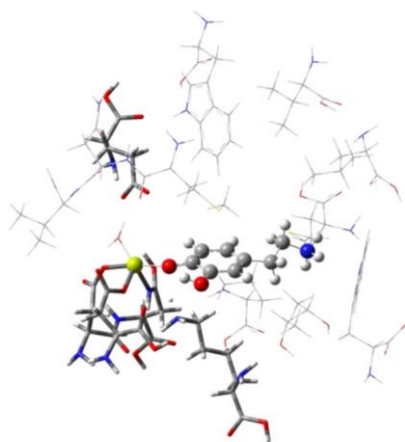
Figure 9: Optimized COMT active site complex, with dopamine bound in the 3-dp position. Key amino acid residues (Lys144, Asp149, Asp169/Asn170, and Glu199) indicated in medium resolution on the right hand side of the active site model.

In the VR model and throughout the subsequent models, dopamine was analyzed to establish a basis of comparison for relative ligand affinity of the proposed derivatives. For a proposed derivative to be a favorable inhibitor, it must have a stronger interaction energy in the active site than dopamine. In the VR model, dopamine had interaction energies of -235.2 and -234.6 kcal/mol when calculated with M06L and MP2, respectively. The interaction energy of dopamine and all proposed ligands are described in Tables 1 and 2.

Table 1: Summary of counterpoise corrected interaction energies for first generation ligands in the VR optimization model (rigid active site, vacuum conditions). Energies were calculated with moth M06L and MP2 and are presented in kcal/mol.

Molecule		Method	Mg^{2+}	Asp169/ Asn170	Lys144	Glu199	Asp141	Total
Dopamine	3-dp	M06L	-217.1	12.6	-59.0	14.8	31.4	-235.2
		MP2	-220.7	14.2	-57.4	15.5	32.7	-234.6
	4-dp	M06L	-208.0	22.0	-55.9	-0.3	23.0	-249.6
		MP2	-211.7	24.8	-55.5	0.5	32.0	-241.1
BIA 8-176	--	M06L	-310.9	-36.9	-93.4	57.5	52.3	-345.6
		MP2	-314.4	-37.5	-91.5	61.1	53.7	-346.4
Resveratrol	--	M06L	-94.9	2.8	-13.9	-3.8	0.4	-109.6
		MP2	-123.3	3.5	-12.2	-4.9	1.6	-146.1
6-Hydroxydopamine	3-dp	M06L	-216.5	25.7	-57.5	11.0	23.3	-230.3
		MP2	-216.7	26.0	-55.9	12.4	31.4	-219.6
	4-dp	M06L	-193.9	13.0	-61.7	-47.7	27.1	-267.8
		MP2	-198.4	14.5	-60.1	-44.9	29.7	-264.5
1,2,3,4-Tetrahydroisoquinolin e-6,7-diol	3-dp	M06L	-183.1	9.9	-53.2	-17.4	25.8	-228.3
		MP2	-186.6	11.3	-51.6	-15.9	26.3	-227.9
	4-dp	M06L	-196.8	19.0	-54.4	-10.0	27.5	-226.5
		MP2	-195.4	20.3	-53.1	-8.5	28.4	-221.4
6-Nitrodopamine	3-dp	M06L	-190.3	15.1	-30.5	15.1	8.5	-202.9
		MP2	-193.9	19.0	-31.4	18.8	10.6	-197.9
	4-dp	M06L	-198.9	16.3	-37.3	6.1	18.4	-217.9
		MP2	-204.5	14.4	-37.5	7.5	18.3	-223.5
6-Bromodopamine	3-dp	M06L	-214.4	18.7	-39.5	22.6	18.2	-218.8
		MP2	-217.2	23.7	-38.7	29.2	20.8	-207.5
	4-dp	M06L	-223.7	14.9	-43.7	17.5	23.8	-237.7
		MP2	-226.3	19.0	-38.7	29.2	25.3	-209.6
6-Cyanodopamine	3-dp	M06L	-205.6	18.3	-33.7	19.7	14.7	-201.5
		MP2	-209.4	22.4	-34.5	22.5	16.3	-200.1
	4-dp	M06L	-209.8	13.6	-40.1	13.0	20.9	-225.2
		MP2	-214.1	17.5	-40.1	15.0	21.9	-222.1
6-Ethenyldopamine	3-dp	M06L	-206.3	24.4	-58.9	12.4	23.6	-223.5
		MP2	-212.5	26.7	-57.5	13.7	31.1	-214.8
	4-dp	M06L	-207.2	24.4	-55.1	-0.3	24.9	-232.5
		MP2	-209.1	26.7	-54.8	0.5	27.3	-230.2
6-Carboxydopamine	3-dp	M06L	-325.5	68.4	-120.5	55.4	69.7	-265.4
		MP2	-324.1	69.5	-118.1	55.7	70.5	-259.1
	4-dp	M06L	-320.4	64.2	-116.2	45.8	75.5	-259.7
		MP2	-319.5	64.8	-114.1	46.3	67.5	-262.5

In the VR model, BIA 8-176 was found to be the most strongly bound ligand. The ligand, which is a known COMT inhibitor, had overall interaction energies of -345.6 and -346.4 kcal/mol with methods M06L and MP2, respectively. BIA 8-176 bound to COMT with a significantly stronger interaction energy than dopamine, making it a favorable inhibitor. BIA 8-176 was also stronger than any of the currently proposed derivatives. Though BIA 8-176 was very favorable in this model, the results may be unreliable because the crystal structure was resolved with BIA 8-176

Table 2: Summary of counterpoise corrected interaction energies for second generation ligands in the VR optimization model (rigid active site, vacuum conditions). Energies were calculated with moth M06L and MP2 and are presented in kcal/mol.

Molecule		Method	Mg^{2+}	Asp169/ Asn170	Lys144	Glu199	Asp141	Total
3,4-Dihydroxybenzonitrile	3-dp	M06L	-327.5	51.4	-83.7	65.6	56.9	-246.8
		MP2	-331.7	55.2	-82.8	67.8	58.1	-245.2
	4-dp	M06L	-334.1	56.1	-81.4	70.3	57.4	-249.8
		MP2	-337.4	61.3	-81.0	72.3	58.6	-246.8
2-(3,4-Dihydroxyphenyl) acetonitrile	3-dp	M06L	-341.2	50.3	-85.5	80.7	61.0	-248.3
		MP2	-344.9	55.1	-84.8	74.5	62.0	-253.5
	4-dp	M06L	-341.0	56.9	-86.7	60.8	70.5	-258.4
		MP2	-344.0	62.0	-85.3	61.5	72.6	-250.7
3-(3,4-Dihydrozyphenyl) propanenitrile	3-dp	M06L	-342.4	59.4	-87.9	68.3	59.6	-259.6
		MP2	-345.1	64.0	-86.3	70.6	60.9	-255.0
	4-dp	M06L	-342.1	51.3	-87.5	69.2	58.8	-268.3
		MP2	-344.8	55.1	-86.0	71.0	59.8	-264.2
4-(3,4-Dihydroxyphenyl) butanenitrile	3-dp	M06L	-125.6	-17.4	-16.1	-3.6	1.3	-172.7
		MP2	-126.6	-11.8	-16.6	-1.9	2.2	-168.1
	4-dp	M06L	-346.4	50.7	-88.2	69.8	60.2	-275.3
		MP2	-348.8	54.8	-86.8	71.6	61.2	-269.5
3-(4,5-Dihydroxy-2-nitrophenyl) propanenitrile	3-dp	M06L	-304.8	47.7	-78.2	56.0	50.4	-242.4
		MP2	-310.4	53.9	-77.6	57.0	51.7	-241.0
	4-dp	M06L	-285.3	60.8	-91.9	50.3	56.9	-220.3
		MP2	-284.2	62.0	-91.3	50.2	58.3	-218.6
4-(4,5-Dihydroxy-2-nitrophenyl) butanenitrile	3-dp	M06L	-324.6	54.3	-77.7	65.7	53.5	-242.6
		MP2	-328.9	60.0	-78.2	68.5	55.7	-239.4
	4-dp	M06L	-308.8	48.0	-79.6	56.4	51.4	-248.7
		MP2	-314.4	50.7	-78.9	57.6	52.6	-249.2
3-(2-(2-Aminoethyl)-4,5-dihydroxyphenyl) propanenitrile	3-dp	M06L	-207.5	28.7	-55.5	9.5	27.1	-211.6
		MP2	-211.6	29.9	-52.8	10.1	28.8	-210.7
	4-dp	M06L	27.7	-100.3	-26.9	-95.6	-97.3	-349.5
		MP2	14.6	-39.3	-119.0	-46.2	-66.6	-288.7
4-(2-(2-Aminoethyl)-4,5-dihydroxyphenyl) butanenitrile	3-dp	M06L	-247.7	10.7	-41.6	28.3	24.0	-250.8
		MP2	-252.2	11.0	-41.4	31.1	25.4	-262.5
	4-dp	M06L	-221.6	45.0	-40.8	-30.2	18.1	-246.4
		MP2	-227.5	61.1	-40.8			
4-Nitrobenzene-1,2-diol	3-dp	M06L	-81.6	-11.4	-16.7	-50.5	-5.3	-169.0
		MP2	-87.5	-5.06	-16.4	-44.1	-3.4	-161.3
	4-dp	M06L	-108.4	-5.0	-10.6	-42.0	-9.4	-181.5
		MP2	-113.4	3.2	-12.5	-37.6	-2.05	-169.3

Table 3: Summary of counterpoise corrected interaction energies for first generation ligands in the SR optimization model (rigid active site, solvated conditions). Energies were calculated with moth M06L and MP2 and are presented in kcal/mol.

Molecule		Method	Mg^{2+}	Asp169/ Asn170	Lys144	Glu199	Asp141	Total
Dopamine	3-dp	M06L	-216.3	30.6	-60.6	13.8	33.0	-216.9
		MP2	-221.8	32.2	-59.1	14.3	34.6	-218.4
	4-dp	M06L	-210.0	21.3	-53.5	0.5	22.6	-248.0
		MP2	-213.7	24.2	-53.3	1.2	31.7	-239.4
BIA 8-176	--	M06L	-320.5	52.4	-93.4	59.2	59.2	-260.6
		MP2	-324.2	57.8	-91.7	63.0	63.0	-253.7
Resveratrol	--	M06L	-96.8	6.4	-15.9	-1.4	1.2	-111.7
		MP2	-129.4	7.5	-0.5	-2.3	2.3	-145.1
6-Hydroxydopamine	3-dp	M06L	-201.7	13.6	-55.9	-44.6	26.9	-267.1
		MP2	-205.4	-4.9	-55.5	-42.7	30.0	-284.4
	4-dp	M06L	-200.4	11.3	-55.6	-44.7	24.3	-270.9
		MP2	-204.1	13.3	-54.4	-42.2	29.7	-264.5
1,2,3,4-Tetrahydroisoquinoline-6,7-diol	3-dp	M06L	-188.2	11.9	-49.8	-0.3	26.2	-209.9
		MP2	-191.7	13.1	-48.5	0.5	26.8	-210.2
	4-dp	M06L	-197.6	23.8	-52.2	-2.7	27.9	-214.0
		MP2	-202.2	25.4	-51.1	-2.8	28.9	-216.5
6-Nitrodopamine	3-dp	M06L	-214.2	15.9	-31.4	20.1	11.8	-237.3
		MP2	-218.6	22.2	-32.4	25.4	14.1	-229.3
	4-dp	M06L	-208.9	18.6	-38.6	10.4	20.7	-219.9
		MP2	-214.3	22.7	-38.4	11.8	16.2	-225.4
6-Bromodopamine	3-dp	M06L	-15.0	-110.5	28.1	-45.3	-39.5	-201.0
		MP2	-16.2	-103.6	28.1	-44.0	-38.5	-194.9
	4-dp	M06L	-237.6	19.3	-43.3	18.7	27.0	-240.5
		MP2	-240.7	26.2	-42.5	22.8	23.4	-235.6
6-Cyanodopamine	3-dp	M06L	-2.5	-118.7	30.2	-50.7	-44.1	-202.4
		MP2	-4.8	-114.1	29.3	-49.0	-42.3	-199.5
	4-dp	M06L	-221.5	19.5	-40.3	15.4	13.0	-231.3
		MP2	-225.8	24.8	-40.0	17.9	19.2	-228.5
6-Ethenyldopamine	3-dp	M06L	-202.5	26.5	-53.0	5.3	28.1	-208.0
		MP2	-207.4	28.4	-52.0	5.8	29.8	-209.9
	4-dp	M06L	-208.1	20.6	-57.7	-0.4	25.5	-236.1
		MP2	-211.0	0.0	-57.3	0.4	28.4	-257.3
6-Carboxydopamine	3-dp	M06L	-325.5	68.4	-120.6	55.4	69.7	-265.7
		MP2	-324.1	69.5	-118.1	55.6	70.5	-262.6
	4-dp	M06L	-332.4	64.0	-113.9	46.1	68.9	-274.5
		MP2	-325.3	65.0	-112.0	46.5	69.8	-265.0

bound in the active site. Thus, the active site residues were favorably oriented in the resolved crystal structure to maximize interaction with BIA 8-176. Optimization of the active site residues may alter the binding affinity of BIA 8-176 and other ligands.

The least strongly bound ligand in the VR model was resveratrol, with overall interaction energies of -109.6 and -146.1 kcal/mol when calculated with M06L and MP2, respectively. Among the proposed novel ligands, several molecules had higher affinities in the active site than dopamine. Favorable ligands from the first generation include 6-hydroxydopamine (4-dp) and 6-carboxydopamine (3-dp) while favorable ligands from

the second generation include 2-(3,4-dihydroxyphenyl)acetonitrile (4-dp), 4-(3,4-dihydroxyphenyl)butanenitrile (4-dp), 3-(3,4-dihydroxyphenyl)propanenitrile (3-dp;4-dp), and 3-(2-(2-Aminoethyl)-4,5-dihydroxyphenyl)propanenitrile (4-dp).. Interaction energies of all ligands studied in the VR active site model, including interaction energies with key residues and total energy, are given in Table 1 and 2.

4.3.   SR Model Interaction Energies

Because the VR model is optimized with gas phase conditions, it is not biologically relevant. In order to prepare a more biologically relevant model, the optimized complexes from the VR model were re-optimized with the application of implicit solvation via the Polarizable Continuum Model. The model simulates the presence of water as a solvent, surrounding the ligand and active site with a field that mimics the electrostatic and hydrostatic forces that would be created by an aqueous environment. In order to maximize the efficiency of the optimization, the fully optimized structures from the VR model were optimized with solvation to produce the SR model structures. This allows for comparison of results between models while minimizing computational costs compared to explicit solvation.

Counterpoise corrected interaction energies were calculated using both M06L and MP2 with the 6-311+G* basis set (Table 3 and Table 4). In the SR model, dopamine had interaction energies of -216.9 and -218.4 kcal/mol when calculated with M06L and MP2, respectively. BIA 8-176 was no longer the most favorable inhibitor, as it had been in the VR model. In the VR model, BIA 8-176 had interaction energies of -345.6 and -348.6 kcal/mol when calculated with M06L and MP2, respectively. In the SR model, however,

BIA 8-176 had interaction energies of -260.6 and -253.7 kcal/mol when calculated with

M06L and MP2, respectively. The decrease in affinity with the addition of implicit

solvation makes BIA 8-176 less favorable as an inhibitor though it is still competitive

with and slightly more favorable than dopamine (-216.9 kcal/mol with M06L in the SR

model).

The most favorable first generation ligands in the SR model included 6-

hydroxydopamine and 6-carboxydopamine, which were both comparable in overall

interaction energy to BIA 8-176. 6-Hydroxydopamine was comparably favorable in both

the 3-dp and 4-dp position, with respective interaction energies of -267.1 and -270.9

Table 4: Summary of counterpoise corrected interaction energies for second generation ligands in the SR optimization model (rigid active site, solvated conditions). Energies were calculated with moth M06L and MP2 and are presented in kcal/mol.

Molecule		Method	Mg^{2+}	Asp169/Asn170	Lys144	Glu199	Asp141	Total
3,4-Dihydroxybenzonitrile	3dp	M06L	-117.1	-30.9	-10.6	-5.3	-1.6	-171.3
		MP2	-120.1	-23.5	-10.9	-3.6	-0.2	-166.2
	4dp	M06L	-116.5	-27.5	-9.0	-2.8	-2.0	-165.7
		MP2	-119.6	-21.0	-9.6	-1.5	-0.4	-162.2
2-(3,4-Dihydroxyphenyl) acetonitrile	3dp	M06L	-124.3	-21.5	-12.6	-0.3	2.2	-165.1
		MP2	-126.8	-15.4	-12.7	1.1	3.2	-161.0
	4dp	M06L	-123.7	-22.6	-14.1	-2.8	2.1	-169.5
		MP2	-126.0	-16.7	-13.7	-1.5	3.1	-165.4
3-(3,4-Dihydrozyphenyl) propanenitrile	3dp	M06L	-128.1	-17.7	-13.0	-1.7	0.0	-167.6
		MP2	-130.2	-12.2	-12.8	-0.6	1.5	-164.0
	4dp	M06L	-127.1	-18.0	-13.4	-1.3	-0.3	-169.2
		MP2	-129.3	-12.4	-13.1	-0.2	1.2	-163.9
4-(3,4-Dihydroxyphenyl) butanenitrile	3dp	M06L	-132.0	-16.7	-13.8	-0.2	2.1	-172.2
		MP2	-133.6	-11.0	-13.9	1.2	3.2	-168.4
	4dp	M06L	-131.7	-17.2	-14.9	-1.4	1.6	-175.8
		MP2	-133.3	-11.5	-14.6	-0.2	2.8	-169.4
3-(4,5-Dihydroxy-2-nitrophenyl) propanenitrile	3dp	M06L	-282.6	59.2	-89.7	50.6	56.8	-215.9
	4dp	M06L	-311.3	-141.9	-74.5	57.3	50.6	-433.2
		MP2	-317.7	-190.9	-74.4	58.5	52.0	-488.8
4-(4,5-Dihydroxy-2-nitrophenyl) butanenitrile	3dp	M06L	-113.5	-35.4	-6.1	-5.9	-4.0	-176.1
	4dp	M06L	-313.5	46.9	-72.6	57.8	51.9	38.4
		MP2	-314.3	53.7	-75.7	59.1	53.2	46.8
3-(2-(2-Aminoethyl)-4,5-dihydroxyphenyl) propanenitrile	3dp	M06L	-208.9	26.7	-53.6	9.7	25.8	-214.3
		MP2	-212.5	28.9	-52.7	11.1	28.6	-209.8
	4dp	M06L	--	--	--	--	--	--
		MP2	--	--	--	--	--	--
4-(2-(2-Aminoethyl)-4,5-dihydroxyphenyl) butanenitrile	3dp	M06L	-45.0	-99.4	279	-41.5	-31.7	-213.9
		MP2	-48.3	-92.5	27.0	-39.8	-30.3	-209.1
	4dp	M06L	-247.5	52.7	-35.6	-41.6	23.1	-269.0
4-Nitrobenzene-1,2-diol	3dp	M06L	-106.5	-6.6	-14.9	-43.4	-2.0	-178.0
	4dp	M06L	-112.9	-6.9	-10.6	-35.4	11.4	-161.0
		MP2	-120.8	3.8	-12.5	-31.4	-1.4	-169.0

when calculated with M06L. 6-Carboxydopamine was also equally favorable in both the

3-dp and 4-dp position, with respective interaction energies of -265.7 and -274.5 kcal/mol

when calculated with M06L. In the second generation of ligands, 3-(4,5-dihydroxy-2-

nitrophenyl)propanenitrile (4-dp) was the most favorable ligand while 4-(4,5-dihydroxy-

2-nitrophenyl)butanenitrile (4-dp) was the least strongly bound. Strong agreement was

seen between M06L and MP2 results for both ligands. The least favorable ligand in the

SR model was resveratrol, with interaction energies of -111.7 and -145.1 kcal/mol when

calculated with M06L and MP2.

Two trends were seen in the transition from the *in vacuo* optimization model to

the solvated model. The first generation of ligands (6-hydroxydopamine, 1,2,3,4-

tetrahydroisoquinoline-6,7-diol, 6-nitrodopamine, 6-bromodopamine, 6-cyanodopamine,

6-ethenyldopamine, and 6-carboxydopamine) retained similar interaction energies in both

the VR and SR models. The interaction energies determined with M06L and MP2

remained comparable across both models as well. The second trend observed in the

transition from VR to SR model conditions was seen with the decrease in favorability of

several second generation (3,4-dihydroxybenzonitrile, 2-(3,4-

dihydroxyphenyl)acetonitrile, 3-(3,4-dihydroxyphenyl)propanenitrile, 4-(3,4-

dihydroxyphenyl)butanenitrile) with the addition of implicit solvation. The loss of ligand

binding affinity results from alterations in protonation states with the application of

implicit solvation. The catecholic derivatives containing nitrile substituents would, in

some cases, extract a proton from Asn170, which is coordinated with the magnesium ion

in the active site. When the proton is extracted by the ligand, the ligand becomes more

neutral, decreasing its interaction with charged amino acids and with the magnesium ion.

The alterations of ion-ion interaction to ion-dipole interaction results in weaker interactions between the ligand and each individual amino acid, and thus the ligand has a lower affinity overall. The interaction between the tail of the ligands and the hydrophobic residues on the back side of the active site remains consistent because the nitrile substituent does change charge when solvated.

4.4.   SX Model Interaction Energies

The final computational model, which retained the implicit solvation conditions present in the SR model, also allowed for the optimization of the amino acid side chains in addition to the optimization of the ligand. This model, called the SR model, is the most biologically relevant and is thus the most reliable model as a measure of potential biological activity. The interaction energies, determined after optimization of the SX model structures, are shown in Table 3. Interaction energies in the SR model were calculated with M06L only. M06L is less computationally expensive but is less reliable than MP2. In the previous models, however, M06L and MP2 showed strong agreement. Thus, in the SR model, the MP2 model was omitted and M06L was used as the only method in the determination of counterpoise corrected interaction energies.

In the SR model, resveratrol was the most favorable inhibitor, with an overall interaction energy of -309.8 kcal/mol. The interaction energy of resveratrol in this model was significantly stronger than in the previous models, in which resveratrol was the weakest ligand overall. The most significant decrease in interaction energy between the SR and SX model was seen in 1,2,3,4-tetrahydroisoquinoline-6,7-diol (-210.2 kcal/mol in the SR model, -62.4 kcal/mol in the SX model).

The first generation ligands (6-hydroxydopamine, 6-nitrodopamine, 6-bromodopamine, 6-cyanodopamine, 6-ethenyldopamine and 6-carboxydopamine) remained relatively consistent in overall binding affinity between the two models with the exception of 1,2,3,4-tetrahydroisoquinoline-6,7-diol, which decreased in affinity (Table 5). The second generation derivatives (3,4-dihydroxybenzonitrile, 2-(3,4-

Table 5. Summary of counterpoise corrected interaction energies for all ligands in the SX optimization model (non-rigid active site, solvated conditions). Energies were calculated with moth M06L and MP2 and are presented in kcal/mol.

Molecule		Method	Mg^{2+}	Asp169/ Asn170	Lys144	Glu199	Asp141	Total
Dopamine	3-dp	M06L	-219.8	26.4	-63.2	13.5	31.3	-224.9
	4-dp	M06L	-215.7	19.4	-75.5	-2.3	24.0	-292.5
BIA 8-176	--	M06L	-288.7	60.2	-90.9	52.2	50.0	-232.9
Resveratrol	--	M06L	-337.1	-337.1	-337.1	-337.1	-337.1	-337.1
6-Hydroxydopamine	3-dp	M06L	-225.0	11.4	-71.8	-11.5	33.3	-275.6
	4-dp	M06L	-209.5	11.6	-64.3	-55.2	31.4	-293.6
1,2,3,4-Tetrahydroisoquinoline-6,7-diol	3-dp	M06L	-200.4	-9.3	-56.0	-9.4	226.2	-62.4
	4-dp	M06L	-211.8	21.6	-69.3	0.5	32.0	-249.3
6-Nitrodopamine	3-dp	M06L	-185.3	27.5	-25.0	16.1	9.5	-177.8
	4-dp	M06L	-178.9	21.5	-36.7	1.5	11.9	-198.1
6-Bromodopamine	3-dp	M06L	-232.8	25.8	-42.5	-1.7	17.4	-258.4
	4-dp	M06L	-222.3	25.2	-42.9	-3.0	19.1	-251.1
6-Cyanodopamine	3-dp	M06L	-204.7	25.8	-33.0	1.8	15.7	-215.8
	4-dp	M06L	-208.8	18.6	-40.1	-4.9	12.9	-248.8
6-Ethenyldopamine	3-dp	M06L	-207.7	23.6	-73.3	2.8	29.3	-245.6
	4-dp	M06L	-212.8	20.0	-62.1	-2.6	27.7	-245.5
6-Carboxydopamine	3-dp	M06L	-343.8	70.1	-116.4	61.1	74.5	-271.6
	4-dp	M06L	-334.8	60.4	-116.4	47.2	69.8	-278.7
3,4-Dihydroxybenzonitrile	3-dp	M06L	-303.2	58.7	-102.7	53.0	65.4	-245.0
	4-dp	M06L	-301.7	64.4	-101.3	55.1	64.3	-227.6
2-(3,4-Dihydroxyphenyl) acetonitrile	3-dp	M06L	-127.7	-8.1	-10.5	3.3	5.6	-138.2
	4-dp	M06L	-350.0	59.9	-85.3	65.5	62.4	-263.4
3-(3,4-Dihydrozyphenyl) propanenitrile	3-dp	M06L	-352.1	61.0	-85.0	64.0	61.9	-265.9
	4-dp	M06L	-314.0	60.3	-72.1	51.9	61.4	-221.5
4-(3,4-Dihydroxyphenyl) butanenitrile	3-dp	M06L	-318.4	59.4	-100.4	52.3	67.0	-215.4
	4-dp	M06L	-357.0	65.3	-92.9	66.8	47.0	-288.7
3-(4,5-Dihydroxy-2-nitrophenyl) propanenitrile	3-dp	M06L	-290.6	58.3	-97.8	53.7	59.7	-229.4
	4-dp	M06L	-318.0	56.1	-73.9	51.7	52.9	-242.4
4-(4,5-Dihydroxy-2-nitrophenyl) butanenitrile	3-dp	M06L	--	--	--	--	--	--
	4-dp	M06L	--	--	--	--	--	--
3-(2-(2-Aminoethyl)-4,5-dihydroxyphenyl) propanenitrile	3-dp	M06L	-323.5	60.4	-112.8	49.7	65.5	-355.5
	4-dp	M06L	--	--	--	--	--	--
4-(2-(2-Aminoethyl)-4,5-dihydroxyphenyl) butanenitrile	3-dp	M06L	-216.8	-13.7	-73.0	-56.6	27.6	-321.7
	4-dp	M06L	-235.5	25.9	-76.3	8.1	31.7	-265.4
4-Nitrobenzene-1,2-diol	3-dp	M06L	--	--	--	--	--	--
	4-dp	M06L	-303.8	48.4	-87.7	56.8	58.8	-241.8

dihydroxyphenyl)acetonitrile, 3-(3,4-dihydroxyphenyl)propanenitrile, 4-(3,4-dihydroxyphenyl)butanenitrile) became more favorable overall in the SX model (Table 5). In the SX model, the nitrile derivatives yielded electronic interaction energies ranging between -221.5 kcal/mol and -288.7 kcal/mol, with M06L, as compared to SR interaction energies ranging between -150.1 kcal/mol and -175.8 kcal/mol.

While optimizing the ligand-active site complexes with the SX conditions (non-rigid amino acid side chains, implicit solvation), an artifact was identified in the crystal structure. One of the residues coordinated with magnesium, Asn170, was resolved in the crystal structure with the oxygen on its side chain protonated while the amino substituent on the side chain had only one proton. This conformation is not realistic at physiological pH, so two computational models were established to determine the energetic difference in the conformation of the residue as resolved in the crystal structure versus the conformation of the residue in its native state at physiological pH. Each model contained dopamine as a ligand and the structures were optimized using the SX conditions. It was shown that the corrected model (Asn170 in its native state) is 36.9 kcal/mol more stable than the uncorrected model (Asn170 in the crystal structure conformation). Due to the greater energetic stability of the corrected model, all SX model structures were optimized with the corrected asparagine conformation, which was allowed to optimize along with the other amino acid side chains and the ligand.

4.5.   *Deprotonation in the 3-position versus the 4-position*

Catecholic and dopaminergic ligands are characterized by the presence of two phenolic hydroxyl groups, and these ligands bind in the COMT active site through

coordination of a hydroxyl group with the magnesium ion. The orientation of the bound ligand can dictate the metabolite formed through metabolism via COMT based on which hydroxyl group is bound and which is closer in proximity to Lys144, which deprotonates the ligand for methylation. Thus, there are two possible metabolites, resulting from deprotonation and subsequent methylation of either the 3-OH group or the 4-OH group (Figure 6).

In the VR and SR models, no strong preference for either deprotonation position was shown, thus indicating that the proposed ligands would be equally favorable in both the 3-dp and 4-dp positions (Tables 1-4). In the SX model, however, several ligands exhibited significantly different interaction energies in the 3-dp position versus the 4-dp position (Tables 5). These ligands include dopamine, 1,2,3,4-tetrahydroisoquinoline-6,7-diol, 6-nitrodopamine, 6-cyanodopamine, and 2-(3,4-dihydroxyphenyl)acetonitrile. The only ligand that displayed preference for the 3-dp position was 3-(3,4-dihydroxyphenyl)propanenitrile. Other ligands were slightly more favorable in one position than in the either, but the difference was not significant enough to indicate that the ligands could not bind competitively in either position.

The preference of dopamine to bind in the 4-dp rather than the 3-dp position is contrary to experimental results, but no strong preference has been demonstrated for known dopaminergic derivatives in experimental analysis thus far.[10] In experimental analysis, dopamine is preferentially deprotonated and methylated in the 3-position, as evidenced by the 3-*O*-methoxy group on dopamine metabolite homovanillic acid. The contrary computational results may have arisen because co-factor SAM was not included in the active site model. Inclusion of SAM in the model may have induced steric effects

causing dopamine to bind in the 3-dp position, rather than the 4-dp position as shown in

the computational results.

Table 6. Summary of interaction energies across computational models (VR, SR and SX model). Total interaction energies are displayed (measured in kcal/mol).

Molecule		VR Model		SR Model		SX Model
		M06L	MP2	M06L	MP2	M06L
Dopamine	3-dp	-235.6	-234.6	-216.9	-218.4	-224.9
	4-dp	-249.6	-242.3	-248.0	-239.4	-292.5
BIA 8-176	--	-345.6	-346.4	-260.6	-253.7	-232.9
resveratrol	--	-109.6	-146.1	-111.7	-145.1	-309.8
6-Hydroxydopamine	3-dp	-230.3	-219.6	-267.1	-284.4	-275.6
	4-dp	-267.8	-264.5	-270.9	-264.5	-293.6
1,2,3,4-Tetrahydroisoquinoline-6,7-diol	3-dp	-228.3	-227.9	-209.9	-210.2	-62.4
	4-dp	-226.5	-221.4	-214.0	-216.5	-249.3
6-Nitrodopamine	3-dp	-202.9	-197.9	-237.3	-229.3	-117.8
	4-dp	-217.9	-223.5	-219.9	-225.4	-198.1
6-Bromodopamine	3-dp	-218.8	-207.5	-201.0	-194.9	-258.4
	4-dp	-237.7	-209.6	-240.5	-235.6	-251.1
6-Cyanodopamine	3-dp	-201.5	-200.1	-202.4	-199.5	-215.8
	4-dp	-225.2	-222.1	-231.3	-228.5	-248.8
6-Ethenyldopamine	3-dp	-223.5	-214.8	-208.0	-209.9	-245.6
	4-dp	-232.4	-230.2	-236.1	-257.3	-245.5
6-Carboxydopamine	3-dp	-265.4	-259.1	-265.7	-262.6	-271.6
	4-dp	-259.7	-262.5	-274.5	-265.0	-278.7
3,4-Dihydroxybenzonitrile	3-dp	-246.8	-245.2	-171.3	-166.2	-245.0
	4-dp	-249.8	-246.8	-165.7	-162.2	-227.6
2-(3,4-Dihydroxyphenyl) acetonitrile	3-dp	-248.3	-253.5	-165.1	-161.0	-138.2
	4-dp	-258.4	-254.1	-169.5	-165.4	-263.4
3-(3,4-Dihydroxyphenyl) propanenitrile	3-dp	-259.6	-255.0	-168.2	-164.0	-265.9
	4-dp	-268.3	-264.2	-169.2	-163.9	-221.5
4-(3,4-Dihydroxyphenyl) butanenitrile	3-dp	-172.7	-168.1	-150.1	-162.9	-251.4
	4-dp	-275.3	-269.5	-175.8	-169.4	-288.7
3-(4,5-Dihydroxy-2-nitrophenyl) propanenitrile	3-dp	-220.3	-218.7	-215.9	-217.0	-229.4
	4-dp	-242.2	-241.0	-433.2	-488.8	-242.4
4-(4,5-Dihydroxy-2-nitrophenyl) butanenitrile	3-dp	-242.6	-239.4	-176.1	-172.2	--
	4-dp	-248.7	-249.2	38.4	46.8	--
3-(2-(2-Aminoethyl)-4,5-dihydroxyphenyl) propanenitrile	3-dp	-211.6	-210.7	-214.3	-209.8	-355.5
	4-dp	-349.5	-288.7	--	--	--
4-(2-(2-Aminoethyl)-4,5-dihydroxyphenyl) butanenitrile	3-dp	-250.8	-262.5	-213.9	-209.1	-321.8
	4-dp	-246.4	--	-269.0	--	-265.4
4-Nitrobenzene-1,2-diol	3-dp	-169.0	-161.3	-178.0	--	--
	4-dp	-181.5	-169.3	-161.0	-169.0	-241.8

4.6.   Overall trends in ligand affinity across computational models

As results of binding affinity are compared across computational models, several trends were present. First, strong agreement between computational methods was demonstrated in both the VR and SR model. The methods, M06L and MP2, were demonstrated to be consistent in previous work by this group,[13] and the results from the first two models further confirmed the reliability of M06L, allowing for the omission of MP2 in the SX model in order to maximize computational efficiency.

When analyzing changes in ligand affinity across computational models (Table 4), dopamine remained relatively consistent in overall affinity in VR, SR and SX model, with the exception of the increased affinity in the 4-dp position in the SX model. BIA 8-176 became less favorable across models, and is less favorable than dopamine (4-dp) in the SX model. Resveratrol increased in affinity across computational models and is the most favorable ligand in the SX model. The first generation of ligands (6-hydroxydopamine, 1,2,3,4-tetrahydroisoquinoline-6,7-diol, 6-nitrodopamine, 6-bromodopamine, 6-cyanodopamine, 6-ethenyldopamine, and 6-carboxydopamine) remained relatively consistent in binding affinity across VR, SR, and SX models, though strong preferences for the 4-dp position became evident in the SX model. The second generation of ligands (3,4-dihydroxybenzonitrile, 2-(3,4-dihydroxyphenyl)acetonitrile, 3-(3,4-dihydroxyphenyl)propanenitrile, 4-(3,4-dihydroxyphenyl)butanenitrile) became significantly less favorable with the application of solvation in the SR model, but regained favorability in the SX model when the Asn170 artifact was corrected and amino

acid side chains were optimized in solvation. Like the first generation ligands, the second generation ligands showed preference for 4-dp when position preference was present.

4.7. Computational determination of lipophilicity

Lipophilicity of the proposed ligands was measured through computational determination of logP and logD (when applicable) according to Equations 1-3 and Equations 4-12, respectively. LogP, the partition coefficient of ligands in octanol and water systems, was determined for all ligands. LogD was determined for ligands containing ionizable substituents that exist in different protonation states (namely, amino groups or carboxyl groups). The values for computationally determined logP and logD are presented in Table 7.

Table 7. LogP and LogD values for all proposed ligands, including catechol and caffeine for reference. Ligands are ranked in order of least hydrophilic to most hydrophilic (based on logP).

Molecule	LogP	LogD	Rank
Catechol	-0.75	--	--
Caffeine	-1.31	--	--
4-(3,4-dihydroxyphenyl)butanenitrile	-0.77	--	1
4-nitrobenzene-1,2-diol	-0.97		2
3,4-dihydroxybenzonitrile	-1.09	--	3
3-(3,4-dihydroxyphenyl)propanenitrile	-1.22	--	4
2-(3,4-dihydroxyphenyl)acetonitrile	-1.35	--	5
4-(4,5-dihydroxy-2-nitrophenyl)butanenitrile	-1.60	-1.55	6
3-(4,5-dihydroxy-2-nitrophenyl)propanenitrile	-1.70	--	7
Dopamine	-4.83	-1.31	8
6-bromodopamine	-4.92	-1.03	9
1,2,3,4-tetrahydroisoquinoline-6,7-diol	-4.96	2.61	10
6-hydroxydopamine	-5.74	-1.55	11
6-cyanodopamine	-5.79	-1.32	12
3-(2-(2-aminoethyl)-4,5-dihydroxyphenyl)propanenitrile	-6.22	-1.85	13
6-nitrodopamine	-6.24	-1.44	14
6-ethenyldopamine	-6.27	-0.78	15
4-(2-(2-aminoethyl)-4,5-dihydroxyphenyl)butanenitrile	-6.47	--	16
6-carboxydopamine	-8.01	-1.65	17

When optimizing the structures for logP calculations with either n-octanol- or water-based implicit solvation conditions, considerations were made for the conformation of the ligand in the respective solvent system. Because a hydrophobic ligand may establish a more folded conformation in an aqueous solution or, conversely, a more extended conformation in a non-polar solution, all structures were started with ethylamine group and 6-position substituents in an intermediate position (bent, but not folded or extended) allowing the ligand to establish the structural conformation most favorable in the applied solvent system.

LogP serves as a measure of lipophilicity by indicating the degree to which ligands are soluble in aqueous versus non-polar solutions. Ligands with a lower (more negative) logP or logD value prefer more aqueous environments. Catechol was included, in addition to dopamine, as a basis of comparison and as a means to establish and test the computational method. Caffeine was included in the computational study in order to validate relative lipophilicity determined computationally to the lipophilicity determined experimentally. Caffeine was used as a reference standard for method validation in the experimental shake flask procedure and was thus included in the computational study as well.

The most hydrophilic ligand in the study was 6-carboxydopamine, while the least hydrophilic (most hydrophobic) was 4-(3,4-dihydroxyphenyl)butanenitrile (Table 7). The logP values of the nitrile derivatives (3,4-dihydroxybenzonitrile, 2-(3,4-dihydroxyphenyl)acetonitrile, 3-(3,4-dihydroxyphenyl)propanenitrile, 4-(3,4-dihydroxyphenyl)butanenitrile, 3-(4,5-dihydroxy-2-nitrophenyl)propanenitrile, 4-(4,5-

dihydroxy-2-nitrophenyl)butanenitrile) were the most hydrophobic. The addition of aminoethyl tail to the nitrile derivatives (3-(2-(2-aminoethyl)-4,5-dihydroxyphenyl)propanenitrile, 4-(2-(2-aminoethyl)-4,5-dihydroxyphenyl)butanenitrile) significantly increase the hydrophilicity of the nitrile ligands, while the addition of the nitro substituent (3-(4,5-dihydroxy-2-nitrophenyl)propanenitrile, 4-(4,5-dihydroxy-2-nitrophenyl)butanenitrile) did not.

In the first generation ligands, 6-carboxydopamine was the most hydrophilic, while 1,2,3,4-tetrahydroisoquinoline-6,7-diol was the least hydrophilic. The calculated hydrophilicity of 6-carboxydopamine follows chemical logic because 6-carboxydopamine contains both the ethylamine tail and the carboxyl substituent, providing more opportunities for hydrogen bonding with water compared to the other ligands. The calculated logP of 1,2,3,4-tetrahydroisoquinoline was most similar to that of dopamine, which contains the same functional group but in a linear form rather than in a cyclic form.

4.8.   Synthesis of 3,4-dihydroxybenzonitrile, 2-(3,4-dibydroxyphenyl)acetonitrile, 3-(3,4-dihydroxyphenyl)propanenitrile

Ligands 3,4-dihydroxybenzonitrile (**2**), 2-(3,4-dihydroxyphenyl)acetonitrile (**4**) and 3-(3,4-dihydroxyphenyl)propanenitrile (**8**) were successfully synthesized according to Schemes 1 and 2. The structure of all products was confirmed via ^{1}H-NMR and HRMS (Appendix E and Appendix G). Purity was confirmed via HPLC (Appendix F).

Scheme 1: Synthesis of 3,4-dihydroxybenzonitrile (**2**) and
2-(3,4-dihydroxyphenyl)acetonitrile (**4**)

1: n = 0
3: n = 1

2: n = 0
4: n = 1
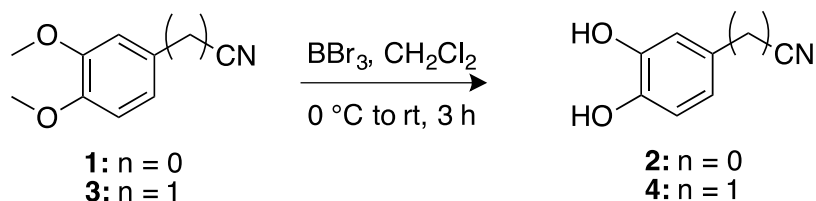
Scheme 2: Synthesis of 3-(3,4-dihydroxyphenyl)propanenitrile (**8**)
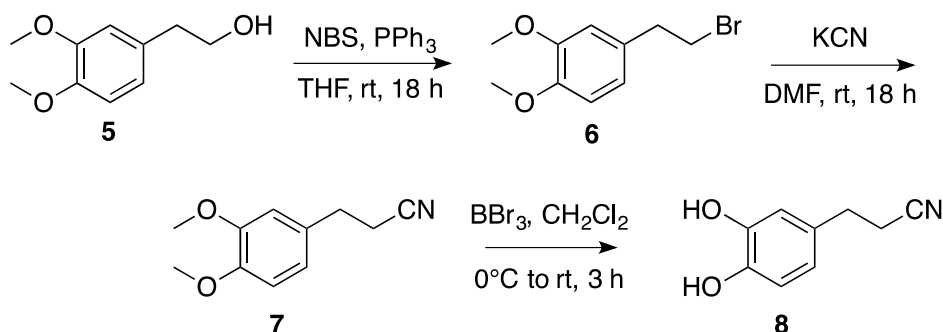
3,4-Dihydroxybenzonitriles (**2**) was synthesized from commercially available starting

material, 3,4-dimethoxybenzonitrile (**1**), via deprotection with boron tribromide (BBr₃).

BBr₃ was added dropwise to starting material **1** in solution with dichloromethane. The

solution was stirred for one hour at 0 °C, allowed to slowly warm to room temperature,

and stirred for an additional two hours. The solution was condensed under reduced

pressure and redissolved in ethyl acetate, followed by an aqueous workup. In initial

attempts to deprotect starting material **1**, the product was not isolated through an aqueous

workup. Rather, the reaction solution was quenched with a small volume (one to two

milliliters) of water or methanol and precipitation through the addition of diethyl ether

was used to isolate the product. Because the nitrile tail of the product is not protonated,

the product did not form a salt and precipitate out of solution. HBr salt precipitated and

the product remained in the diethyl ether solution. The workup was modified to remove salt byproducts like HBr through aqueous washes, allowing for the isolation of a pure product (**2**). Similar issues arose in the workup of 2-(3,4-dihydroxyphenyl)acetonitrile (**4**), which was produced through deprotection of 2-(3,4-dimethoxyphenyl)acetonitrile (**3**) with BBr_3. When an aqueous workup was used rather than precipitation, 2-(3,4-dihydroxyphenyl)acetonitrile (**4**) was yielded as an off-white solid.

3-(3,4-Dihydroxyphenyl)propanenitrile (**8**) was synthesized in three steps from 2-(3,4-dimethoxyphenyl)ethan-1-ol (**5**). Starting material **5** was first brominated through triphenylphosphine and N-bromosuccinimide in tetrahydrofuran to produce intermediate **6**. The reaction was stirred at room temperature overnight, quenched with an aqueous solution of sodium thiosulfate, diluted with dichloromethane, and washed with 1M sodium hydroxide and water. The reaction produces triphenylphosphine oxide as a by-product, which was partially removed through precipitation following the addition of diethyl ether. Further purification was required, and flash chromatography was used to remove excess triphenylphosphine oxide and yield intermediate **6** as a pure product.

4-(2-Bromoethyl)-1,2-dimethoxybenzene (**6**) was cyanated by the addition of potassium cyanide in dimethylformamide. The solution was stirred at room temperature overnight and quenched with water. The solution was extracted with dichloromethane. The combined organic layer was dried and condensed under reduced pressure. The product was purified through flash chromatography with a 1:1 hexanes:ethyl acetate solvent system. The starting material did not fully react due to the limited solubility of potassium cyanide in dimethylformamide.

In the synthesis of 3,4-dihydroxybenzonitrile (**2**), 2-(3,4-dihdyroxyphenyl)acetonitrile (**4**) and 3-(3,4-dihydroxyphenyl)propanenitrile (**8**), various conditions were used to improve the deprotection of the methyl ethers via BBr_3. The deprotection reaction is water sensitive as water or source of OH^- can quench the BBr_3 and render it inactive. Thus, anhydrous conditions were maintained and the number of equivalents of BBr_3 relative to the starting or intermediate material was varied to ensure complete deprotection. Trials were completed with between 1 and 6 equivalents of BBr_3. Maximum yield was achieved with 4 to 6 equivalents of BBr_3. The conditions of the workup were also varied in order to prevent the loss of product into aqueous phases or in the recrystallization process. The most efficient deprotection was achieved when the reaction solution was not quenched with water or methanol prior to workup. Rather, the solution was concentrated without quenching and immediately redissolved with ethyl acetate, which acted to sufficiently quench the unreacted BBr_3. Maximum yields of 3,4-dihydroxybenzonitrile, 2-(3,4-dihdyroxyphenyl)acetonitrile and 3-(3,4-dihydroxyphenyl)propanenitrile were 57%, 72% and 61% for the three molecules, respectively.

5.   **Conclusions**

Proposed dopaminergic (first generation) and catecholic (second generation) ligands were analyzed in three computational models (VR, SR, and SX). The VR model applied gas phase conditions with rigid amino acid side chains, while SR and SX applied implicit solvation with rigid and non-rigid amino acid side chains, respectively. Dopamine was analyzed in all models to provide a basis against which proposed derivatives would be compared to determine relative inhibitory capacity. BIA 8-176, a known COMT inhibitor, and resveratrol, a natural product, were analyzed in all models in addition to the proposed ligands.

In the VR model, BIA 8-176 was the most favorable inhibitor because it had the strongest interaction energy in the COMT active site. Of the proposed first generation ligands, 6-hydroxydopamine and 6-carboxydopamine were the most favorable inhibitors while 2-(3,4-dihydroxyphenyl)acetonitrile, 3-(3,4-dihydroxyphenyl)propanenitrile, 4-(3,4-dihydroxyphenyl)butanenitrile and 3-(2-(2-aminoethyl-4,5-dihydroxyphenyl)propanenitrile were the most favorable inhibitors in the second generation. Overall, the second generation inhibitors had slightly stronger interaction energies in the COMT active site.

Because the VR model was optimized in gas phase conditions, it did not provide a biologically relevant model. Implicit solvation was applied in the SR model, simulating aqueous conditions around the active site and docked ligand. In the SR model, BIA 8-176 did not interact as strongly in the COMT active site and was not longer the most favorable inhibitor. 6-Hydroxydopamine and 6-carboxydopamine were the most favorable first generation ligands and both had interaction energies comparable to BIA 8-

176. In the second generation ligands, 3-(4,5-dihydroxy-2-nitrophenyl)propanenitrile (4-dp) was the most favorable ligand while 4-(4,5-dihydroxy-2-nitrophenyl)butanenitrile (4-dp) was the least strongly bound ligand. Resveratrol was also a very unfavorable ligand in the SR model.

In the SR model, the first generation ligands retained similar binding affinities after the application of solvation while several of the second generation ligands decreased in binding affinity and, subsequently, favorability. Changes in favorability resulted from changes in the protonation and overall charge of the ligands with the application of solvation.

The SX model allowed for the optimization of the amino acid side chains in aqueous condition, providing the most biologically relevant model. The SX model complexes were optimized from the completed SR model complexes to minimize computational expense. M06L was the only method used due to strong agreement between M06L and MP2 in previous work and in the previous models, further minimizing computational expense. An artifact was identified in the crystal structure where an asparagine residue was resolved in an unfavorable protonation state, so the residue was corrected to its physiologically relevant state through the SX optimization.

In the SX model, BIA 8-176 showed a significant decrease in binding affinity, making it a weaker ligand than dopamine and an unfavorable inhibitor. The most favorable ligands in the first generation were 6-hydroxydopamine and 6-carboxydopamine while 1,2,3,4-tetrahydroisoqinoline-6,7-diol was the least favorable ligand. In the second generation of ligands, 3-(2-2-aminoethyl)-4,5-dihydroxyphenyl)propanenitrile was the most favorable ligand. Overall, the first

generation of ligands remained consistent in their binding affinity trends while the second generation ligands became more favorable overall.

Following the analysis of ligand-active site complexes, all ligands were studied computationally to determine lipophilicity as logP and logD where applicable. The ligands were optimized with both water and octanol applied through the Polarizable Continuum Model. LogP was determined for all ligands while logD was determined for ligands that have substituents that can exist in various protonation states (i.e. carboxyl group or amino group).Overall, the first generation ligands were more hydrophilic than the second generation ligands.

In the synthesis of 3,4-dihydroxybenzonitirle (**2**), 2-(3,4-dihydroxyphenyl)acetonitrile (**4**) and 3-(3,4-dihydroxyphenyl)propanenitrile (**8**), all compounds were synthesized in moderate yields. All products were analyzed with ^{1}H NMR and HRMS while purity was confirmed with HPLC. For all three ligands, the final deprotection via boron tribromide required an aqueous workup rather than a precipitation to produce the final product. Intermediates in the synthesis of 3-(3,4-dihydroxyphenyl)propanenitrile required purification via flash chromatography to remove unreacted starting material or byproducts. Overall, the synthesis of the three nitrile ligands provided sufficient product to allow for further studies of stability, lipophilicity or biological activity.

6.   References:

1.   Bonifacio, M. J.; Palma, P. N.; Almeida, L.; Soares-da-Silva, P., Catechol-O-methyltransferase and its inhibitors in Parkinson's disease. *CNS Drug Reviews* **2007,** *13* (3), 352-379.

2.   Palma, P. N.; Rodrigues, M. L.; Archer, M.; Bonifacio, M. J.; Loureiro, A. I.; Learmonth, D. A.; Carrondo, M. A.; Soares-da-Silva, P., Comparative study of ortho- and meta-nitrated inhibitors of catechol-O-methyltransferase: interactions with the active site and regioselectivity of O-methylation. *Mol.Pharm.***2006,** *70* (1), 143-153.

3.   Axelrod, J.; Tomchick, R., Enzymatic O-methylation of epinephrine and other catechols. *J. Biol. Chem.* **1958,** *233* (3), 702-5.

4.   Rodrigues, M. L.; Bonifacio, M. J.; Soares-da-Silva, P.; Carrondo, M. A.; Archer, M., Crystallization and preliminary x-ray diffraction studies of a catechol-O-methyltransferase/inhibitor complex. *Acta Crystallographica, Section F: Structural Biology and Crystallization Communications* **2005,** *61* (1), 118-120.

5.   Baas, H.; Beiske, A. G.; Ghika, J.; Jackson, M.; Oertel, W. H.; Poewe, W.; Ransmayr, G., Catechol-O-methyltransferase inhibition with tolcapone reduces the "wearing off" phenomenon and levodopa requirements in fluctuating parkinsonian patients. *Neurology* **1998,** *50* (5, Suppl. 5), S46-S53.

6.   Ohtsuki, S.; Terasaki, T., Contribution of Carrier-Mediated Transport Systems to the Blood-Brain Barrier as a Supporting and Protecting Interface for the Brain; Importance for CNS Drug Discovery and Development. *Pharm. Research* **2007,** *24* (9), 1745-1758.

7.   Cedarbaum, J. M., Clinical pharmacokinetics of anti-parkinsonian drugs. *Clin. Pharmacokinet.* **1987,** *13* (3), 141-78.

8.   Iwaki, H.; Nishikawa, N.; Nagai, M.; Tsujii, T.; Yabe, H.; Kubo, M.; Ieiri, I.; Nomoto, M., Pharmacokinetics of levodopa/benserazide versus levodopa/carbidopa in healthy subjects and patients with Parkinson's disease. *Neurology and Clinical Neuroscience* **2015,** *3* (2), 68-73.

9.   Mamisto, P. T.; Kaakkola, S., Rationale for selective COMT inhibitors as adjuncts in the drug treatment of Parkinson's disease. *Pharmacology & Toxicology (Oxford, United Kingdom)* **1990,** *66* (5), 317-23.

10.   Ross, S.B.; Haljasamaa, O. Catechol-O-methyltransferase inhibitors. In vivo inhibition in mice. *Acta. Pharmacol. Toxicol.* **1964,** *21*, 215-225.

11.   Giles, R.E.; Miller, J.W.; The caetchol-O-methyltransferase activity and endogenous catecholamine content of carious tiddues in the rat and the effect of administration of U-0521. *J. Pharmacol. Exp. Ther.* **1967,** *158,* 189-194.

12.   Reches, A.; Fahn, S.; Catechol-O-methyltransferse and Parkinson's disease, *Adv. Neurol.* **1984,** *40,* 171.

13.   Archer, S.; Arnold, A.; Kullnig, R.L.; Wylie, D. The enzymatic methylation of pyrogallol. *Arch. Biochem. Biophys.* **1960,** *87,* 53-154.

14.   Booth, A.N.; Masri, M.; Robbins, D.J.; Emerson, O.H.; Jones. F.T.; Deeds, F. The metabolic fate of gallic acid and related compunds. *J. Biol. Chem.* **1959,** *234,* 3014-3016.

15.   Kiss, L.F. and Soares-da-Silva, P. Medicinial chemistry of catechol-O-methyltransferase inhibitors and their therapeutic utility. *J. Med. Chem.* **2014**, *57,* 8692-8717.

16.   Borgulya, J.; Bruderer, H.; Bernauer, K.; Zurcher,G.; Da Prada, M.; Catechol-O-methyltransferase-inhibiting pyrocatechol derivatives: Synthesis and structure-activity studies. *Helv. Chim. Acta* **1989** 72, 952-968.

17.   Nissinen, E.; Linden, L.B.; Schultz, E.; Kaakkola, S.; Mannisto, P. Inhibition of catechol-o-mthyltransferase activity by two novel disubstituted catechols in the rat. *Eur. J. Pharmacol.* **1988,** *153,* 263-269.

18.   Schultz, E.; Nissinen. E.; Inhibition of rat liver and duodenum soluble catechol-O-methyltransferase by a tight binding inhibitor OR-462. *Biochem. Pharmacol.* **1989,** *38,* 3953-3956.

19.   Mannisto, P.; Toumainen, T.; Toumainen, R.L. Different in vivo properties of three new inhibitors of catechol-O-methyltransferase in the rat. *Br. J. Pharmacol.* **1992,** *105,* 569-574.

20.   Keranen, T.; Gordn, A.; Karlsson, M.; Korpela, L.; Pentikainen, P.J.; Rita, H.; Schultz, E.; Seppala, L.; Wikberg, T.; Inhibition of solubel catechol-O-methyltransferase and single dose pharmacokinetics after oral and intravenous administration of entacapone. *Eur. J. Clin. Pharmacol.* **1994,** *46,* 151-157.

21.   Zurcher, G.; Dingemanse, J.; Da Prada, M. Potenti CoMT ihibition by Ro40-7592 in the periphery and in the brain: preclinical and clinical findings. *Adv Neurol.* **1993,** *60,* 641-647.

22.   Zurcher, G.; Keller, H.H.; Kettler, R.; Borgulya, J.; Bonetti, E.P.; Eigenmann, R.; Da Prada, M. R40-7592, a novel, very potentin and orally active inhibiros of catechol-O-methyltransferase: a pharacological study in rats. *Adv. Neruol.* **1990,** *53*, 497-503.

23.   Learmonth, D.A.; Viera,-Coelho, M.A.; Benes, J.; Alves, P.C.; Borges, N.; Freitas, A.P.; Soares-da-silva, P. Synthesis of 1-(3,4-dihydroxy-5-nitrophenyl)-2-phenyl-ethanone and derivatives as potent and long-acting peripheral inhibitors of catechol-O-methyltransferase. *J. Med. Chem.* **2002,** *45,* 685-695.

24.   Bonifacio, M.J.; Archer, M.; Rodrigues, M.L.; Matias, P.M.; Leramont, D.A.; Carrondo, M.A.; Soares-da-Silva, P. Kinetics and crystal structure of catechol-O-methyltransferase complex with co-substrate and a novel inhibitor with potential therapeutic application. *Mol. Pharmacol.* **2002,** *62,* 795-805.

25.   Tomasi, J.; Mennucci, B.; Cammi, R., Quantum Mechanical Continuum Solvation Models. *Chemical Reviews (Washington, DC, United States)* **2005,** *105* (8), 2999-3093.

26.   Zhao, Y.; Truhlar, D. G., Density Functionals for Noncovalent Interaction Energies of Biological Importance. *J. Chem. Theor. Comp.* **2007,** *3* (1), 289-300.

27.   Zhao, Y.; Truhlar, D. G., Design of Density Functionals That Are Broadly Accurate for Thermochemistry, Thermochemical Kinetics, and Nonbonded Interactions. *J. Phys. Chem.* **2005,** *109* (25), 5656-5667.

28.   Bigler, D. J.; Peterson, L. W.; Cafiero, M., Effects of implicit solvent and relaxed amino acid side chains on the MP2 and DFT calculations of ligand-protein structure and electronic interaction energies of dopaminergic ligands in the SULT1A3 enzyme active site. *Comp. Theor. Chem.* **2015,** *1051*, 79-92.

29.   Zhao, Y.; Truhlar, D. G., A new local density functional for main-group thermochemistry, transition metal bonding, thermochemical kinetics, and noncovalent interactions. *J. Chem. Phys.* **2006,** *125* (19), 194101/1-194101/18.

30.   Moller, C.; Plesset, M. S., Note on the approximation treatment for many-electron systems. *Physical Review* **1934,** *46*, 618-22.

31.   Sinnokrot, M. O.; Sherrill, C. D., High-Accuracy Quantum Mechanical Studies of π-π Interactions in Benzene Dimers. *J. Chem. Phys. A* **2006,** *110* (37), 10656-10668.

32.   Rote, J.C.; Bailey, G.E.; Cochrane, C.S.; Brown, N.S.; Cafiero, N.; Peterson, L.W. Synthesis of a series of dopamine derivatives, *in preparation.*

33.   Kurkela, M.; Siiskonen, A.; Finel, M.; Tammela, P.; Taskinen, J.; Vuorela, P. Microplate screening assay to identify inhibitors of human catechol-O-methyltransferase. *Anal. Biochem.* **2004,** *331,* 198-200.

34.   Andres, A.; Roses, M.l Fafols, C.; Bosch, E.; Espinosa, S.; Segarra, V.; Huerta, J.M. Setup and validation of shake-flask prodcedures for the determination of partition coefficients (logD) from low drug amounts. *Eur. J. Pharm. Sci.* **2015**, *76,* 181-191.

7.   Appendix

Appendix A: Figures of all optimized ligand-active site complexes in both the 3- and 4- deprotonation position in the VR (vacuum, rigid) model.
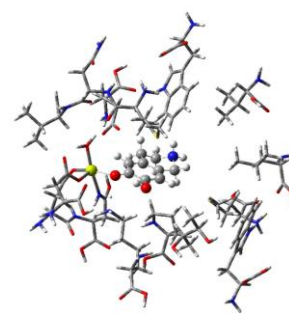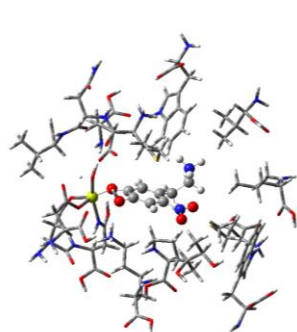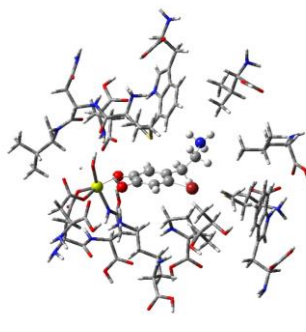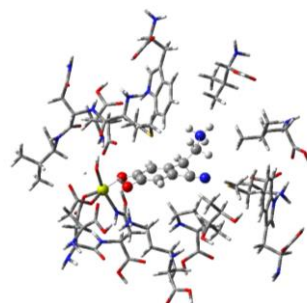

Dopamine (3-dp)

6-Hydroxydopamine (3-dp)

1,2,3,4-Tetrahydroisoquinoline -6,7-diol (3-dp)

6-Nitrodopamine (3-dp)

6-Bromodopamine (3-dp)

6-Cyanodopamine (3-dp)

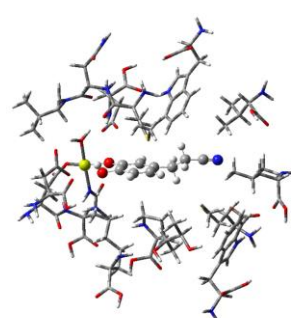6-Ethenyldopamine (3-dp)

6-Carboxydopamine (3-dp)
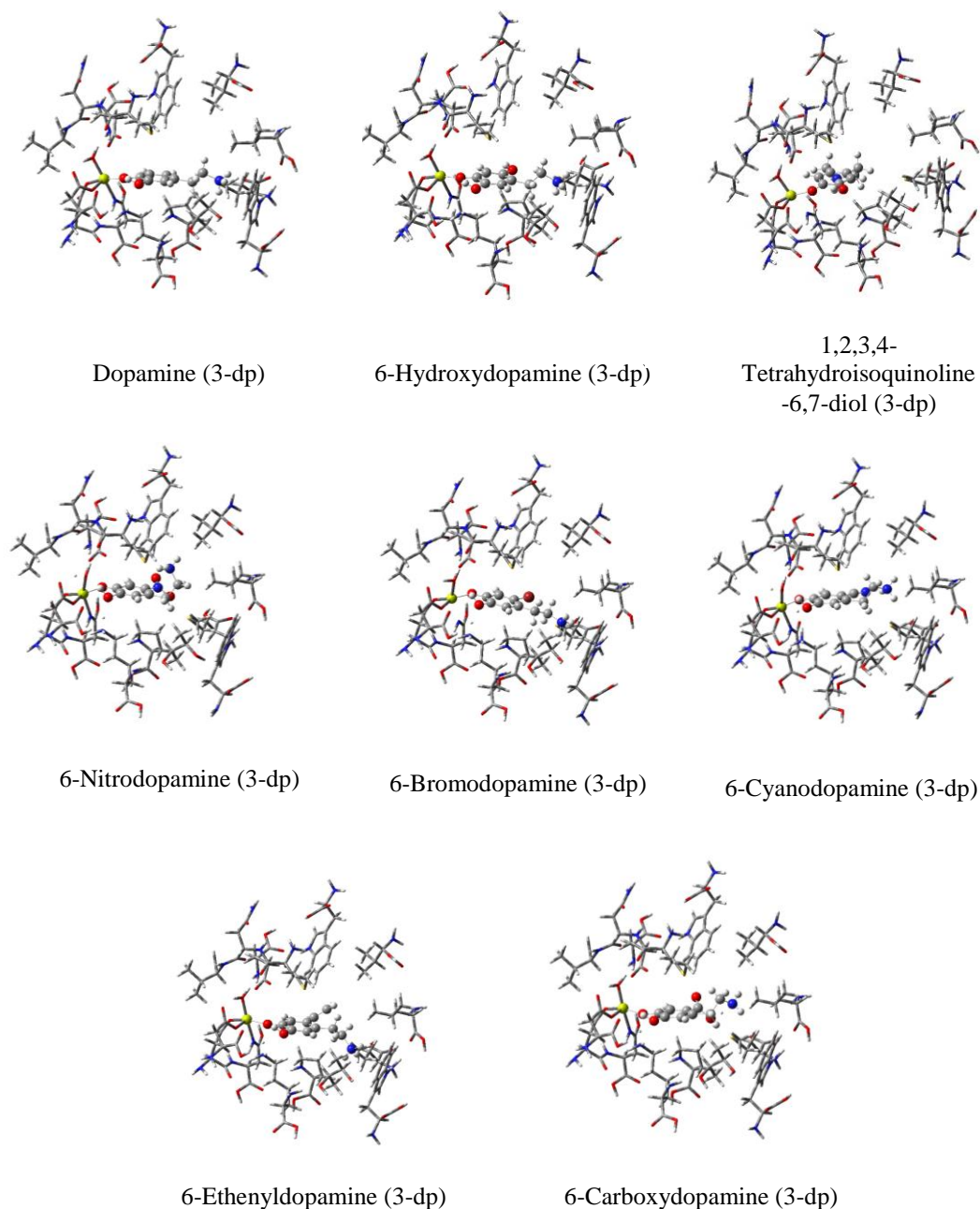
Appendix A-1: Optimized models of the first generation ligands, with dopamine, in the vacuum rigid active site model. Ligands are positioned with the 3-position hydroxyl group nearer to Lys144 and represent metabolism via deprotonation in the 3-position.
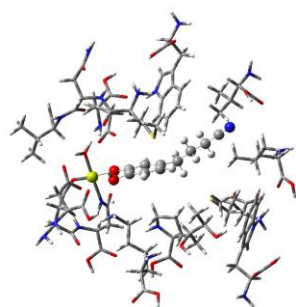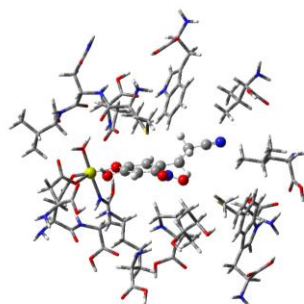
3,4-Dihydroxybenzonitrile
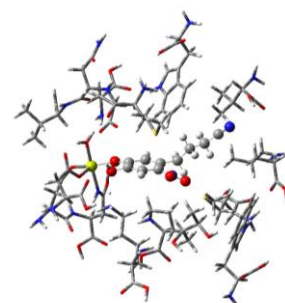(3-dp)
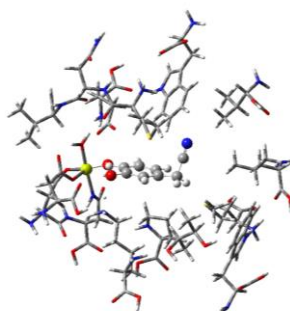
2-(3,4-Dihydroxyphenyl)
acetonitrile (3-dp)
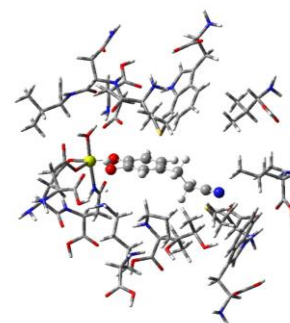
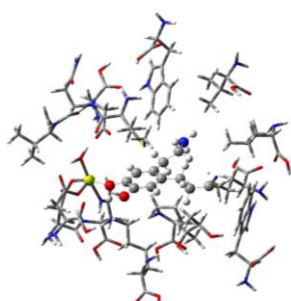3-(3,4-Dihydroxyphenyl)
propanenitrile (3-dp)
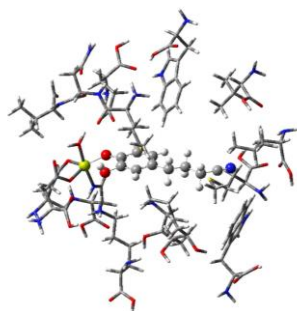
4-(3,4-Dihydroxyphenyl)
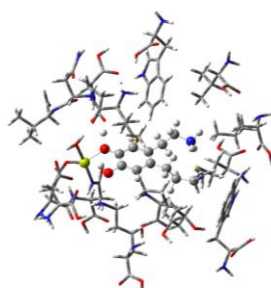butanenitrile (3-dp)
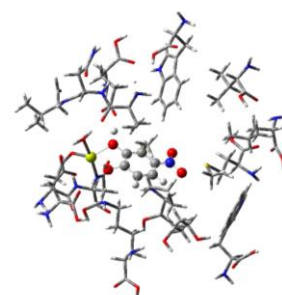
3-(4,5-Dihydroxy-2-nitrophenyl)
propanenitrile
(3-dp)

4-(4,5-Dihydroxy-2-nitrophenyl)
butanenitrile
(3-dp)

3-(2-(2-Aminoethyl)-4,5-
dihydroxyphenyl)
propanenitrile (3-dp)

4-(2-(2-Aminoethyl)-4,5-
dihydroxyphenyl)
butanenitrile (3-dp)

4-Nitrobenzene-1,2-diol
(3-dp)

Appendix A-2: Optimized models of the second generation ligands in the vacuum rigid active site model. Ligands are positioned with the 3-position hydroxyl group nearer to Lys144 and represent metabolism via deprotonation in the 3-position.
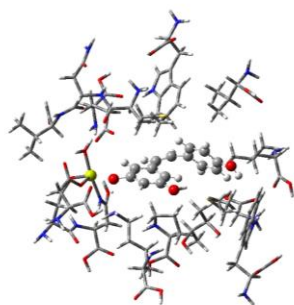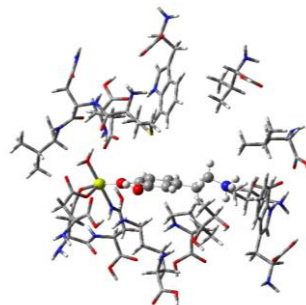
Resveratrol   BIA 8-176

Appendix A-3: Optimized models of resveratrol and BIA 8-176 in the vacuum rigid
active site model.
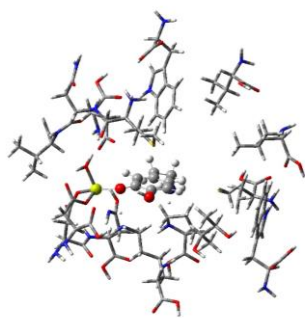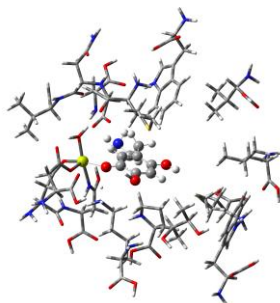
Dopamine (4-dp)

6-Hydroxydopamine (4-dp)

1,2,3,4-Tetrahydroisoquinoline
-6,7-diol (4-dp)

6-Nitrodopamine (4-dp)

6-Bromodopamine (4-dp)

6-Cyanodopamine (4-dp)
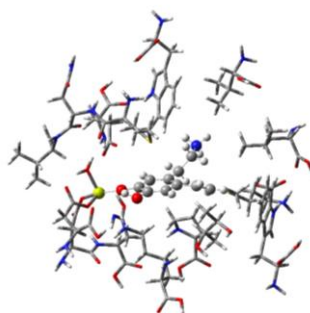
6-Ethenyldopamine (4-dp)
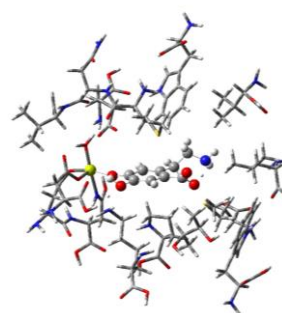
6-Carboxydopamine (4-dp)

Appendix A-4: Optimized models of the first generation ligands, with dopamine, in the vacuum rigid active site model. Ligands are positioned with the 4-position hydroxyl group nearer to Lys144 and represent metabolism via deprotonation in the 4-position.
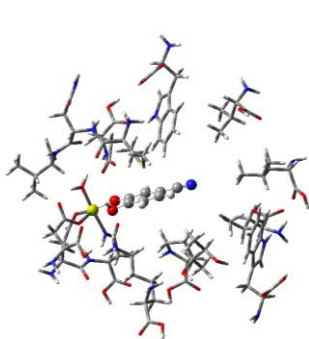
3,4-Dihydroxybenzonitrile
(4-dp)
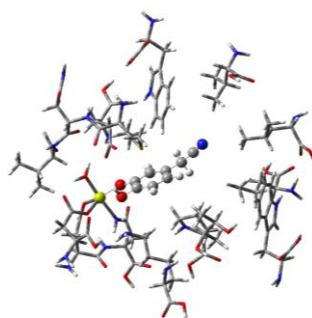
2-(3,4-Dihydroxyphenyl)
acetonitrile (4-dp)

3-(3,4-Dihydroxyphenyl)
propanenitrile (4-dp)

4-(3,4-Dihydroxyphenyl)
butanenitrile (4-dp)

3-(4,5-Dihydroxy-2-nitrophenyl)
propanenitrile
(4-dp)

4-(4,5-Dihydroxy-2-nitrophenyl)
butanenitrile
(4-dp)

3-(2-(2-Aminoethyl)-4,5-
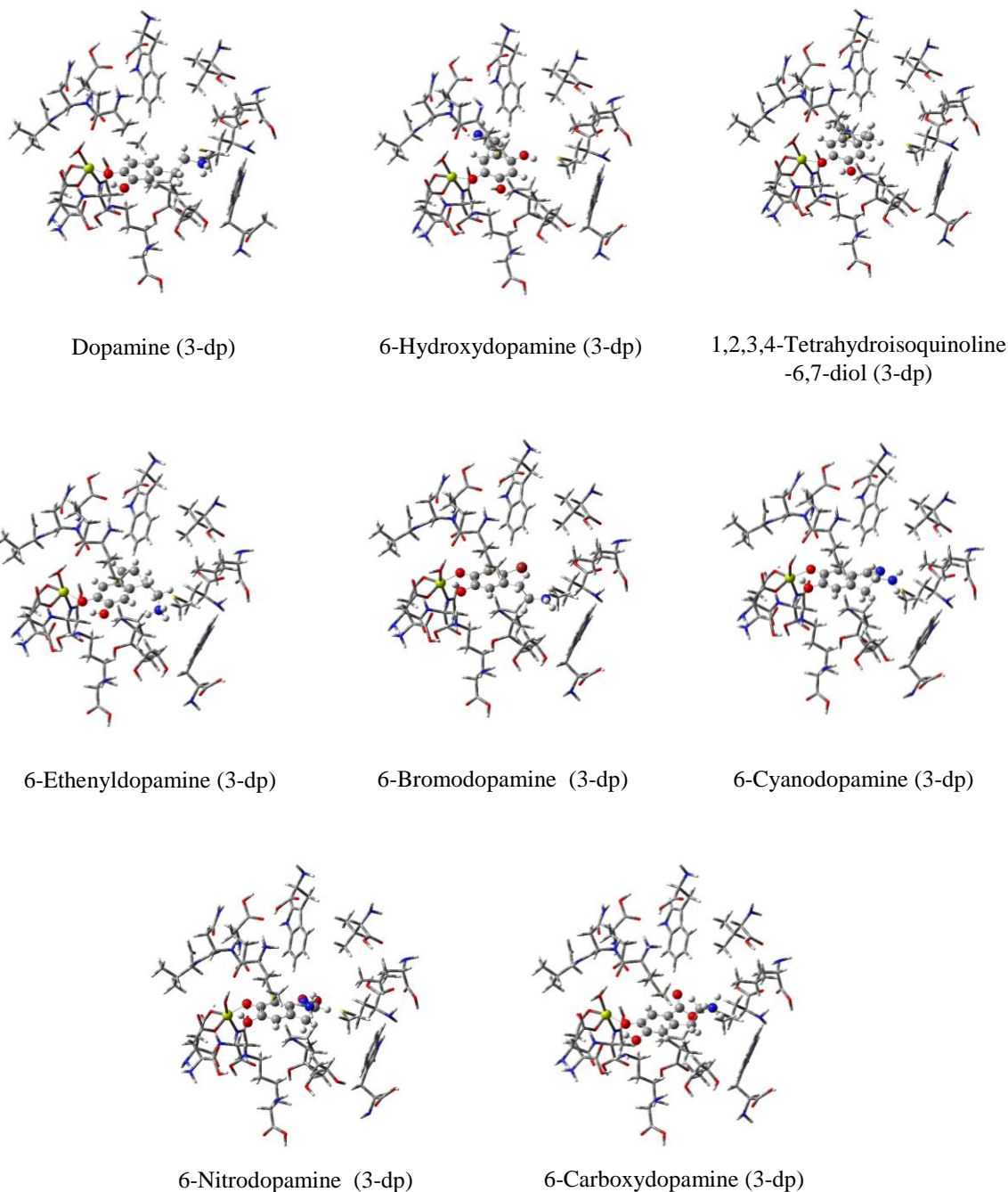dihydroxyphenyl)
propanenitrile (4-dp)

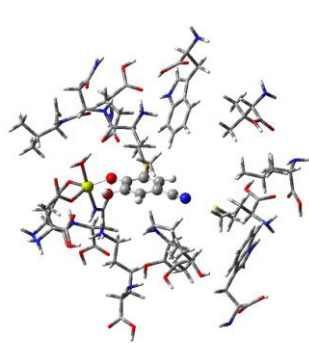4-(2-(2-Aminoethyl)-4,5-
dihydroxyphenyl)
butanenitrile (4-dp)

4-Nitrobenzene-1,2-diol
(4-dp)

Appendix A-5: Optimized models of the second generation ligands in the vacuum rigid active site model. Ligands are positioned with the 4-position hydroxyl group nearer to Lys144 and represent metabolism via deprotonation in the 4-position.
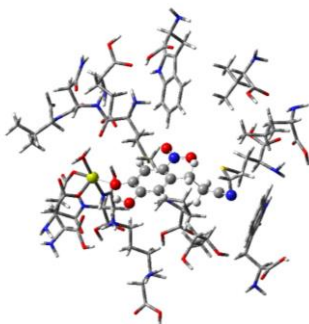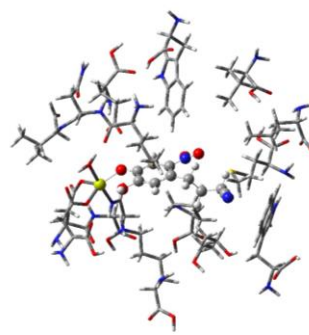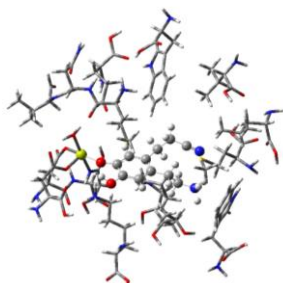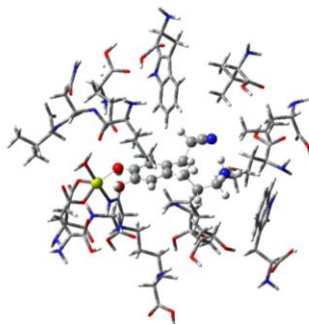
Appendix B: Figures of all optimized ligand-active site complexes in both the 3- and 4- deprotonation position in the SR (solvated, rigid) model.

Dopamine (3-dp)   6-Hydroxydopamine (3-dp)   1,2,3,4-Tetrahydroisoquinoline -6,7-diol (3-dp)

6-Ethenyldopamine (3-dp)   6-Bromodopamine (3-dp)   6-Cyanodopamine (3-dp)

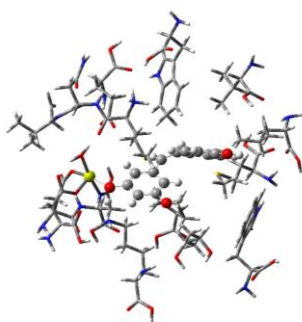6-Nitrodopamine (3-dp)   6-Carboxydopamine (3-dp)

Appendix B-1: Optimized models of the first generation ligands, with dopamine, in the solvated rigid active site model. Ligands are positioned with the 3-position hydroxyl group nearer to Lys144 and represent metabolism via deprotonation in the 3-position.

3,4-Dihydroxybenzonitrile (3-dp)
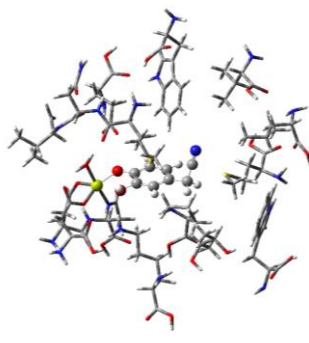
2-(3,4-Dihydroxyphenyl)
acetonitrile (3-dp)
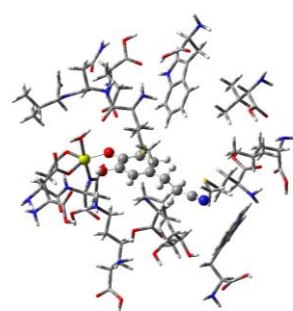
3-(3,4-Dihydroxyphenyl)
propanenitrile (3-dp)
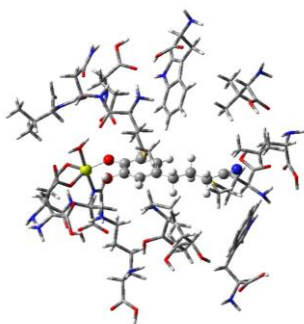
4-(3,4-Dihydroxyphenyl)
butanenitrile (3-dp)

3-(4,5-Dihydroxy-2-nitrophenyl)
propanenitrile
(3-dp)

4-(4,5-Dihydroxy-2-nitrophenyl)
butanenitrile
(3-dp)

3-(2-(2-Aminoethyl)-4,5-
dihydroxyphenyl)
propanenitrile (3-dp)

4-(2-(2-Aminoethyl)-4,5-
dihydroxyphenyl)
butanenitrile (3-dp)
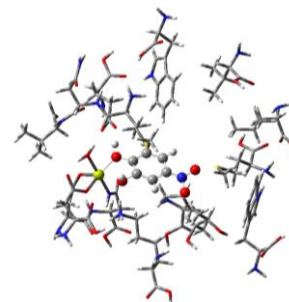
4-Nitrobenzene-1,2-diol
(3-dp)

Appendix B-2: Optimized models of the second generation ligands in the solvated rigid active site model. Ligands are positioned with the 3-position hydroxyl group nearer to Lys144 and represent metabolism via deprotonation in the 3-position.
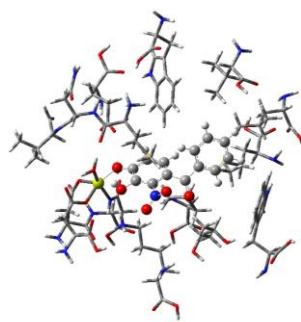
Resveratrol   BIA 8-176

Appendix B-3: Optimized models of resveratrol and BIA 8-176 in the solvated rigid active site model.

Dopamine (4-dp)

6-Hydroxydopamine (4-dp)

1,2,3,4-Tetrahydroisoquinoline-6,7-diol (4-dp)

6-Nitrodopamine (4-dp)

6-Bromodopamine (4-dp)

6-Cyanodopamine (4-dp)

6-Ethenyldopamine (4-dp)

6-Carboxydopamine (4-dp)

Appendix B-4: Optimized models of the first generation ligands, with dopamine, in the solvated rigid active site model. Ligands are positioned with the 4-position hydroxyl group nearer to Lys144 and represent metabolism via deprotonation in the 4-position.
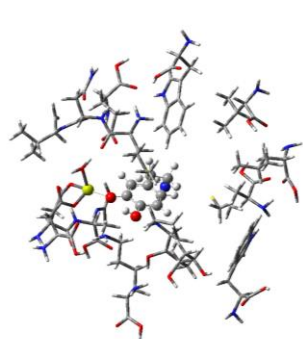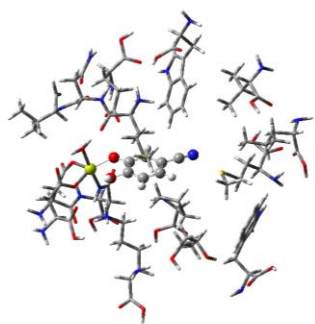
3,4-Dihydroxybenzonitrile
(4-dp)
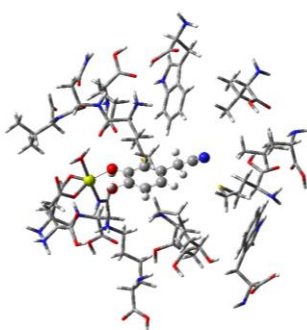
2-(3,4-Dihydroxyphenyl)
acetonitrile (4-dp)

3-(3,4-Dihydroxyphenyl)
propanenitrile (4-dp)

4-(3,4-Dihydroxyphenyl)
butanenitrile (4-dp)

3-(4,5-Dihydroxy-2-nitrophenyl)
propanenitrile (4-dp)

4-(4,5-Dihydroxy-2-nitrophenyl)
butanenitrile (4-dp)

4-(2-(2-Aminoethyl)-4,5-
dihydroxyphenyl)
butanenitrile (4-dp)
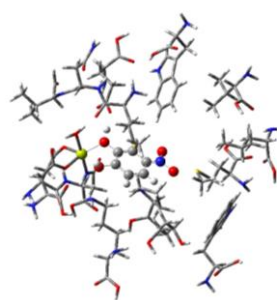
4-Nitrobenzene-1,2-diol
(4-dp)

Appendix B-5: Optimized models of the second generation ligands in the solvated rigid active site model. Ligands are positioned with the 4-position hydroxyl group nearer to Lys144 and represent metabolism via deprotonation in the 4-position.
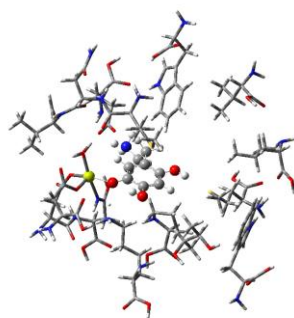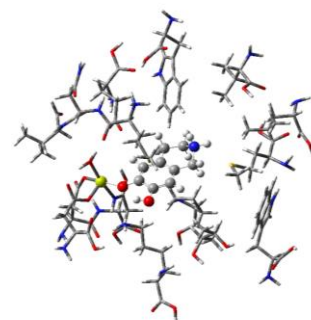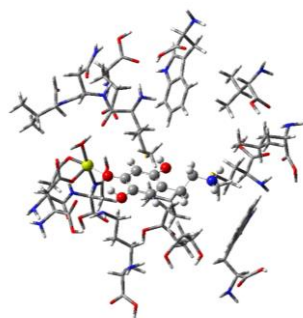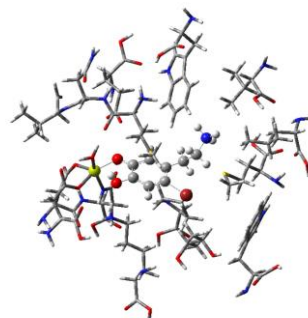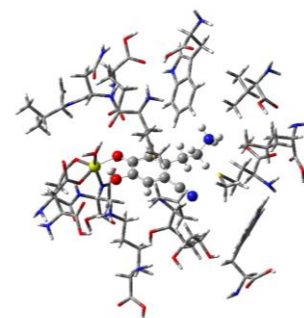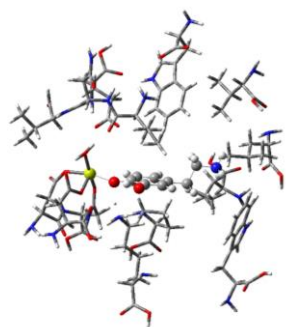
Dopamine (3-dp)
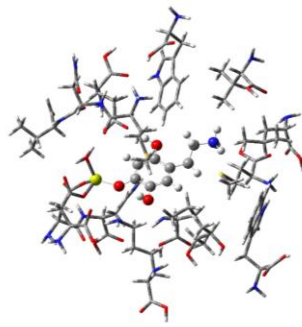
6-Hydroxydopamine (3-dp)
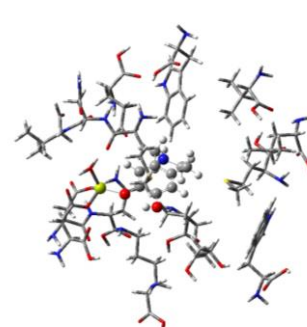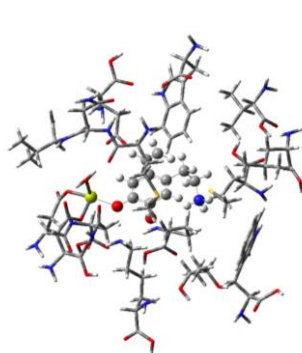
1,2,3,4-
Tetrahydroisoquinoline-
6,7-diol (3-dp)

6-Ethenyldopamine (3-dp)
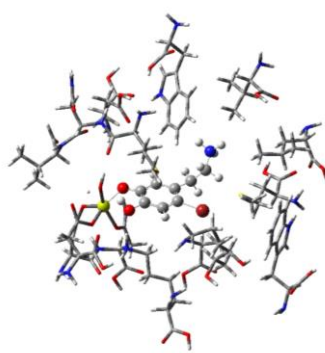
6-Bromodopamine (3-dp)
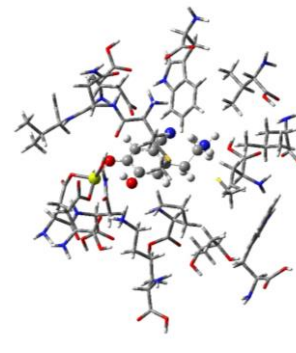
6-Cyanodopamine (3-dp)
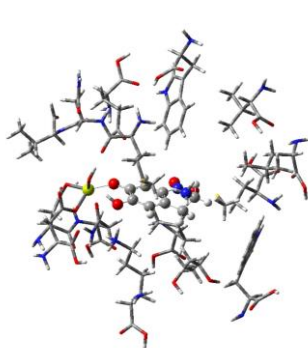
6-Nitrodopamine (3-dp)
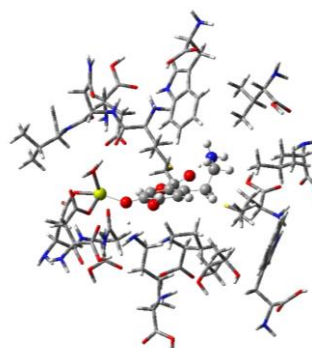
6-Carboxydopamine (3-dp)

Appendix C-1: Optimized models of the first generation ligands, with dopamine, in the solvated, non-rigid active site model. Ligands are positioned with the 3-position hydroxyl group nearer to Lys144 and represent metabolism via deprotonation in the 3-position.

3,4-Dihydroxybenzonitrile
(3-dp)
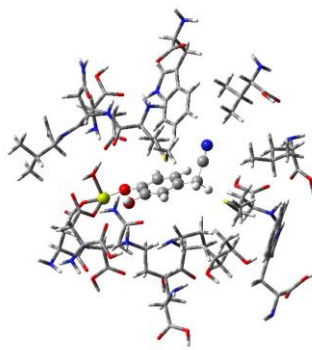
2-(3,4-Dihydroxyphenyl)
acetonitrile (3-dp)
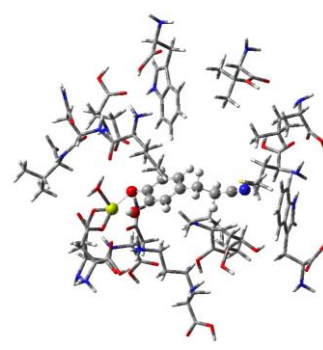
3-(3,4-Dihydroxyphenyl)
propanenitrile (3-dp)
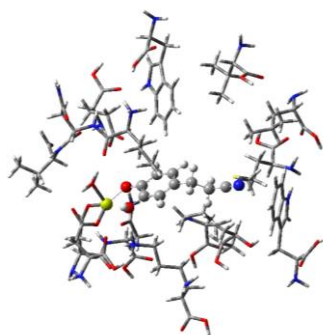
4-(3,4-Dihydroxyphenyl)
butanenitrile (3-dp)

3-(4,5-Dihydroxy-2-nitrophenyl)
propanenitrile (3-dp)

4-(4,5-Dihydroxy-2-nitrophenyl)
butanenitrile (3-dp)

3-(2-(2-Aminoethyl)-4,5-
dihydroxyphenyl)
propanenitrile (3-dp)
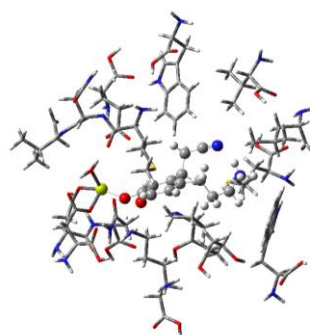
4-(2-(2-Aminoethyl)-4,5-
dihydroxyphenyl)
butanenitrile (3-dp)

Appendix C-2: Optimized models of the second generation ligands in the solvated, non-rigid active site model. Ligands are positioned with the 3-position hydroxyl group nearer to Lys144 and represent metabolism via deprotonation in the 3-position
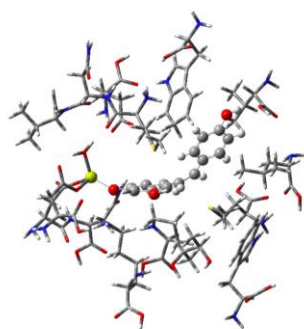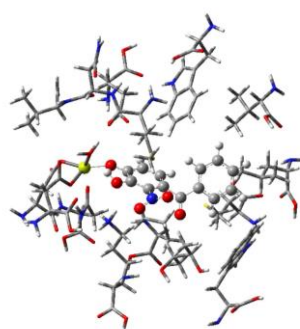
Resveratrol   BIA 8-176

Appendix C-3: Optimized models of resveratrol and BIA 8-176 in the solvated, rigid active site model.

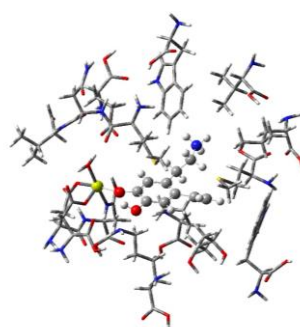Dopamine (4-dp)　　6-Hydroxydopamine (4-dp)　　1,2,3,4-Tetrahydroisoquinoline-6,7-diol (4-dp)
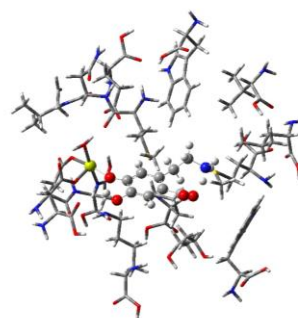
6-Nitrodopamine (4-dp)　　6-Bromodopamine (4-dp)　　6-Cyanodopamine (4-dp)

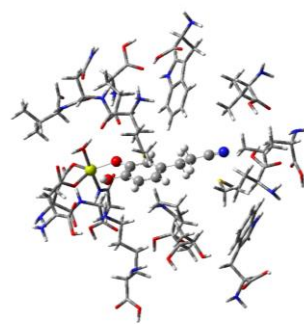6-Ethenyldopamine (4-dp)　　6-Carboxydopamine (4-dp)

Appendix C-4: Optimized models of the first generation ligands, with dopamine, in the solvated, non-rigid active site model. Ligands are positioned with the 4-position hydroxyl group nearer to Lys144 and represent metabolism via deprotonation in the 4-position.
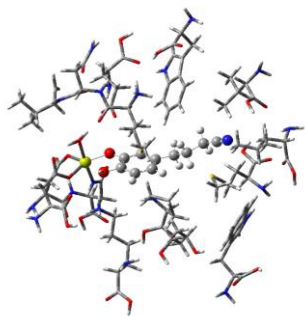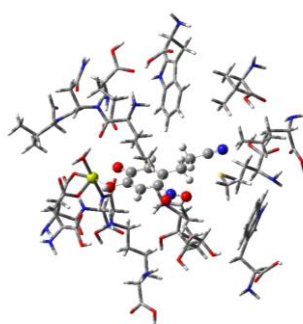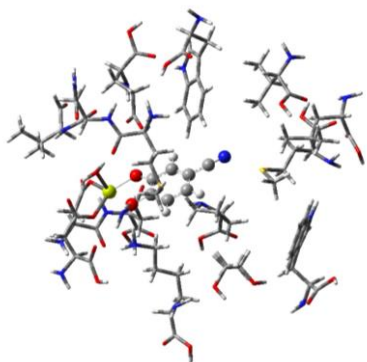
3,4-Dihydroxybenzonitrile
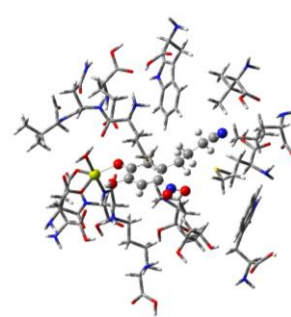(4-dp)
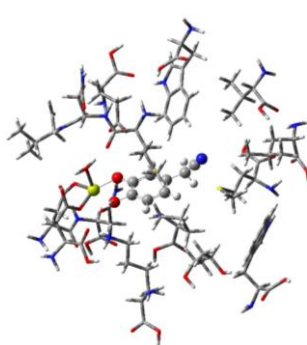
2-(3,4-Dihydroxyphenyl)
acetonitrile (4-dp)
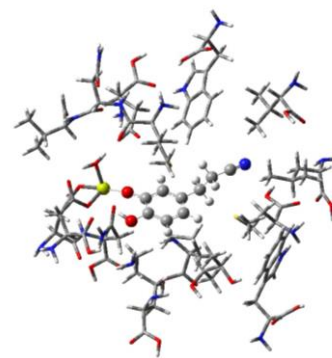
3-(3,4-Dihydroxyphenyl)
propanenitrile (4-dp)
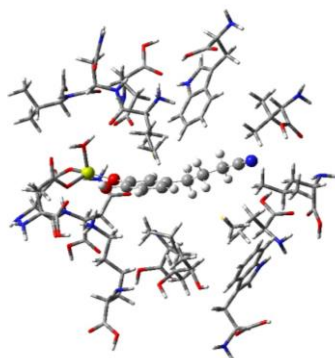
4-(3,4-Dihydroxyphenyl)
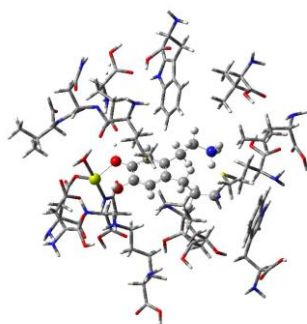butanenitrile (4-dp)
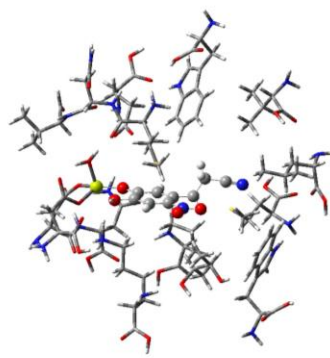
3-(4,5-Dihydroxy-2-nitropheny
propanenitrile (4-dp)

3-(2-(2-Aminoethyl)-4,5-
dihydroxyphenyl)
propanenitrile (4-dp)
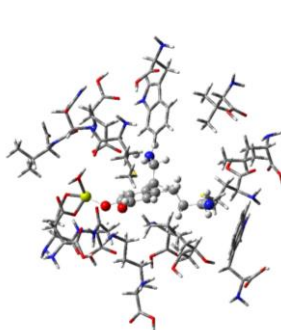
4-(2-(2-Aminoethyl)-4,5-
dihydroxyphenyl)
butanenitrile (4-dp)
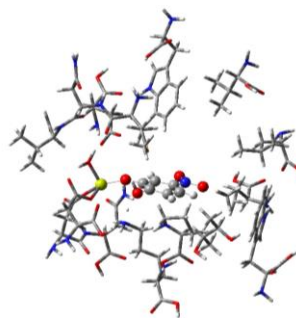
4-Nitrobenzene-1,2-diol (4-dp)

Appendix C-5: Optimized models of the second generation ligands, with dopamine, in the solvated, non-rigid active site model. Ligands are positioned with the 4-position hydroxyl group nearer to Lys144 and represent metabolism via deprotonation in the 4-position.

**Appendix D.** Supplementary interaction energy data from computational study of ligand binding in the COMT active site.

Table D-1. Supplementary data for first generation ligands in the VR model

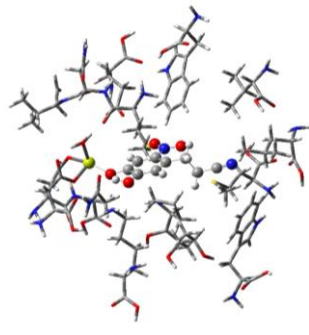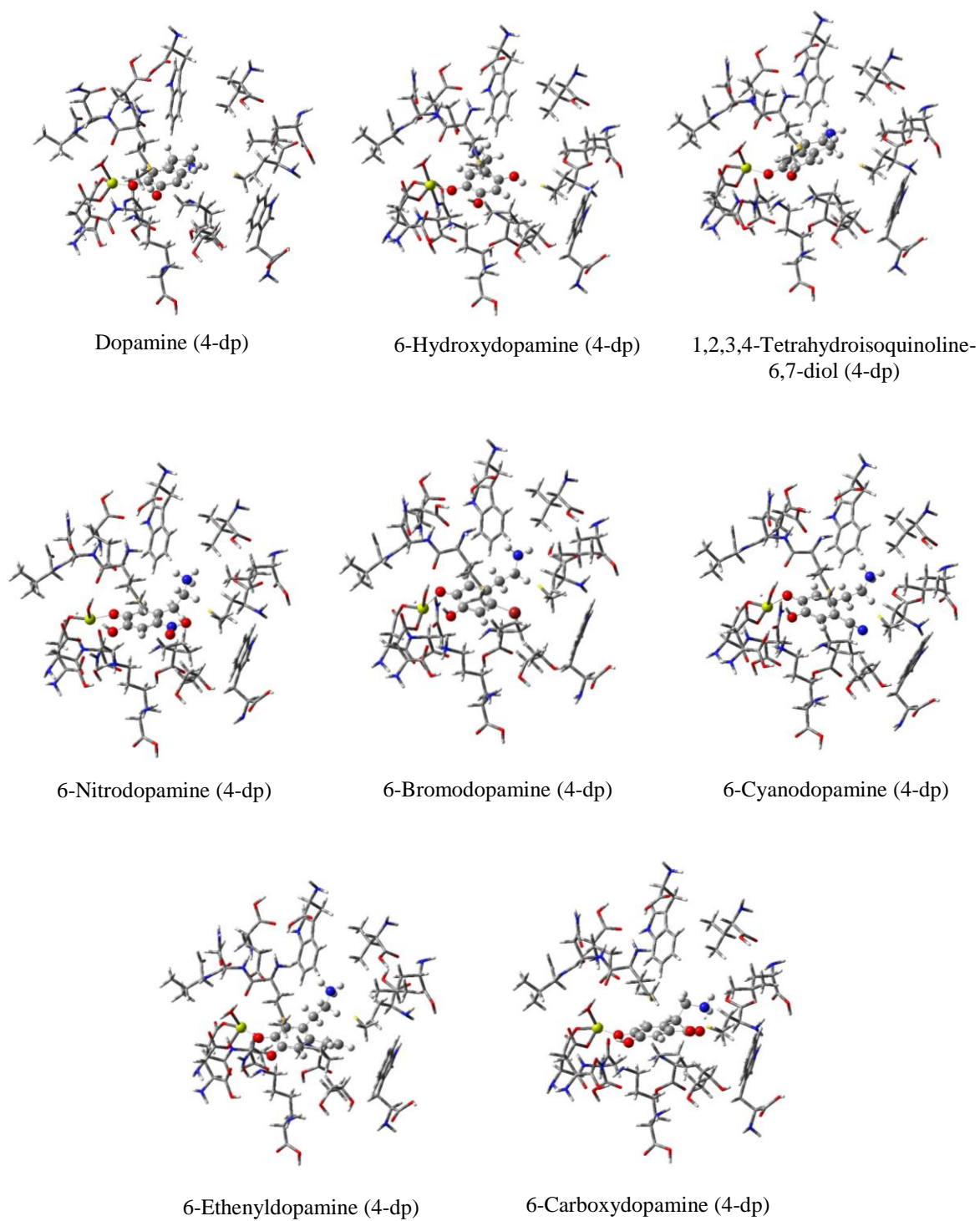| Molecule			Trp253	Leu413	Mg²⁺	Asp169/ Asn170	Pro174	Met416	Val388	Lys144	Trp38	Met40	Val42	Asn41	Glu199	Asp141	Total
Dopamine	3-dp	M06L	-12.0	0.1	-217.1	12.6	-4.1	0.4	-0.4	-59.0	-1.2	0.8	-1.5	-0.1	14.8	31.4	-235.2
		MP2	-13.2	-0.3	-220.7	14.2	-2.6	1.3	-0.5	-57.4	-1.7	0.3	-1.9	-0.2	15.5	32.7	-234.6
	4-dp	M06L	0.5	-0.4	-208.0	22.0	-20.5	-7.3	0.0	-55.9	-0.7	1.5	-1.6	-1.9	-0.3	23.0	-249.6
		MP2	0.3	-0.5	-211.7	24.8	-18.2	-8.3	-0.1	-55.5	-1.5	1.2	-1.9	-2.2	0.5	32.0	-241.1
BIA 8-176	--	M06L	-0.2	-1.2	-310.9	-36.9	-4.8	-0.8	-1.0	-93.4	-2.7	-2.5	-2.1	1.2	57.5	52.3	-345.6
		MP2	-0.9	-1.2	-314.4	-37.5	-5.4	-1.0	-1.2	-91.5	-3.2	-3.3	-2.6	1.1	61.1	53.7	-346.4
Resveratrol	--	M06L	-3.0	0.0	-94.9	2.8	-2.2	0.4	-0.6	-13.9	8.2	-1.7	-0.3	-0.4	-3.8	0.4	-109.6
		MP2	-3.7	-0.1	-123.3	3.5	-2.5	0.7	-0.9	-12.2	1.0	-2.7	-0.5	-0.6	-4.9	1.6	-146.1
6-Hydroxy dopamine	3-dp	M06L	-11.3	-0.1	-216.5	25.7	-2.0	0.3	-0.4	-57.5	-0.9	0.9	-1.3	-1.6	11.0	23.3	-230.3
		MP2	-12.5	-0.3	-216.7	26.0	0.0	1.0	-0.4	-55.9	-1.4	0.3	-1.5	-1.9	12.4	31.4	-219.6
	4-dp	M06L	0.3	-0.1	-193.9	13.0	-4.3	-0.6	0.0	-61.7	2.0	1.8	-2.1	-1.5	-47.7	27.1	-267.8
		MP2	0.2	-0.2	-198.4	14.5	-4.3	-1.0	-0.1	-60.1	2.5	1.7	-2.3	-1.8	-44.9	29.7	-264.5
1,2,3,4-Tetrahydro isoquinoline-6,7-diol	3-dp	M06L	0.4	-0.2	-183.1	9.9	-5.8	-2.0	0.0	-53.2	-0.5	0.8	-1.4	-1.7	-17.4	25.8	-228.3
		MP2	0.2	-0.3	-186.6	11.3	-4.5	-2.5	-0.1	-51.6	-1.0	0.2	-1.6	-1.9	-15.9	26.3	-227.9
	4-dp	M06L	0.4	-0.3	-196.8	19.0	-3.7	-2.4	-0.2	-54.4	-5.0	1.5	-1.4	-0.7	-10.0	27.5	-226.5
		MP2	0.2	-0.6	-195.4	20.3	-3.4	-2.8	-0.3	-53.1	-4.8	1.3	-1.6	-0.9	-8.5	28.4	-221.4
6-Nitro dopamine	3-dp	M06L	-0.6	0.1	-190.3	15.1	-1.7	0.0	-0.5	-30.5	-4.5	-13.4	-0.6	0.7	15.1	8.5	-202.9
		MP2	-1.0	-0.2	-193.9	19.0	-2.1	-0.5	-0.8	-31.4	-3.8	-11.9	-1.0	0.4	18.8	10.6	-197.9
	4-dp	M06L	-11.1	-1.9	-198.9	16.3	-3.7	-4.6	-1.2	-37.3	1.7	-1.6	-0.9	0.8	6.1	18.4	-217.9
		MP2	-10.7	-1.9	-204.5	14.4	-3.5	-4.7	-0.5	-37.5	1.1	-0.9	-1.2	0.7	7.5	18.3	-223.5
6-Bromo dopamine	3-dp	M06L	-12.0	-0.1	-214.4	18.7	-3.5	-0.3	-0.4	-39.5	-2.3	-3.3	-1.3	-1.3	22.6	18.2	-218.8
		MP2	-13.0	-0.3	-217.2	23.7	-2.0	0.7	-0.5	-38.7	-2.9	-3.9	-1.6	-1.8	29.2	20.8	-207.5
	4-dp	M06L	0.2	-1.9	-223.7	14.9	-2.7	-2.2	-1.7	-43.7	-12.3	-3.8	-1.3	-0.9	17.5	23.8	-237.7
		MP2	-0.2	-1.9	-226.3	19.0	-2.3	-2.3	-1.2	-38.7	-2.9	-3.9	-1.6	-1.8	29.2	25.3	-209.6
6-Cyano dopamine	3-dp	M06L	-1.8	-0.4	-205.6	18.3	-2.1	0.2	-1.4	-33.7	-4.3	-2.6	-1.0	-1.3	19.7	14.7	-201.5
		MP2	-2.3	-0.6	-209.4	22.4	-2.5	0.3	-1.6	-34.5	-4.5	-3.1	-1.4	-1.8	22.5	16.3	-200.1
	4-dp	M06L	1.4	-2.1	-209.8	13.6	-3.0	-2.4	-1.7	-40.1	-12.3	-2.6	-0.9	1.0	13.0	20.9	-225.2
		MP2	-12.0	-2.0	-214.1	17.5	-3.1	-2.6	-1.0	-40.1	0.8	-1.9	-1.3	0.9	15.0	21.9	-222.1
6-Ethenyl dopamine	3-dp	M06L	-12.4	-0.1	-206.3	24.4	-3.2	-0.3	-0.4	-58.9	-1.0	0.1	-1.2	0.0	12.4	23.6	-223.5
		MP2	-13.7	-0.3	-212.5	26.7	-2.3	0.4	-0.6	-57.5	-1.6	3.4	-1.4	-0.2	13.7	31.1	-214.8
	4-dp	M06L	0.0	-1.5	-207.2	24.4	-3.0	-2.3	-1.7	-55.1	-9.6	1.8	-1.1	-1.8	-0.3	24.9	-232.5
		MP2	-0.7	-1.7	-209.2	26.7	-2.5	-2.4	-1.9	-54.8	-9.5	1.3	-1.3	-2.2	0.5	27.3	-230.2
6-Carboxy dopamine	3-dp	M06L	0.6	-0.3	-325.5	68.4	-4.2	-0.7	-0.2	-120.5	-2.6	-0.8	-2.5	-2.3	55.4	69.7	-265.4
		MP2	0.2	-0.5	-324.1	69.5	-4.5	-1.0	-0.4	-118.1	0.0	-0.9	-2.7	-2.7	55.7	70.5	-259.1
	4-dp	M06L	1.2	-0.1	-320.4	64.2	-2.9	-0.1	-0.1	-116.2	-0.7	-1.2	-2.4	-2.3	45.8	75.5	-259.7
		MP2	0.8	-0.3	-319.5	64.8	-3.2	-0.2	-0.3	-114.1	-0.7	1.7	-2.6	-2.6	46.3	67.5	-262.5

Table D-2. Supplementary data for second generation ligands in the VR model

Molecule			Trp253	Leu413	Mg²⁺	Asp169/Asn170	Pro174	Met416	Val388	Lys144	Trp38	Met440	Val42	Asn41	Glu199	Asp141	Total
3,4-Dihydroxy benzonitrile	3-dp	M06L	0.8	-0.4	-327.5	51.4	-3.1	-0.2	-0.3	-83.7	-1.9	-2.8	-2.6	0.9	65.6	56.9	-246.8
		MP2	0.6	-0.4	-331.7	55.2	-3.5	-0.2	-0.4	-82.8	-2.6	-3.0	-3.0	0.6	67.8	58.1	-245.2
	4-dp	M06L	0.4	-0.9	-334.1	56.1	-3.7	-0.8	-0.7	-81.4	-2.0	-5.4	-2.6	-2.5	70.3	57.4	-249.8
		MP2	0.3	-1.0	-337.4	61.3	-3.9	-0.9	-0.9	-81.0	-2.6	-5.5	-3.1	-3.0	72.3	58.6	-246.8
2-(3,4-Dihydroxyphenyl) acetonitrile	3-dp	M06L	0.2	-0.3	-341.2	50.3	-4.2	0.2	-0.4	-85.5	-4.1	-3.9	-2.3	1.0	80.7	61.0	-248.3
		MP2	0.0	-0.4	-344.9	55.1	-4.4	0.2	-0.5	-84.8	-4.6	-3.8	-2.7	0.8	74.5	62.0	-253.5
	4-dp	M06L	0.4	-0.9	-341.0	56.9	-4.1	-0.4	-0.8	-86.7	-3.3	-4.4	-2.6	-2.7	60.8	70.5	-258.4
		MP2	0.2	-1.0	-344.0	62.0	-4.4	-0.5	-0.9	-85.3	-3.4	-4.9	-2.9	-3.2	61.5	72.6	-254.1
3-(3,4-Dihydrozyphenyl) propanenitrile	3-dp	M06L	0.0	-0.3	-342.4	59.4	-3.0	0.1	-0.2	-87.9	-2.3	-5.7	-2.6	-2.8	68.3	59.6	-259.6
		MP2	-0.4	-0.4	-345.1	64.0	-3.4	0.0	-0.3	-86.3	-2.9	-5.6	-2.8	-3.3	70.6	60.9	-255.0
	4-dp	M06L	0.4	-1.4	-342.1	51.3	-3.3	-0.1	-0.5	-87.5	-2.6	-5.1	-2.7	-2.7	69.2	58.8	-268.3
		MP2	0.1	-1.3	-344.8	55.1	-3.6	-0.3	-0.8	-86.0	-2.4	-4.9	-3.1	-3.2	71.0	59.8	-264.2
4-(3,4-Dihydroxyphenyl) butanenitrile	3-dp	M06L	-1.7	-1.0	-125.6	-17.4	-0.9	-0.7	0.1	-16.1	-1.0	-5.4	-0.3	-0.4	-3.6	1.3	-172.7
		MP2	-2.1	-0.9	-126.6	-11.8	-1.3	-0.9	-0.2	-16.6	-1.4	-5.3	-0.6	-0.7	-1.9	2.2	-168.1
	4-dp	M06L	0.5	-0.4	-346.4	50.7	-3.4	0.1	-3.3	-88.2	-4.6	-4.7	-2.8	-2.8	69.8	60.2	-275.3
		MP2	0.3	-0.6	-348.8	54.8	-3.8	-0.1	-2.2	-86.8	-4.0	-4.6	-3.2	-3.3	71.6	61.2	-269.5
3-(4,5-Dihydroxy-2-nitrophenyl) propanenitrile	3-dp	M06L	-0.4	-0.6	-285.3	60.8	-3.0	-0.5	-0.3	-91.9	-1.1	-1.1	-2.1	-1.9	50.3	56.9	-220.3
		MP2	-0.8	-0.7	-284.2	62.0	-3.3	-0.7	-0.5	-91.3	-1.5	-1.5	-2.3	-2.3	50.2	58.3	-218.7
	4-dp	M06L	0.8	-1.4	-304.8	47.7	-2.9	-0.4	-0.6	-78.2	-1.4	-3.6	-2.1	-1.9	56.0	50.4	-242.4
		MP2	0.5	-1.5	-310.4	53.9	-3.4	-0.6	-0.8	-77.6	-1.2	-3.8	-2.4	-2.4	57.0	51.7	-241.0
4-(4,5-Dihydroxy-2-nitrophenyl) butanenitrile	3-dp	M06L	-1.9	-0.5	-324.6	54.3	-3.8	-0.4	-0.4	-77.7	-2.0	-0.4	-2.2	-2.3	65.8	53.5	-242.6
		MP2	-2.3	-0.7	-328.9	60.0	-3.9	-0.3	-0.7	-78.2	-2.9	--	-2.8	-2.8	68.5	55.7	-239.4
	4-dp	M06L	1.0	-0.5	-308.8	48.0	-3.1	-0.3	-3.8	-79.6	-3.5	-1.8	-2.2	-2.0	56.4	51.4	-248.7
		MP2	0.6	-0.8	-314.4	50.7	-3.6	-0.5	-2.9	-78.9	-3.0	-1.7	-2.5	-2.5	57.6	52.6	-249.2
3-(2-(2-Aminoethyl)-4,5-dihydroxyphenyl) propanenitrile	3-dp	M06L	-10.4	-0.1	-207.5	28.7	-0.3	-0.2	-0.6	-55.0	0.8	-1.0	-1.2	-1.6	9.5	27.1	-211.6
		MP2	-11.3	-0.6	-211.6	29.9	0.4	0.1	-0.7	-52.8	1.6	-1.4	-1.4	-1.8	10.1	28.8	-210.7
	4-dp	M06L	0.0	-7.7	27.7	-100.3	-8.2	-9.5	-0.9	-26.9	-18.7	-13.7	1.0	0.5	-95.6	-97.3	-349.5
		MP2	-25.1	-0.9	14.6	-39.3	-0.6	--	-1.0	-119.0	0.8	-6.3	0.7	0.3	-46.2	-66.6	-288.7
4-(2-(2-Aminoethyl)-4,5-dihydroxyphenyl) butanenitrile	3-dp	M06L	-9.4	0.2	-247.7	10.7	-1.2	-0.5	-0.6	-41.6	-2.3	-4.4	-4.4	-1.8	28.3	24.0	-250.8
		MP2	-9.2	0.0	-252.2	--	-1.0	-0.1	-0.8	-41.4	-2.2	-4.9	-4.9	-2.3	31.1	25.4	-262.5
	4-dp	M06L	-3.8	-0.5	-221.6	45.0	-1.3	-0.6	-1.8	-40.8	-4.1	-3.7	-1.6	0.5	-30.2	18.1	-246.4
4-Nitrobenzene-1,2-diol	3-dp	M06L	0.9	-0.2	-81.6	-11.4	-1.3	-1.1	0.1	-16.7	-0.2	-2.0	0.5	-0.2	-50.5	-5.3	-169.0
	4-dp	M06L	0.2	-0.2	-108.4	-5.0	-1.4	-1.4	0.0	-10.6	-0.3	-3.1	0.3	-0.3	-42.0	-9.4	-181.5
		MP2	-0.1	-0.3	-113.4	3.2	-0.6	-1.3	-0.1	-12.5	-0.7	-2.9	0.0	-0.5	-37.6	-2.5	-169.3

Table D-3. Supplementary data for first generation ligands in the SR model

Molecule			Trp253	Leu413	Mg²⁺	Asp169/Asn170	Pro174	Met416	Val388	Lys144	Trp38	Met40	Val42	Asn41	Glu199	Asp141	Total
Dopamine	3-dp	M06L	-10.2	0.1	-216.3	30.6	-3.6	0.4	-0.2	-60.6	-1.6	0.6	-1.2	-1.7	13.8	33.0	-216.9
		MP2	-11.1	-0.1	-221.8	32.2	-2.6	0.6	-0.4	-59.1	-1.9	0.5	-1.6	-2.0	14.3	34.6	-218.4
	4-dp	M06L	0.6	-0.4	-210.0	21.3	-18.8	-7.8	0.0	-53.5	-0.8	1.7	-1.6	-1.8	0.5	22.6	-248.0
		MP2	0.4	-0.5	-213.7	24.2	-16.5	-8.6	-0.1	-53.3	-1.5	1.4	-1.9	-2.2	1.2	31.7	-239.4
BIA 8-176	--	M06L	-0.3	-1.2	-320.5	52.4	-5.0	-0.7	-1.1	-93.4	-2.7	-2.1	-2.2	-2.1	59.2	59.2	-260.6
		MP2	-0.9	-1.2	-324.2	57.8	-5.4	-0.9	-1.3	-91.7	-3.4	-3.0	-2.7	-2.6	63.0	63.0	-253.7
Resveratrol	--	M06L	-0.2	1.0	-96.8	6.4	-2.0	-0.4	-0.8	-15.9	0.2	-2.2	-0.3	-0.4	-1.4	1.2	-111.7
		MP2	-0.8	-0.1	-129.4	7.5	-2.4	-0.8	-14.1	-0.5	-0.5	-2.9	-0.4	-0.6	-2.3	2.3	-145.1
6-Hydroxy dopamine	3-dp	M06L	0.4	-0.1	-201.7	13.6	-4.0	0.4	0.0	-55.9	1.3	1.8	-2.3	-2.8	-44.6	26.9	-267.1
		MP2	0.2	-0.2	-205.4	-4.9	-3.5	0.2	-0.1	-55.5	1.7	1.6	-2.6	-3.1	-42.7	30.0	-284.4
	4-dp	M06L	0.3	-0.1	-200.4	11.3	-4.1	-0.5	0.0	-55.6	1.3	2.2	-2.3	-2.7	-44.7	24.3	-270.9
		MP2	0.2	-0.2	-204.1	13.3	-3.8	-0.9	-0.1	-54.4	1.4	2.1	-2.5	-3.0	-42.2	29.7	-264.5
1,2,3,4-Tetrahydroisoquinoline-6,7-diol	3-dp	M06L	0.4	-0.2	-188.2	11.9	-5.8	-2.1	0.0	-49.8	-0.3	1.8	-1.4	-1.9	-0.3	26.2	-209.9
		MP2	0.2	-0.3	-191.7	13.1	-4.3	-2.6	-0.1	-48.5	-0.8	0.0	0.0	0.0	0.0	0.0	-235.0
	4-dp	M06L	-0.1	-0.5	-197.6	23.8	-3.7	-1.4	-0.5	-52.2	-5.3	1.2	-1.1	-1.8	-2.7	27.9	-214.0
		MP2	-0.4	-0.8	-202.2	25.4	-3.4	-1.5	-0.7	-51.1	-5.1	0.8	-1.3	-2.1	-2.8	28.9	-216.5
6-Nitro dopamine	3-dp	M06L	-1.0	0.0	-214.2	15.9	-2.7	-0.1	-0.1	-31.4	-2.8	-16.1	-0.7	-1.0	20.1	11.8	-237.3
		MP2	-1.4	-0.2	-218.6	22.2	-2.6	-14.8	-0.3	-32.4	-3.3	-14.8	-1.1	-1.5	25.4	14.1	-229.3
	4-dp	M06L	1.2	-1.8	-208.9	18.6	-2.9	-2.3	-1.8	-38.6	-11.7	-0.8	-0.8	-1.3	10.4	20.7	-219.9
		MP2	0.8	-1.8	-214.3	22.7	-3.0	-2.4	-1.2	-38.4	-11.5	-1.4	-1.1	-1.7	11.8	16.2	-225.4
6-Bromo dopamine	3-dp	M06L	-9.8	-0.1	-15.0	-110.5	-0.7	-0.4	-0.5	28.1	-1.6	-6.8	0.7	0.3	-45.3	-39.5	-201.0
		MP2	-10.8	-0.3	-16.2	-103.6	-0.8	-0.5	-0.6	28.1	-1.5	-6.9	0.6	0.1	-44.0	-38.5	-194.9
	4-dp	M06L	0.1	-1.3	-237.6	19.3	-2.9	-1.2	-1.8	-43.3	-11.4	-4.4	-1.2	-0.6	18.7	27.0	-240.5
		MP2	-0.3	-1.6	-240.7	26.2	-2.6	-1.4	-1.6	-42.5	-11.7	-2.1	-1.4	-2.1	22.8	23.4	-235.6
6-Cyano dopamine	3-dp	M06L	-3.2	0.0	-2.5	-118.7	-0.5	-0.1	-0.8	30.2	-3.7	-9.5	0.9	0.4	-50.7	-44.1	-202.4
		MP2	-3.6	-0.2	-4.8	-114.1	-0.9	-0.6	-1.0	29.3	-3.9	-9.3	0.7	0.2	-49.0	-42.3	-199.5
	4-dp	M06L	1.0	-1.3	-221.5	19.5	-2.8	-1.1	-2.0	-40.3	-7.1	-1.8	-0.9	-1.4	15.4	13.0	-231.3
		MP2	0.5	-1.5	-225.8	24.8	-3.2	-1.4	-1.5	-40.0	-12.1	-2.2	-1.3	-1.9	17.9	19.2	-228.5
6-Ethenyl dopamine	3-dp	M06L	-4.6	0.2	-202.5	26.5	-2.4	0.8	-0.3	-53.0	-1.9	-1.7	-1.1	-1.5	5.3	28.1	-208.0
		MP2	-5.4	-0.1	-207.4	28.4	-2.3	0.6	-0.5	-52.0	-1.6	-2.0	-1.4	-1.9	5.8	29.8	-209.9
	4-dp	M06L	0.1	-1.1	-208.1	20.6	-2.8	-1.8	-1.5	-57.7	-7.9	1.9	-1.1	-1.8	-0.4	25.5	-236.1
		MP2	-0.8	-1.3	-211.0	0.0	-2.3	-1.9	-1.7	-57.3	-7.9	1.5	-1.3	-2.1	0.4	28.4	-257.3
6-Carboxy dopamine	3-dp	M06L	0.6	-0.3	-325.5	68.4	-4.2	-0.7	-0.2	-120.6	-2.6	-0.9	-2.5	-2.3	55.4	69.7	-265.7
		MP2	0.2	-0.5	-324.1	69.5	-4.5	-1.0	-0.4	-118.1	-3.2	-1.1	-2.7	-2.7	55.6	70.5	-262.6
	4-dp	M06L	1.2	0.0	-332.4	64.0	-3.7	0.1	-0.3	-113.9	-1.2	1.8	-2.5	-2.5	46.1	68.9	-274.5
		MP2	0.6	-0.2	-325.3	65.0	-3.8	-0.1	-0.4	-112.0	-1.3	1.7	-2.7	-2.9	46.5	69.8	-265.0

Table D-4. Supplementary data for second generation ligands in the SR model

| Molecule			Trp253	Leu413	Mg²⁺	Asp169/ Asn170	Pro174	Met416	Val388	Lys144	Trp38	Met40	Val42	Asn41	Glu199	Asp141	Total
3,4-Dihydroxy benzonitrile	3-dp	M06L	0.4	-0.1	-117.1	-30.9	-0.8	-0.3	0.0	-10.6	-0.2	-4.2	-0.3	-0.3	-5.3	-1.6	-171.3
		MP2	0.1	-0.1	-120.1	-23.5	-1.2	-0.5	0.0	-10.9	-0.9	-4.2	-0.5	-0.6	-3.6	-0.2	-166.2
	4-dp	M06L	-0.1	-0.3	-116.5	-27.5	-1.3	-0.6	-0.1	-9.0	-0.2	-4.6	-0.3	-0.3	-2.8	-2.0	-165.7
		MP2	-0.2	-0.4	-119.6	-21.0	-1.6	-0.9	-0.3	-9.6	-0.8	-4.7	-0.6	-0.6	-1.5	-0.4	-162.2
2-(3,4-Dihydroxyphenyl) acetonitrile	3-dp	M06L	-0.4	0.0	-124.3	-21.5	-1.2	0.0	0.0	-12.6	-1.4	-4.8	-0.5	-0.4	-0.3	2.2	-165.1
		MP2	-0.7	-0.1	-126.8	-15.4	-1.4	-0.2	-0.1	-12.7	-2.0	-4.8	-0.6	-0.7	1.1	3.2	-161.0
	4-dp	M06L	0.0	-0.4	-123.7	-22.6	-1.4	-0.6	-0.2	-14.1	-1.5	-3.4	-0.5	-0.5	-2.8	2.1	-169.5
		MP2	-0.2	-0.6	-126.0	-16.7	-1.7	-0.9	-0.3	-13.7	-1.6	-3.8	-0.7	-0.8	-1.5	3.1	-165.4
3-(3,4-Dihydroxyphenyl) propanenitrile	3-dp	M06L	-0.8	0.0	-128.1	-17.7	-0.7	-0.1	-0.1	-13.0	-0.3	-4.8	-0.4	-0.5	-1.7	0.0	-168.2
		MP2	-1.2	-0.1	-130.2	-12.2	-1.0	-0.3	-0.2	-12.8	-1.0	-4.6	-0.6	-0.8	-0.6	1.5	-164.0
	4-dp	M06L	-0.4	-0.7	-127.1	-18.0	-0.9	-0.3	-0.1	-13.4	-1.4	-4.5	-0.4	-0.5	-1.3	-0.3	-169.2
		MP2	0.0	-0.7	-129.3	-12.4	-1.2	-0.6	-0.4	-13.1	-1.3	-4.5	-0.6	-0.8	-0.2	1.2	-163.9
4-(3,4-Dihydroxyphenyl) butanenitrile	3-dp	M06L	-2.0	-1.0	-132.0	-16.7	-1.0	-0.4	0.1	-13.8	-0.9	-5.3	-0.5	-0.6	-0.2	2.1	-172.2
		MP2	-2.4	-1.2	-133.6	-11.0	-1.3	-0.7	-0.3	-13.9	-1.4	-5.5	-0.7	-0.9	1.2	3.2	-168.4
	4-dp	M06L	-0.3	-0.3	-131.7	-17.2	-0.9	-0.2	-1.9	-14.9	-3.3	-4.3	-0.5	-0.6	-1.4	1.6	-175.8
		MP2	-0.7	-0.3	-133.3	-11.5	-1.3	-0.6	-1.0	-14.6	-2.8	-4.3	-0.7	-0.8	-0.2	2.8	-169.4
3-(4,5-Dihydroxy-2-nitrophenyl) propanenitrile	3-dp	M06L	-0.5	-0.6	-282.6	59.2	-3.0	-0.4	-0.4	-89.7	-1.3	0.0	-2.1	-1.9	50.6	56.8	-215.9
		MP2	-0.9	-0.8	-284.5	60.4	-3.2	-0.5	-0.6	-89.3	-1.8	0.0	-2.3	-2.4	50.4	58.3	-217.0
	4-dp	M06L	0.8	-1.6	-311.3	-141.9	-3.4	-0.6	-0.5	-74.5	-1.1	-2.8	-2.1	-2.1	57.3	50.6	-433.2
		MP2	0.4	-1.5	-317.7	-190.9	-3.8	-0.8	-0.9	-74.4	-1.3	-3.2	-2.5	-2.5	58.5	52.0	-488.8
4-(4,5-Dihydroxy-2-nitrophenyl) butanenitrile	3-dp	M06L	-3.1	-0.1	-113.5	-35.4	-1.4	-0.3	-0.2	-6.1	-0.6	-5.1	-0.3	-0.2	-5.9	-4.0	-176.1
		MP2	-3.6	-0.3	-116.5	-28.4	-1.4	-0.4	-0.4	-7.4	-1.4	-5.3	-0.5	-0.6	-4.0	-2.0	-172.2
	4-dp	M06L	1.1	0.0	-313.5	49.6	-3.6	0.0	0.8	-72.6	-3.5	-2.5	-1.8	274.6	57.8	51.9	38.4
		MP2	0.6	-0.8	-314.4	53.8	-4.0	-0.5	-1.8	-75.7	-3.4	-3.0	-2.1	285.7	59.2	53.2	46.8
3-(2-(2-Aminoethyl)-4,5-dihydroxyphenyl) propanenitrile	3-dp	M06L	-8.9	0.4	-208.9	26.7	-1.1	-0.7	-0.4	-53.6	-0.9	0.3	-1.2	-1.6	9.7	25.8	-214.3
		MP2	-8.7	0.3	-212.5	28.9	0.1	0.1	-0.6	-52.7	-1.1	-0.2	-1.4	-1.9	11.1	28.6	-209.8
	4-dp	M06L	--	--	--	--	--	--	--	--	--	--	--	--	--	--	--
		MP2	--	--	--	--	--	--	--	--	--	--	--	--	--	--	--
4-(2-(2-Aminoethyl)-4,5-dihydroxyphenyl) butanenitrile	3-dp	M06L	-10.0	-0.8	-45.0	-99.4	-0.7	-1.7	-0.7	27.9	-3.9	-5.4	-0.1	-1.0	-41.5	-31.7	-213.9
		MP2	-10.6	-0.9	-48.3	-92.5	-0.1	-1.6	-0.7	27.0	-4.0	-5.8	-0.3	-1.1	-39.8	-30.3	-209.1
	4-dp	M06L	-4.2	-0.6	-247.5	52.7	-1.5	-1.0	-1.9	-35.6	-4.1	-4.2	0.0	-2.5	-41.6	23.1	-269.0
		MP2	-4.3	-0.9	-227.5	61.1	-1.3	-0.4	-2.0	-40.8	-3.5	-4.0	-2.1	0.3			
4-Nitrobenzene-1,2-diol	3-dp	M06L	1.1	-0.2	-106.5	-6.6	-2.1	-1.1	0.1	-14.9	0.0	-2.1	0.3	-0.4	-43.4	-2.0	-178.0
	4-dp	M06L	0.2	-0.2	-112.9	-7.0	-1.7	-1.3	0.0	-10.6	-0.4	-3.2	0.3	-0.3	-35.4	11.4	-161.0
		MP2	--	-0.3	-120.8	3.8	-0.8	-1.2	-0.1	-12.5	-0.9	-2.8	0.0	-0.6	-31.4	-1.4	-169.0

**Table D-5.** Supplementary data for first generation ligands in the SX model

Molecule			Trp253	Le413	Mg^{2+}	Asp169/Asn170	Pro174	Met416	Val388	Lys144	Trp38	Met40	Val42	Asn41	Glu199	Asp141	Total
Dopamine	3-dp	M06L	-4.1	-0.6	-219.8	26.4	-2.5	0.6	-1.0	-63.2	-3.6	0.7	-1.3	-1.3	13.5	31.3	-224.9
	4-dp	M06L	0.6	-0.3	-215.7	19.4	-28.2	-7.8	0.0	-75.5	-0.8	-1.8	-1.6	-2.3	-2.3	24.0	-292.5
BIA 8-176	--	M06L	-0.2	-1.6	-288.7	60.2	-4.2	-0.6	-1.1	-90.9	-2.8	-1.8	-2.1	-1.1	52.2	50.0	-232.9
Resveratrol	--	M06L	1.1	-0.6	-337.1	37.6	-3.3	0.1	-3.4	-116.3	-2.5	-1.9	-2.3	-1.3	52.1	68.1	-309.8
6-Hydroxy dopamine	3-dp	M06L	-0.3	-1.2	-225.0	11.4	-1.5	-0.6	-2.2	-71.8	-3.3	-0.2	-1.1	-1.5	-11.5	33.3	-275.6
	4-dp	M06L	0.2	-0.1	-209.5	11.6	-5.2	-1.5	0.0	-64.3	0.3	1.9	-1.3	-1.8	-55.2	31.4	-293.6
1,2,3,4-Tetrahydrois oquinoline-6,7-diol	3-dp	M06L	0.4	-0.3	-200.4	-9.3	-8.6	-2.9	0.0	-56.0	-1.1	1.5	-1.4	-1.3	-9.4	226.2	-62.4
	4-dp	M06L	0.2	-0.8	-211.8	21.6	-2.9	-1.5	-0.6	-69.3	-9.2	-4.7	-1.3	-1.4	0.5	32.0	-249.3
6-Nitro dopamine	3-dp	M06L	-1.2	0.0	-185.3	27.5	-2.3	-0.4	-0.1	-25.0	-2.2	-12.7	-0.7	-1.0	16.1	9.5	-177.8
	4-dp	M06L	0.6	-1.1	-178.9	21.5	-1.3	-0.8	-2.3	-36.7	-11.7	-0.6	-0.7	0.5	1.5	11.9	-198.1
6-Bromo dopamine	3-dp	M06L	0.1	-1.7	-232.8	25.8	-1.9	-2.3	-1.7	-42.5	-12.6	-1.6	-1.5	-1.4	-1.7	17.4	-258.4
	4-dp	M06L	0.1	-1.9	-222.3	25.2	-2.1	-2.7	-1.9	-42.9	-14.2	-1.6	-1.4	-1.6	-3.0	19.1	-251.1
6-Cyano dopamine	3-dp	M06L	-0.4	-1.4	-204.7	25.8	-1.6	-4.7	-1.2	-33.0	-5.5	-2.4	-1.7	-2.4	1.8	15.7	-215.8
	4-dp	M06L	1.0	-2.0	-208.8	18.6	-2.6	-2.3	-2.3	-40.1	-14.3	-1.7	-1.1	-1.2	-4.9	12.9	-248.8
6-Ethenyl dopamine	3-dp	M06L	-4.2	-0.3	-207.7	23.6	-2.4	-0.9	-0.6	-73.3	-3.5	-5.3	-1.2	-2.0	2.8	29.3	-245.6
	4-dp	M06L	0.2	-1.1	-212.8	20.0	-2.8	-1.7	-1.3	-62.1	-9.5	2.9	-1.1	-1.3	-2.6	27.7	-245.5
6-Carboxy dopamine	3-dp	M06L	0.8	-0.7	-343.8	70.1	-4.2	1.1	-0.3	-116.4	-6.7	-2.9	-2.4	-1.8	61.1	74.5	-271.6
	4-dp	M06L	0.7	0.0	-334.8	60.4	-3.3	0.5	-0.4	-116.4	-1.7	3.2	-2.4	-1.4	47.2	69.8	-278.7

**Table D-6.** Supplementary data for second generation ligands in the SX model

Molecule			Trp253	Leu413	Mg^{2+}	Asp169/Asn170	Pro174	Met416	Val388	Lys144	Trp38	Met40	Val42	Asn41	Glu199	Asp141	Total
3,4-Dihydroxy benzonitrile	3-dp	M06L	0.6	-1.2	-303.2	58.7	-4.2	-2.2	-0.7	-102.7	-1.6	-3.2	-2.3	-1.4	53.0	65.4	-245.0
	4-dp	M06L	0.2	0.0	-301.7	64.4	-3.9	0.7	-0.6	-101.3	-1.9	0.6	-2.2	-1.4	55.1	64.3	-227.6
2-(3,4-Dihydroxyphenyl) acetonitrile	3-dp	M06L	-0.5	0.0	-127.7	-8.1	1.2	0.1	0.0	-10.5	0.6	-1.0	-0.6	-0.6	3.3	5.6	-138.2
	4-dp	M06L	0.3	-0.3	-350.0	59.9	-2.7	0.4	-0.6	-85.3	-3.4	-4.6	-3.1	-2.1	65.5	62.4	-263.4
3-(3,4-Dihydrozyphenyl) propanenitrile	3-dp	M06L	-0.4	-0.3	-352.1	61.0	-2.9	0.3	-0.2	-85.0	-2.5	-4.6	-3.0	-2.2	64.0	61.9	-265.9
	4-dp	M06L	0.6	-0.9	-314.0	60.3	-3.1	-0.1	-0.5	-72.1	-1.3	0.4	-2.5	-1.8	51.9	61.4	-221.6
4-(3,4-Dihydroxyphenyl) butanenitrile	3-dp	M06L	-2.0	-1.4	-318.4	59.4	-3.5	-0.4	-0.3	-100.4	-0.9	1.2	-2.4	-1.5	52.3	67.0	-251.4
	4-dp	M06L	0.6	-0.5	-357.0	65.3	-3.5	0.3	-2.8	-92.9	-4.7	-2.9	-2.5	-1.8	66.8	47.0	-288.7
3-(4,5-Dihydroxy-2-nitrophenyl) propanenitrile	3-dp	M06L	-0.5	-1.4	-290.6	58.3	-2.9	0.4	-0.7	-97.8	-2.7	-1.7	-2.0	-1.1	53.7	59.7	-229.4
	4-dp	M06L	0.5	-1.5	-318.0	56.1	-3.3	-1.1	-0.5	-73.9	-1.0	-1.2	-2.0	-1.2	51.7	52.9	-242.4
4-(4,5-Dihydroxy-2-nitrophenyl) butanenitrile	3-dp	M06L	--	--	--	--	--	--	--	--	--	--	--	--	--	--	--
	4-dp	M06L	--	--	--	--	--	--	--	--	--	--	--	--	--	--	--
3-(2-(2-Aminoethyl)-4,5-dihydroxyphenyl) propanenitrile	3-dp	M06L	-84.5	-1.2	-323.5	60.4	-3.5		-0.7	-112.8	-1.3	0.2	-2.3	-1.6	49.7	65.5	-355.5
	4-dp	M06L	--	--	--	--	--	--	--	--	--	--	--	--	--	--	--
4-(2-(2-Aminoethyl)-4,5-dihydroxyphenyl) butanenitrile	3-dp	M06L	-2.7	-0.3	-216.8	13.7	-3.1	-2.1	-0.3	-73.0	-1.5	-3.0	-1.7	-1.9	-56.6	27.6	-321.8
	4-dp	M06L	-7.4	-0.3	-235.5	25.9	-2.3	-0.1	-0.1	-76.3	-2.3	-3.7	-1.4	-1.8	8.1	31.7	-265.4
4-Nitrobenzene-1,2-diol	3-dp	M06L	1.1	-0.2	-106.5	-6.6	-2.1	-1.1	0.1	-14.9	0.0	-2.1	0.3	-0.4	-43.4	-2.0	-178.0
	4-dp	M06L	1.3	-0.8	-303.8	48.4	-4.3	-3.1	-0.3	-87.7	-1.1	-2.5	-2.2	-1.5	56.8	58.8	-241.8

Appendix E: NMR Spectroscopy (Data and spectrum)
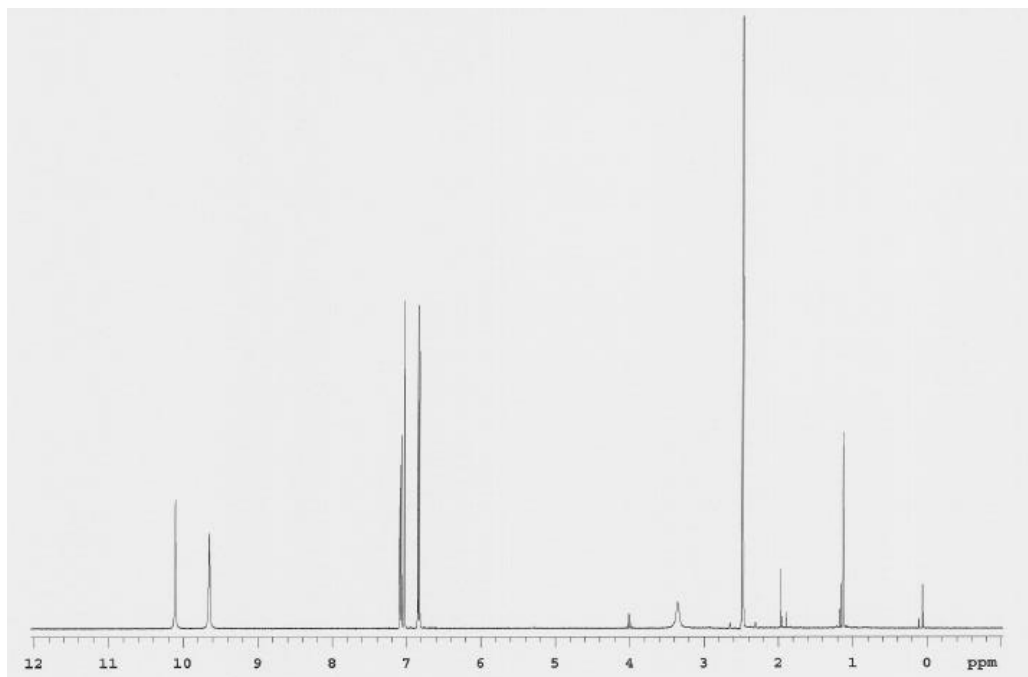
Figure E-1. ^{1}H NMR spectrum for 3,4-dihydroxybenzonitrile **(2)**. ^{1}H NMR (400 MHz, DMSO-d_6) δ ppm 6.86 (d, J=8.22 Hz, 1 H) 7.05 (d, J=1.96 Hz, 1 H) 7.08 (dd, J=8.22, 1.96 Hz, 1 H) 9.66 (br. s., 1 H) 10.12 (s, 1 H)
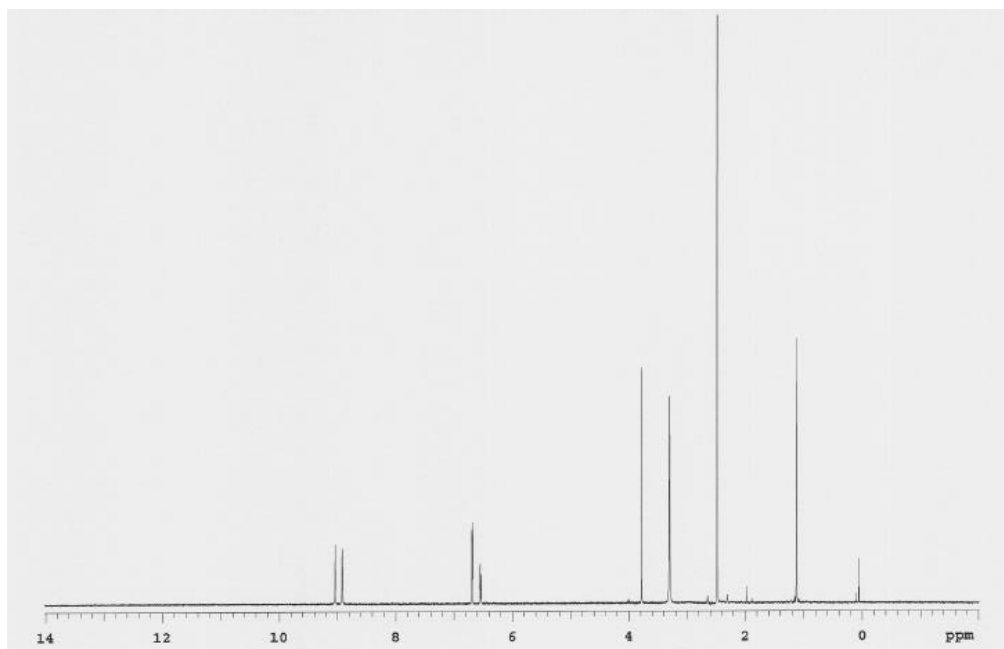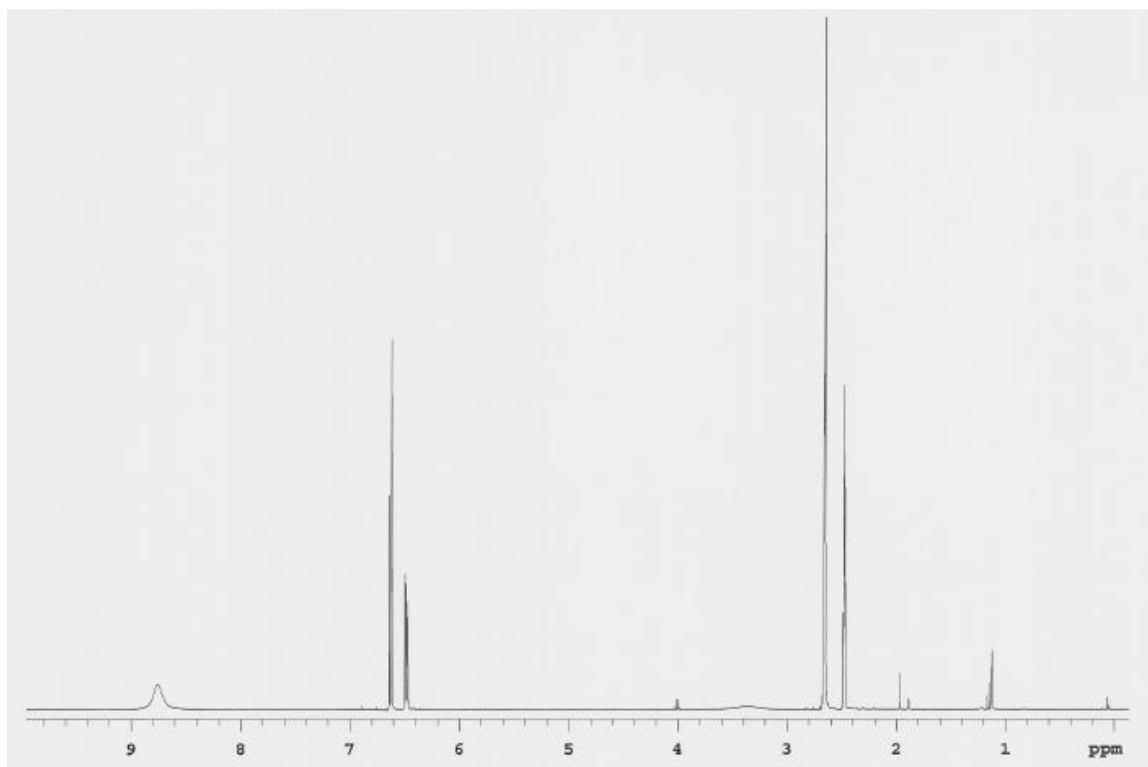

Figure E-2. ^{1}H NMR spectrum for 2-(3,4-dihydroxyphenyl)acetonitrile **(4)**. ^{1}H NMR (400 MHz, DMSO-d_6) δ ppm 3.80 (s, 2 H) 6.57 (dd, J=7.8, 2.0 Hz, 0 H) 6.70 (d, J=7.8 Hz, 0 H) 6.71 (d, J=2.0 Hz, 0 H) 8.94 (s, 1 H) 9.06 (s, 1 H)
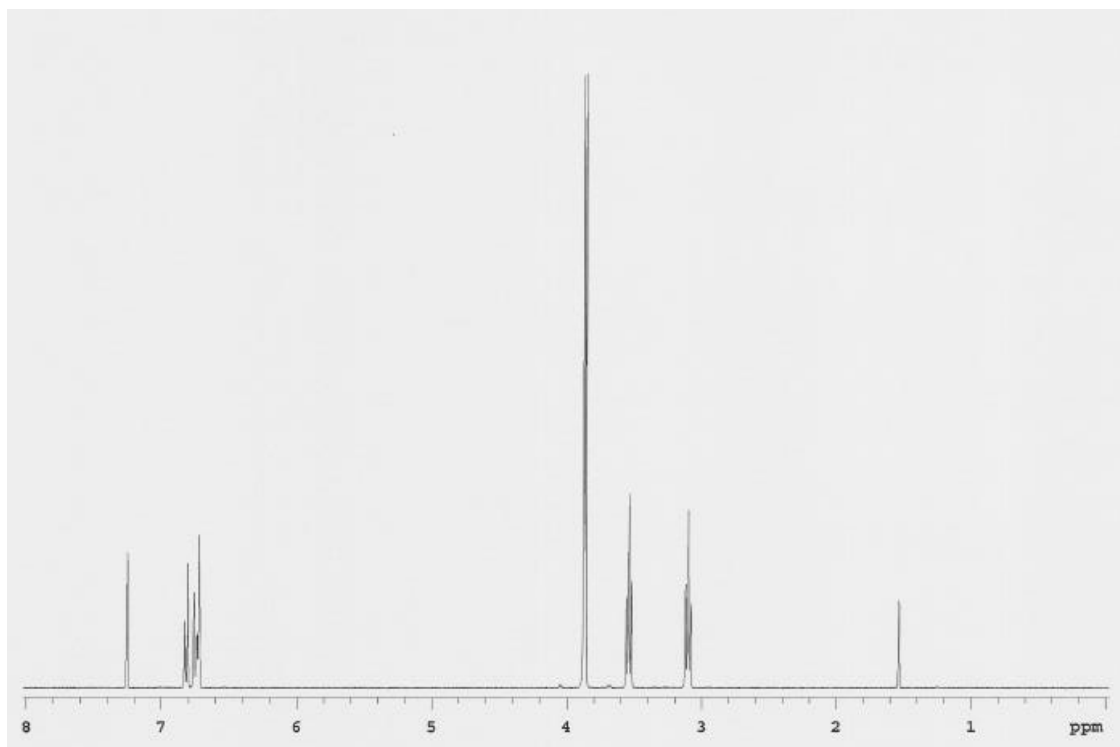
Figure E-3. ^{1}H NMR spectrum for 4-(2-bromoethyl)-1,2-dimethoxybenzene **(6).** ^{1}H NMR (400 MHz, CDCl$_3$-*d*) δ ppm 3.12 (t, *J*=7.83 Hz, 2 H) 3.56 (t, *J*=7.83 Hz, 2 H) 3.88 (s, 3 H) 3.89 (s, 3 H) 6.72 - 6.86 (m, 3 H)
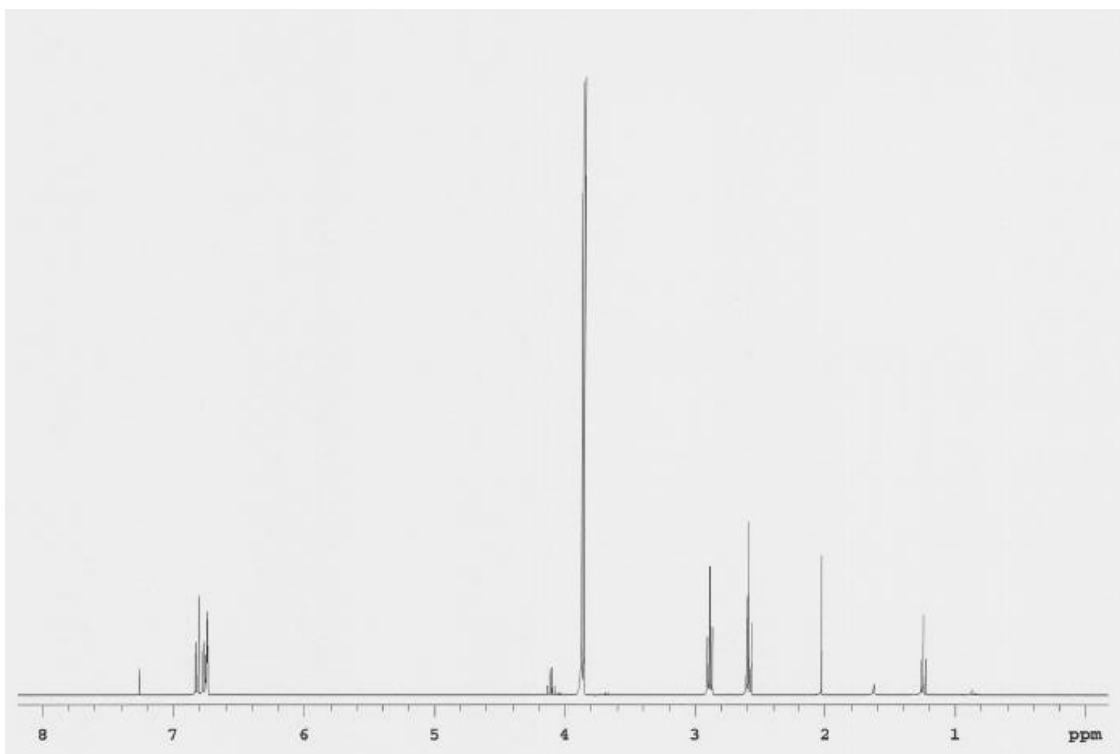

Figure E-4. ^{1}H-NMR spectrum for 3-(3,4-dimethoxyphenyl)propanenitrile **(7).** ^{1}H NMR (400 MHz, CDCl$_3$-*d*) δ ppm 2.60 (t, *J*=7.43 Hz, 2 H) 2.90 (t, *J*=7.43 Hz, 2 H) 3.87 (s, 3 H) 3.88 (s, 3 H) 6.74 - 6.86 (m, 3 H)

Figure E-4. ^{1}H NMR spectrum for 3-(3,4-dihydroxyphenyl)propanenitrile **(8).** ^{1}H NMR (400 MHz, DMSO-d_6) δ ppm 2.68 (s, 4 H) 6.51 (dd, *J*=8.2, 2.0 Hz, 1 H) 6.64 (d, *J*=2.0 Hz, 1 H) 6.65 (d, *J*=8.2 Hz, 1 H) 8.78 (br. s., 2 H)

Appendix F: HPLC Data

HPLC conditions: Acetonitrile and 5% acetonitrile in water, 0.8 mL/min, 30 ˚C oven temp; HPLC method: 20% acetonitrile (0-2 minutes), 50% acetonitrile (2-5 minutes), 65% acetonitrile (5-8 minutes)
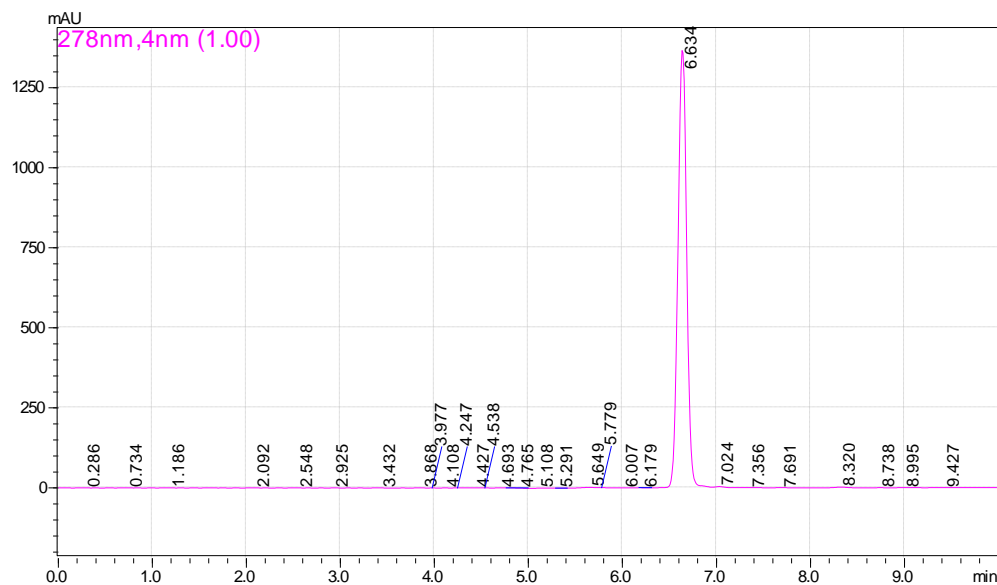
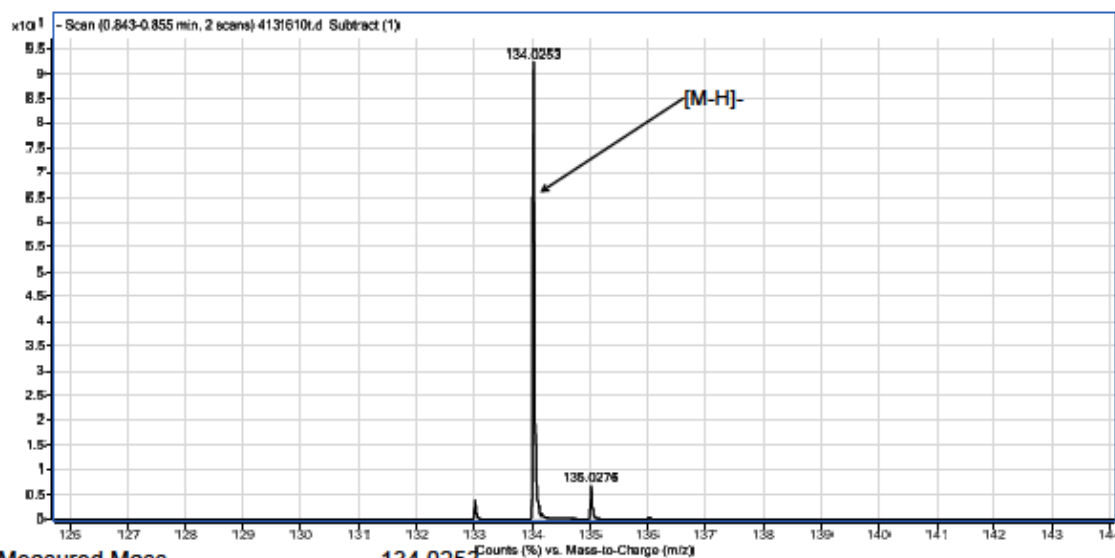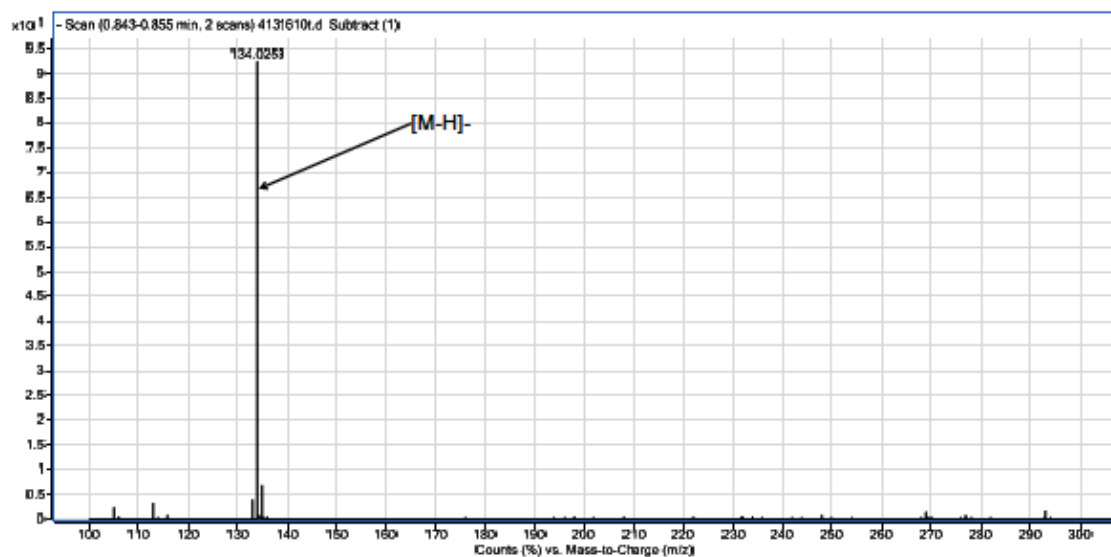**Figure F-1**. HPLC chromatogram of 3,4-dihydroxybenzonitrile (Retention Time: 6.634 minutes)
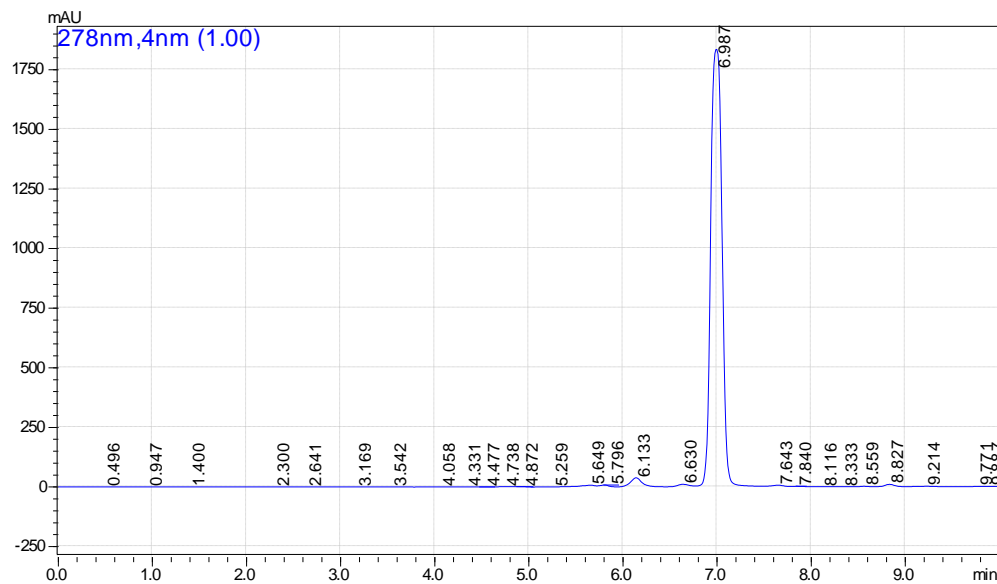
Figure F-2. HPLC chromatogram of 2-(3,4-dihydroxyphenyl)acetonitrile (Retention Time: 6.978 min)
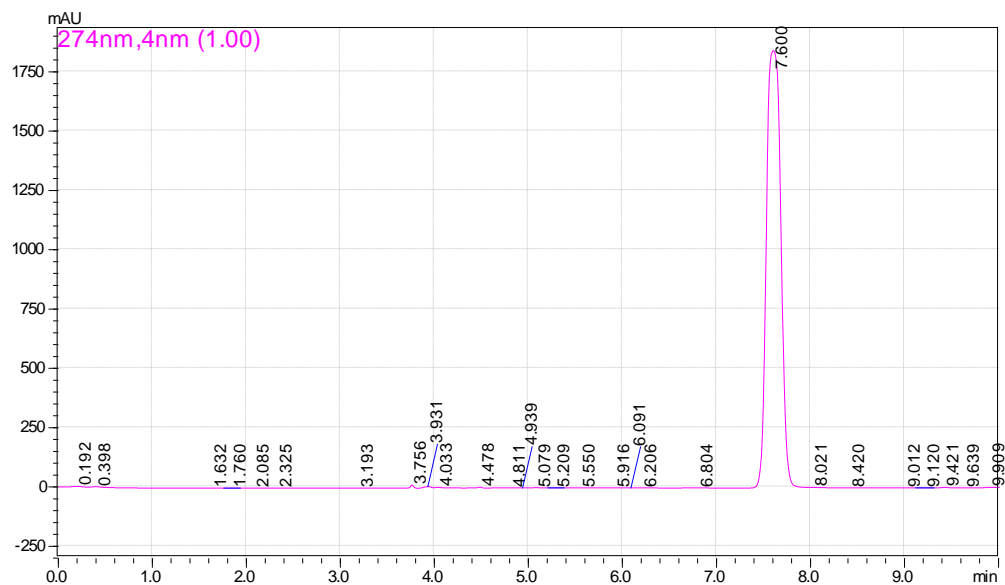
Figure F-3. HPLC chromatogram of 3-(3,4-dihydroxyphenyl)propanenitrile (Retention Time: 7.600 min)

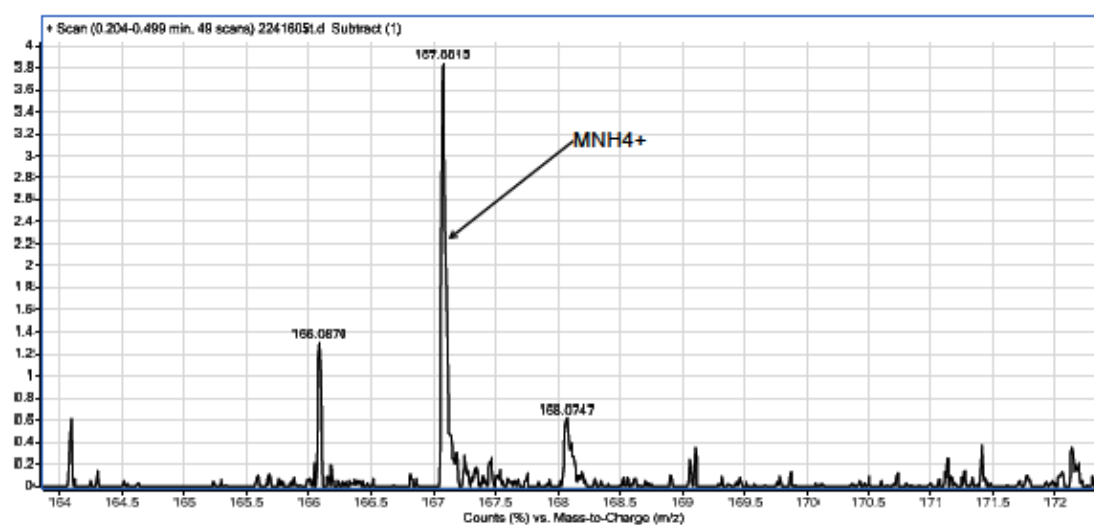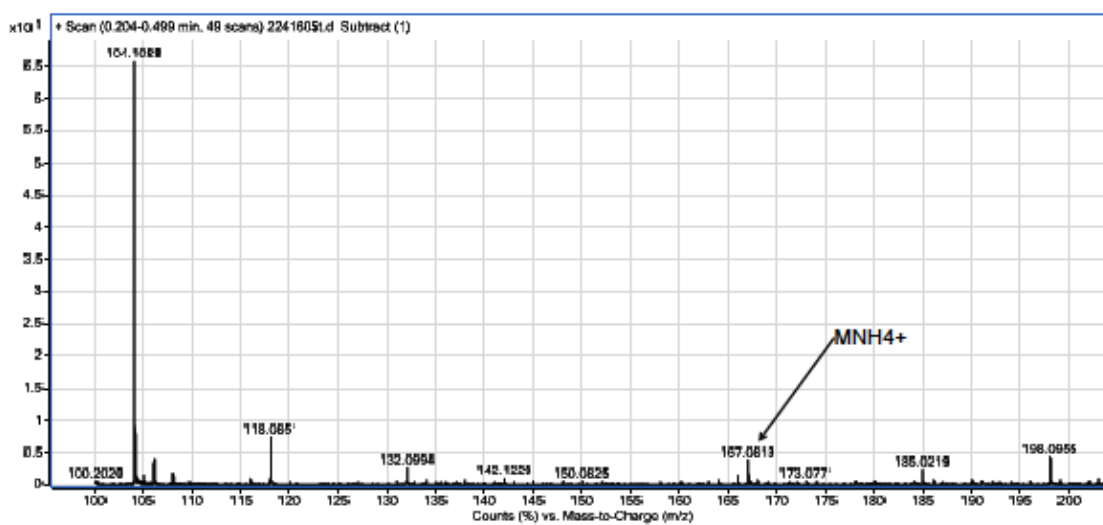**Appendix G: High resolution mass spectrometry analysis**

Measured Mass		134.0253

Element	Low Limit	High Limit
C	2	12
H	0	20
N	0	3
O	0	3

Formula	Calculated Mass	mDaError	ppmError	RDB
C7 H4 N O2	134.0248	0.5	4.1	6.5

Appendix G-1: High resolution mass spec spectrum for (3,4-dihydroxyphenyl)benzonitrile (analyzed at UC Riverside Mass Spec facility)
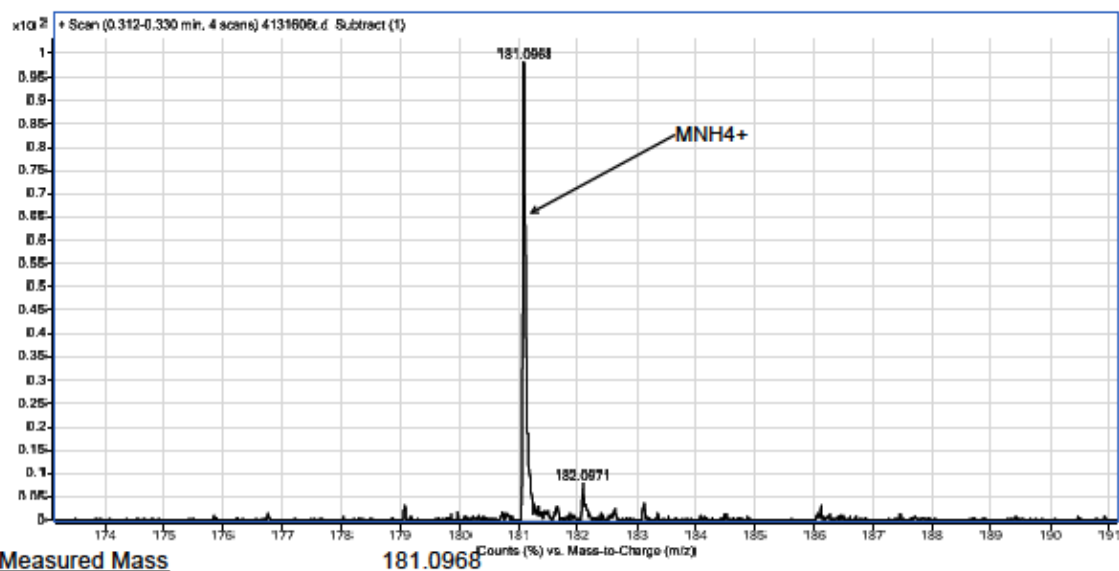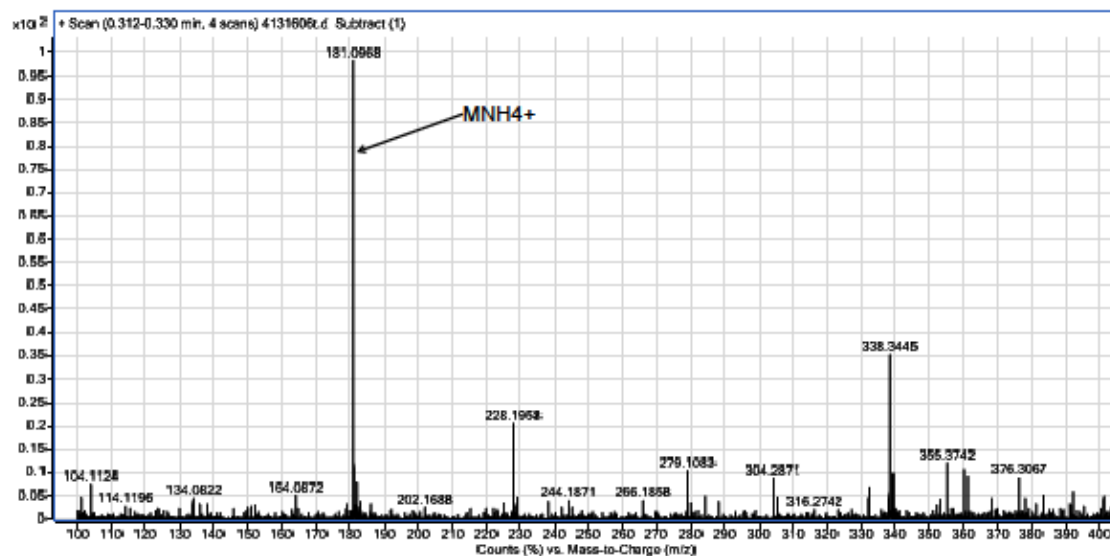
Measured Mass		167.0813	

Element	Low Limit	High Limit
C	3	13
H	0	20
N	0	2
O	0	93

Formula	Calculated Mass	mDaError	ppmError	RDB
C8 H11 N2 O2	167.0815	-0.2	-1.2	4.5

Appendix G-2: High resolution mass spec spectrum for 2-(3,4-dihydroxyphenyl)acetonitrile, doped with NH_4^+ (analyzed at UC Riverside Mass Spec facility)

Measured Mass	181.0968			

Element	Low Limit	High Limit
C	4	14
H	0	20
N	0	3
O	0	3

Formula	Calculated Mass	mDaError	ppmError	RDB
C9 H13 N2 O2	181.0972	-0.4	-2.0	4.5

Appendix G-3: High resolution mass spec spectrum for 3-(3,4-dihydroxyphenyl)propanenitrile (analyzed at UC Riverside Mass Spec facility)